Dissertations, Master's Theses and Master's Reports - Open

Dissertations, Master's Theses and Master's Reports

2006

Development and modeling of thermally conductive resins for fuel cell bipolar plate applications

Michael G. Miller
Michigan Technological University

Development and Modeling of Thermally Conductive Resins for Fuel Cell Bipolar Plate Applications

By

Michael G. Miller

Bachelor of Science, Michigan Technological University, May 2003

A Dissertation

Submitted to the Graduate Faculty

Of The

Michigan Technological University

In partial fulfillment of the requirements

For the degree of

Doctor of Philosophy

In

Chemical Engineering

Houghton, Michigan
September 2006
© 2006 Michael G. Miller

Chapter 0:   Prequel

Section 0.1: Signatures Page

This dissertation, **"Development and Modeling of Thermally Conductive Resins for Fuel Cell Bipolar Plate Applications,"** is hereby approved in partial fulfillment of the requirements for the degree of DOCTOR OF PHILOSPHY in the field of Chemical Engineering.

DEPARTMENT – Chemical Engineering

Signatures

Dissertation Advisor: _____

Dr. Julia A. King

Dissertation Co-Advisor: _____

Dr. Jason M. Keith

Department Chair: _____

Dr. Michael E. Mullins

Date: September 11, 2006_____

Section 0.2: Abstract

Development and Modeling of Thermally Conductive Resins for Fuel Cell Bipolar Plate Applications

By: Michael G. Miller

Committee Chair: Dr. Julia A. King

Committee Co-Chair: Dr. Jason M. Keith

Chemical Engineering

Thermally conductive resins are a class of material that show promise in many different applications. One growing field for their use is in the area of bipolar plate technology for fuel cell applications. In this work, a LCP was mixed with different types of carbon fillers to determine the effects of the individual carbon fillers on the thermal conductivity of the composite resin. In addition, mathematical modeling was performed on the thermal conductivity data with the goal of developing predictive models for the thermal conductivity of highly filled composite resins.

Section 0.3: Acknowledgements

Brian Edwards, Matt Hedlund, Juan Morinelly, Leslie Brown, Andrew Cole, Kara Lenhart, Katherine Lindahl, Jacob Lundmark, Terrence Mazure, Troy Tambling, Samuel Roache, Elaine Venema, Joan Wierzba, Amanda Zalud, Peter Grant, Bryan Klett, and Matt Ponkey.

I'd also like to thank some of my high school teachers for guiding me into chemical engineering along the way. Of particular note are Harlan Larson (chemistry), Dawn Bassuener and Mary Pardun (biology) and Gerry Pardun (physics) for helping me narrow down which field of science I wanted to specialize in and Cindy Goll, Lori Kotarba and John Kriegl (mathematics) for firing my interest in the mathematical side of the sciences.

Section 0.5: List of Figures

Section 0.6: List of Tables

Section 0.7: Table of Nomenclature

A	Nielsen Model equation parameter
A	Trendline equation parameter
B	Nielsen Model equation parameter
B	Trendline equation parameter
C_p	Heat capacity of component (J/kgK)
c	Volumetric heat capacity (J/m^3K)
E_C	Elastic modulus of composite (bar)
E_P	Elastic modulus of polymer (bar)
G_C	Shear modulus of composite (bar)
G_P	Shear modulus of polymer (bar)
K	Thermal conductivity of composite (W/mK)
k	Thermal conductivity (W/mK)
k_b	Boltzmann constant
k_C	Thermal conductivity of composite (W/mK)
k_E	Einstein coefficient
k_i	Thermal conductivity of component (W/mK)
k_{ij}	Direction-dependent thermal conductivity (W/mK)
k_{in}	In-plane thermal conductivity (W/mK)
k_P	Thermal conductivity of polymer (W/mK)
k_{thru}	Through-plane thermal conductivity (W/mK)
N_O	Avogadro's number
P	Power (W)
Q	Power (W)
Q_R	Power per unit length (W/m)
q_i	Heat flux (W/m^2)
R_n	Resistance at time n (Ω)
R_{no}	Resistance at time 0 (Ω)
r'	Radius of sensor 'ring' (m)
T	Temperature (K)
t	Time (s)
u	Speed of sound in a material (m/s)
V_{EXP}	Experimental cell voltage (V)
V_{OCV}	Theoretical cell voltage (V)
W	Mass of component (kg)
x_i	Particle count parameter (non-dimensional)
y_i	Shape factor (non-dimensional)
y_i	Particle count parameter (non-dimensional)

_____

α	Thermal diffusivity (m^2/s)
β	Temperature coefficient of resistance (1/K)
χ	Halpin-Tsai equation parameter
ΔT	Change in temperature (K)

δ	Dirac delta function
$\delta T/\delta x_i$	Temperature gradient (K/m)
ϕ_i	volume fraction of component (non-dimensional)
ϕ_m	maximum packing fraction of component (non-dimensional)
η	Efficiency (non-dimensional)
η_C	Viscosity of composite (kg/m-s)
η_P	Viscosity of polymer (kg/m-s)
φ	McCullough equation parameter
λ	Mean free path (m)Θ
θ_D	Debye temperature (K)
ρ	Density of component (kg/m^3)
ρ_{theo}	Theoretical density of composite (kg/m^3)
ρ_{water}	Density of water (kg/m^3)
τ	Hot Disk equation parameter
ω	Frequency of vibration (1/sec)
ω_D	Debye frequency of vibration (1/sec)
ψ	Particle sphericity (non-dimensional)
ψ	Nielsen Model equation parameter
ζ	Halpin-Tsai equation parameter
$\hbar$	Planck's constant

Chapter 1: Introduction

Section 1.1: Background

Polymers are generally very poor materials to use in thermally conductive applications. By and large, for these types of applications metals are used. However, by adding conductive fillers to polymers it is possible to increase the thermal conductivity of the polymer to values greater than 1 W/mK, at which point they become useful in thermal conductivity applications. These thermally conductive polymers have many advantages over a pure metal: a lower density, improved corrosion / oxidation / chemical resistance and more direct control over the properties of the material.

A prime application for thermally conductive resins is thermal energy regulation. Computers, laptops, fuel cells and transformer housings all need to disperse the thermal energy during use. Heat exchangers and radiators could also benefit from advances in this field. In all of these cases, the polymer composite would need a thermal conductivity greater than 1 W/mK. However, developing the materials with the precise properties necessary for the application at hand is very costly if done by trial and error. Being able to predict the thermal conductivity of a composite material will vastly streamline this process, allowing for savings in time, labor and materials cost.

In recent years, there has been a large increase in the demand for smaller and lighter electronic devices and similar machinery. Industry has also been specializing in materials with properties tailored to the specific needs of the application. More and more often, composite materials are used to fill these specific needs. Composite materials are a mixture of two or more different kinds of materials (such as ceramics, metals, and polymers) which, when combined, produce a material with physical properties that are a

mixture of the constituent materials. Examples of widely used composite materials include fiberglass and concrete. In this study, carbon-filled thermoplastic polymer composites will be investigated. This dissertation will focus on the thermal conductivity of these composites.

Since most polymers are very poor thermal conductors, the most common way to improve them for this application is to add thermally conductive fillers to the polymer matrix. Previous studies have investigated different single-filler additions to a polymer matrix to improve the thermal conductivity of the polymer composite [1-6]. Different types of carbon fillers are used to adjust the thermal and electrical conductivities of these polymer composites dependent on their end use. Carbon filler will increase the conductivity of the composite relative to the neat polymer, but not to the level of the pure carbon filler. Previous work [7-8] has shown that a multiple-filler system has given synergistic effects in the increasing of thermal conductivity; the total increase in thermal conductivity when the fillers are mixed together is greater than the sum of the increase in thermal conductivity in the single-filler systems.

Section 1.2: Thermal Conductivity

Thermal conductivity has had a profound impact on human existence [9]. Materials with low thermal conductivity have helped people in non-tropical climates retain the heat necessary to survive while allowing people in tropical climates to build structures that were effective at keeping the heat out. In more modern times, space vehicles designed for atmospheric passage and re-entry are dependent on materials with a very low thermal conductivity to keep the massive amounts of thermal energy away from the rest of the vessel. Thermal conductivity has been important throughout the ages and promises to be integral to our continued advancement. Table 1.2-1 lists the thermal conductivity of some common materials [10].

Table 1.2-1: Thermal Conductivity of Common Materials [10]

Materials	Thermal Conductivity (W/mK)
Polymers	0.19 to 0.30
PAN-based Carbon Fiber	8 to 70
Pitch-based Carbon Fiber	20 to 1000
Stainless Steel	11 to 24
Aluminum	218 to 243
Copper	385
Silver	418
Diamond	990

Section 1.3: Motivation

The demand for conductive composites continues to grow in the United States. In 1995, the demand for conductive polymer composites was 221 million lbs. It was projected to grow 6.1 percent annually to 565 million pounds (including both resins and additives) by 2004. Its projected value was to reach $1.5 billion by 2004, consisting of the cost of resins and additives, as well as labor and other overhead costs incurred during the production of the conductive compound [11]. It is clear that this increasing demand requires more research and development of conductive polymer composites, both to produce new materials and to streamline the cost and time of production. Most conductive resins in widespread use today are used in electromagnetic frequency interference (EMI) and/or radio frequency interference (RFI) shielding or in electrostatic dissipation (ESD) applications. Research into these composites could allow for multifunctional composite materials. Another application of conductive polymer composites will now be described.

Section 1.4: Fuel Cells

Fundamental and applied research is needed for the development of cost effective fuel cells for stationary and transportation applications. The proton exchange membrane fuel cell (PEMFC) is one of the most promising alternative fuel technologies to power cars and buses. Hydrogen is the fuel which reacts with oxygen (from the air) to produce DC electricity to power motors and auxiliary equipment for the vehicle. The byproducts of the reaction are heat and water [12].

Hydrogen gas flows into the fuel cell on the anode side of the membrane, where it encounters a platinum catalyst, which facilitates the separation of the hydrogen gas into electrons and protons (hydrogen ions). The hydrogen ions pass through the membrane, and, again encounter a platinum catalyst, which helps combine the hydrogen ions, oxygen gas, and electrons on the cathode side to produce water as the product. The electrons, which cannot pass through the membrane, flow from the anode to the cathode side of the fuel cell through an external circuit containing a motor or other electric load, which consumes the power generated by the fuel cell. The voltage generated from one single cell is typically 0.7 volts. The cells are typically arranged in a stack to provide a proportionally larger voltage. Since commercial electric motors often operate at 300 volts, often 430 bipolar plates are needed for a fuel cell assembly [12]. In a PEMFC, the efficiency is expressed by Equation 1.1:

$$\eta = \frac{V_{EXP}}{V_{OCV}} \tag{1.1}$$

In this equation, η is non-dimensional, V_{EXP} is the measured voltage of a single cell (V) and V_{OCV} is the open circuit voltage (V), which is the theoretical maximum voltage output of a single cell. V_{OCV} is dependent on the fuel used in the fuel cell and, in the case of a

PEMFC, the state of the water that comes out (steam or liquid). Using hydrogen as the

fuel and assuming the product comes out as steam results in Equation 1.2:

$$\eta = \frac{V_{EXP}}{1.25V} \qquad (1.2)$$

Assuming the typical 0.7 volt output as discussed above, $\eta = 0.56$. This means

56% of the energy content of the fuel is converted into electrical energy, with the other

44% converted into heat energy. Increasing the electrical conductivity of the material

used in the bipolar plate may increase the measured voltage of the single cell and increase

the efficiency; increasing the thermal conductivity will increase the rate at which heat

energy is pulled out of the bipolar plate and will help with thermal management of the

fuel cell.

Bipolar plates serve many different functions in a fuel cell. They separate the

proton exchange membranes from each other, conduct heat generated by the chemical

reactions and electron flow out of the system, distribute the feed gases uniformly across

the proton exchange membrane, and conduct the electrons generated in the anode half-

reaction into the load circuit to generate work. Current bipolar plate technology uses

conductive resins as the foundation for the bipolar plate, with different fillers being used

to modify the physical properties. A more detailed description follows in the next section.

Section 1.5: Bipolar Plates

Bipolar plate technology plays a key role in fuel cell technology. The bipolar plate separates one cell from the next, with this plate carrying hydrogen gas on one side and air (oxygen) on the other side. The bipolar plate must be made of gas impermeable material. Otherwise, the fuel sources and the electrons they generate are wasted since they cannot be sent to an external circuit to do useful electrical work. In addition, the bipolar plate must be electrically conductive to minimize ohmic losses and be thermally conductive to conduct the generated heat (reaction byproduct) away. Ideally, the bipolar plates should be as thin as possible to minimize electrical resistance and to make the fuel cells stack small [11,13,14]. An illustration of a fuel cell unit is shown in Figure 1.5-1; the bipolar plates are the structures to the left and right of the gas diffusion backings [13].

Figure 1.5-1: Cross Section of Polymer Electrolyte Fuel Cell [13]

The desired properties for bipolar plates for fuel cells are as follows [15-18]:

- Electrical conductivity greater than 50 S/cm

- Thermal conductivity greater than 20 W/mK

- Flexural strength greater than 35 MPa

- Flexural modulus greater than 6 GPa

- Tensile strength greater than 25 MPa

- Tensile modulus greater than 6 GPa

- Unnotched Izod impact strength greater than 0.1 N-m/cm

- Hydrogen permeation rate less than $2 \times 10^{-6}\,\text{cm}^3/(\text{sec-cm}^2)$

In addition, the bipolar plates need to have excellent thermal and dimensional stability up to 150°C for the next generation of fuel cells which will operate at this temperature instead of the current 80°C [16-18].

Section 1.6: Research Objectives

The objectives of this project were to:

1.   Create thermally conductive composites

2.   Characterize and analyze carbon filled polymer composites

3.   Develop a model to predict thermal conductivity of carbon-filled polymer

composites

These objectives have been reached in an experimental study where data was

collected and analyzed. The study centered on the production, testing, and analysis of

single-filler conductive resins. This study examined polymer composites filled with

carbon black, natural flake graphite, synthetic graphite, calcined needle coke, or carbon

fiber in a liquid crystal polymer matrix. Their thermal conductivity was determined for

both the longitudinal and transverse directions. The knowledge gained from this study

forms the foundation for the modeling work.

The transverse thermal conductivity results gathered from this study were then

used to improve a current transverse thermal-conductivity model. The resulting model

more accurately predicts the composite transverse thermal conductivity. The model that

was used is a function of the volume fraction of filler, maximum packing fraction, and

filler thermal conductivities, as well as the polymer volume fraction and thermal

conductivity. The longitudinal thermal conductivity results were used to help derive a

model relating the longitudinal thermal conductivity, the transverse thermal conductivity

and the volume fraction of the carbon fillers in the composite material.

Section 1.7: References

1.   D. M. Bigg, "Thermally Conductive Polymer Compositions". *Polymer Composites*, Vol. 7, No. 3, 1986, pp. 125.

2.   D. Hansen, and G. A. Bernier, "Thermal Conductivity of Polyethylene: The Effects of Crystal Size, Density, and Orientation on the Thermal Conductivity". *Polymer Engineering and Science*, Vol. 12, No. 3, 1972, pp. 204.

3.   Y. Agari, and T. Uno, "Thermal Conductivity of Polymer Filled with Carbon Materials: Effect of Conductive Particle Chains on Thermal Conductivity". *Journal of Applied Polymer Science*, Vol. 30, 1985, pp. 2225-2236.

4.   Y. Agari, A. Ueda, and S. Nagai, "Thermal Conductivities of Composites in Several Types of Dispersion Systems". *Journal of Applied Polymer Science*, Vol. 42, 1991, pp. 1655-1669.

5.   R. C. Progelhof, J. L. Throne, and R. R. Ruetsch, "Methods of Predicting Thermal Conductivity of Composite Systems: A Review". *Reg. Tech. Cond. – Soc. Plast. Eng*, 1975, pp. 221-257.

6.   L. E. Nielsen, "The Thermal and Electrical Conductivity of Two-Phase Systems". *I&EC Fundamentals*, Vol. 13, No. 1, 1974, pp. 17-20.

7.   E. H. Weber, M. L. Clingerman, and J. A. King, "Thermally Conductive Nylon 6,6 and Polycarbonate Based Resin. Part 1: Synergistic Effects of Carbon Fillers", Journal of Applied Polymer Science, Vol. 88, pp. 112-122, 2003.

8.   E. H. Weber, M. L. Clingerman, and J. A. King, "Thermally Conductive Nylon 6,6 and Polycarbonate Based Resin. Part 2: Modelling", Journal of Applied Polymer Science, Vol. 88, pp. 123-130, 2003.

9. J. E. Parrott, and A. D. Stuckes, <u>Thermal Conductivity of Solids</u>. Pion Limited, London, 1975.

10. http://www.matweb.com/search/SearchProperty.asp?e=1, accessed April 14, 2006.

11. The Freedonia Group, Inc., "Conductive Polymers". Cleveland, OH 44143-2326, 2000.

12. S. Gottesfeld, C. F. Keller, S. Moller-Holst A. Redondo and J. Milliken, "Fuel Cells: Green Power", Los Alamos National Laboratory, LA-UR-99-3231, 1999.

13. "Fuel Cells", Los Alamos National Laboratory, http://www.lanl.gov/orgs/ee/fuelcells/index.shtml and http://education.lanl.gov/RESOURCES/H2/gottesfeld/education.html, accessed May 22, 2006.

14. "Material Opportunities in Fuel Cell technology: 2002 & Beyond", Principia Partners, www.principiaconsulting.com/PDF/brochure_fuelcells.pdf, accessed December 23, 2003, Exton, PA, 19341.

15. J. Larminie and A. Dicks, <u>Fuel Cell Systems Explained</u>, 2nd edition, John Wiley& Sons, West Sussex, England, 2003.

16. L. E. Nunnery, Jr., "Fuel Cell Technology", Society of Automotive Engineers (SAE) Conference, 1998.

17. R. Leaversuch, "Fuel Cells Jolt Plastics Innovation", <u>Plastics Technology Online</u>, November 2001, www.plasticstechnology.com/articles/200111fa2.html., accessed May 22, 2006.

18. N. Garland, "Materials for Bipolar Plates",

http://www1.eere.energy.gov/hydrogenandfuelcells/pdfs/nn0123s.pdf,

Department of Energy sponsored research presented May 9-10, 2002 in Golden,

CO, accessed May 22, 2006.

Chapter 2: Fundamentals of Polymers, Heat Transfer and Fuel Cell Bipolar Plates

Section 2.1: Polymeric and Composite Materials

A polymer molecule is a long molecule composed of many repeating units [1-3]. Most polymers have very few intermolecular interactions except for van der Waals forces; however, these forces are not strong enough to hold the molecules together in a solid form. The length of the polymeric molecules allows them to entwine each other and form entanglements that restrict the flow of the molecules. The stability of these entanglements is dependent on the molecular weight, flexibility and steric hindrance of the composite molecules. These entanglements influence the viscoelastic, melt viscosity, and mechanical properties of the polymer [1].

Another quality of the polymer that affects its physical properties is its degree of crystallinity. Most polymers have a very low degree of crystallinity if they possess any at all. Polymers without crystallinity are called amorphous [1]. Figure 2.1-1 shows how the polymer chains are arranged in an amorphous polymer matrix. Amorphous polymers tend to have good mechanical properties, good dimensional stability, consistent shrinking rates during cooling, and tend to be transparent / translucent materials [2].
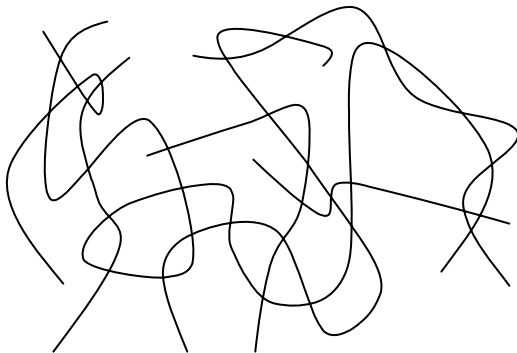
Figure 2.1-1: Representation of Polymer Chains in an Amorphous Polymer [1-2]

In contrast, semi-crystalline polymers generally arrange themselves in a lamellar structure [2]; examples of these structures in nature are the spores of a mushroom or the gills of a fish. For polymer crystallization to occur, the cooling conditions have to allow for time for the polymer chains to orient themselves properly. The crystalline sheets that form may be as thin as $100 - 200$Å, with amorphous regions between them [1]. In polyethylene, it was found that as the thickness of the lamellar structures increased, the thermal conductivity increased as well [4]. Figure 2.1-2 illustrates variations on two-dimensional lamellar structures which can be expanded to account for three dimensions. Semi-crystalline polymers have anisotropic shrinking properties, good electrical properties and are generally chemically resistant [2].

Regular adjacent reentry

Irregular reentry

Irregular reentry
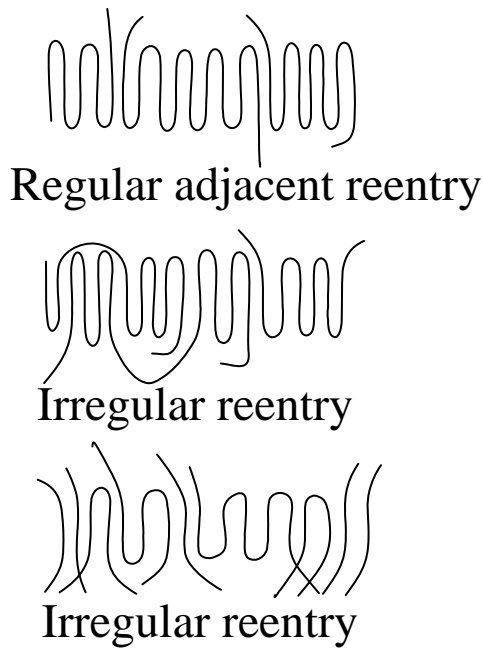
Figure 2.1-2: 2D Representation of Polymer Chains in a Semi-Crystalline Polymer [1,3]

Thermal conductivity has been experimentally shown to increase with increasing crystallinity or orientation of polymer chains [4-6], which implies that amorphous

polymers will be less conductive than semi-crystalline polymers. It has also been shown that filled amorphous polymer systems are less thermally conductive than filled semi-crystalline polymers [7].

Section 2.2: Thermal Conductivity Background

There are three mechanisms of heat transfer: radiation, convection and conduction. In solid systems, the primary mechanism of heat transfer is by conduction, quantified using Fourier's law (Equation 2.1) [8-10].

$$q_i = -k_{ij} \frac{\partial T}{\partial x_i} \qquad\qquad (2.1)$$

This equation shows that heat flux (q_i) is dependent on both the thermal conductivity of the material (k_{ij}) and the temperature gradient in the direction of conduction. In the above equation, the thermal conductivity term is assumed to be a constant value; in reality the thermal conductivity of a material varies with temperature, with the degree of variation being dependent on the material. The material thermal conductivity, referred to in the above equation, is the summation of different heat transfer methods. There are two primary methods of conductive heat transport in solids. These methods are electron transport and phonon transport. In pure metals, electron transport is the dominant method; in dielectric materials such as polymers, phonon transport is the dominant method. Mixtures of these classes of materials can have both forms of transport be significant in the overall heat transport [8-9].

A phonon is the quantum frequency of an atomic vibration. Phonons are carriers of heat energy and transfer this energy by interacting with other phonons and with other subatomic particles [11]. To understand these interactions, imagine a series of atoms with the bonds between them represented by small springs. An atom is excited and vibrates slightly, pushing or pulling on the springs connected to it, which disturbs the atoms connected to those springs, which moves the springs connected to those atoms, and

so on. The energy from the original atomic excitation would be propagated through the array. Figure 2.2-1 shows a two-dimensional example of this mechanism [12].
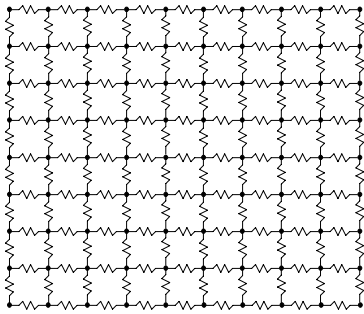
Figure 2.2-1: Two-Dimensional Array of Atoms Connected by Springs

Phonon heat transfer is highly dependent on the scattering of the phonons as they propagate through the material [11]. Different atoms, clustered atoms or missing atoms all have varying effects on the path of the phonon and the energy transferred between atoms. The dominant feature of phonon heat transfer is the distance between scattering incidents. Scattering incidents occur when a phonon encounters an atom and is either absorbed into it or deflects off it in a different direction. The longer the distance between scattering effects, the greater the thermal conductivity of a dielectric material is. This concept is illustrated by the Debye model for heat conduction in dielectric solids [4].

$$k = \frac{1}{3} \cdot c \cdot u \cdot \lambda \qquad (2.2)$$

In this model, k is the thermal conductivity, c is the volumetric heat capacity, u is the velocity of sound in the material, and λ is the mean free path (the average distance between scattering incidents) of the phonons in the material. A high mean free path will lead to a higher thermal conductivity than a low mean free path. For a typical material, the speed of sound is approximately 5×10^5 cm/s and is relatively independent of temperature [13]. The mean free path decreases with an increase in temperature.

The heat capacity of a material can be calculated using the Debye model as found in Equation 2.3 [14]. In this equation, c is the volumetric heat capacity, k_B is the Boltzmann's constant, N_o is Avogadro's number, T is the absolute temperature in Kelvin, θ_D is the Debye temperature in Kelvin, $\hbar$ is Planck's Constant, ω is the frequency of vibration, and ω_D is the Debye frequency of vibration.

$$c = 9 \cdot k_B \cdot N_0 \left(\frac{T}{\theta_D} \right)^3 \int_0^{\theta_D/T} \frac{x^4 \cdot e^x}{\left(e^x - 1 \right)^2} dx \tag{2.3}$$

$$\text{Where: } x = \frac{\hbar \cdot \omega}{k_B \cdot T} \text{ and } \theta_D = \frac{\hbar \cdot \omega_D}{k_B}$$

Heat conduction by phonons is the main conduction method in polymers, carbons, and their composites. Polymers are dielectric materials so they generally follow the Debye model. Many carbon fillers (including all the carbon fillers used in this project) are electrically conductive, but their thermal conductivity is essentially due to phonon transport.

Thermal conductivity in carbon/polymer composites is a bulk property. This is different from electrical conductivity, which is a path-dependent property. Previous experimental research has shown thermal conductivity increases continuously over the whole concentration range, whereas electrical conductivity increases by as many as 10 orders of magnitude over a small range of filler concentration known as the "percolation threshold" [15-16]. At the percolation threshold, the fillers get close enough to conduct current with little resistance. Thermal conductivity does not show a large and sudden increase with increasing filler concentration. This indicates that proximity of filler particles and the contact between them is not a significant factor in thermal conductivity and further indicates that thermal conductivity is a bulk property of a material.

Another way to examine thermal conductivity is to look at the scattering of phonons that occurs with touching filler particles. Assume that there is an array of filler particles touching each other edge to edge. In one case (see Figure 2.2-2a), the fillers are surrounded by vacuum; in another (see Figure 2.2-2b), the fillers are surrounded by a dielectric matrix material. Also, assume that no heat transfer occurs by radiation – all the heat transfer must be accomplished by conduction. In the case of Figure 2.2-2a, phonons are scattered and transmitted only at filler-filler contact points since any phonons scattered into the vacuum are lost by the 'no radiation' assumption. In the case of Figure 2.2-2b, phonons are still scattered and transmitted at filler-filler interface points, but the phonons that scatter at filler edge points connected to the dielectric matrix material are not lost because the matrix material can absorb and transmit the phonons. This matrix allows a far greater heat transfer than the first case. For a path-dependent property, the first and second cases should yield an identical heat transfer, which has been shown experimentally to not be true. This is another indicator that thermal conductivity is a bulk property.
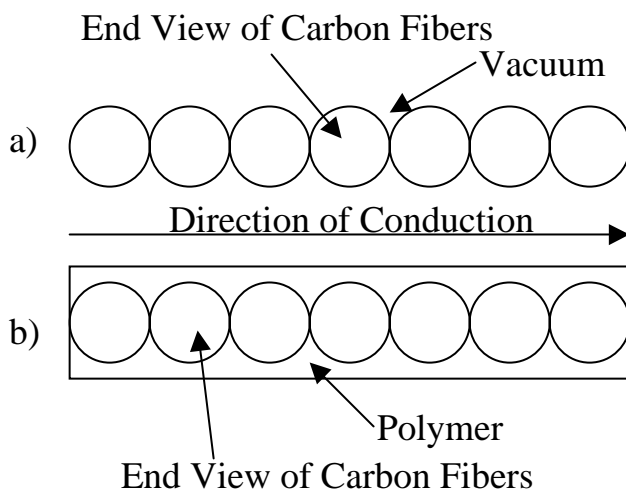
Figure 2.2-2: Fiber Configurations [(a) carbon fiber in a vacuum, (b) carbon fiber in polymer matrix]

Section 2.3: Thermal Conductivity Models

In conductive resins, there are two methods of heat transfer: lattice vibrations and electron transport. Lattice vibrations are the primary method of transfer. There are several different factors that affect the thermal conductivity of a composite material. These factors include the thermal conductivity of the component materials and the crystallinity of the matrix material. The size and shape of the filler particles, the concentration and dispersion (degree of mixing) of the filler particles in the matrix material, and the orientation and bonding between the filler and the matrix material are also important factors. Orientation is significant because most carbon-based fillers are anisotropic, with greatly different thermal conductivities depending on the direction of measurement.

Thermal conductivity has a numerical relationship between a composite material and its pure polymer counterpart; this relationship is similar to phenomena noted in viscosity, tensile modulus, and shear modulus. Equation 2.4 demonstrates these numerical relationships between the composite and the pure polymer [11]. This equation uses k for thermal conductivity, η for the viscosity, E for the elastic modulus, and G for the shear modulus, with the subscripts c and p representing the composite material and the pure polymer respectively.

$$\frac{k_c}{k_p} = \frac{\eta_c}{\eta_p} = \frac{E_c}{E_p} = \frac{G_c}{G_p} \qquad (2.4)$$

Section 2.3.1: Basic Thermal Conductivity Models

The most basic thermal-conductivity models start with the standard mixture rule (Equation 2.5), inverse mixture rule (Equation 2.6), and the geometric mixture rule (Equation 2.7) [17]. These equations use K for the thermal conductivity of the composite, n for the number of constituents in the composite (fillers and matrix materials), i for the index variable for the composite constituents, ϕ for the volume fraction of constituents, and k_i for the thermal conductivity of the ith constituent.

$$K = \sum_{i=1}^{n} \phi_i \cdot k_i \tag{2.5}$$

$$K = \sum_{i=1}^{n} \frac{\phi_i}{k_i} \tag{2.6}$$

$$K = \sum_{i=1}^{n} k_i^{\phi_i} \tag{2.7}$$

To estimate the composite thermal conductivity parallel to the primary filler orientation, the rule of mixtures model is often used. This model is the weighted average of the filler and matrix material conductivities weighted by the volume fractions of the constituents. The premise is that the more volume a constituent occupies in the mixture, the more its thermal conductivity will dominate the composite thermal conductivity. This model is typically used to predict the thermal conductivity of a composite with continuous fiber fillers oriented in a single direction. To estimate the composite thermal conductivity perpendicular to the primary filler orientation, the rule of inverse mixtures model is often used. The geometric mixing rule model is less commonly used.

For this research, four different types of carbon fillers were studied: carbon fibers ($\approx$3.2mm long), carbon black powder (30-100nm), graphite particles (50-300μm), and

calcined needle coke (150-600μm) were used as the conductive filler. These models will be a good starting point for study, but the discontinuous nature of the fillers will require an alteration to the models.

Section 2.3.2: Advanced Thermal Conductivity Models

There are many models currently proposed for composite systems. The basis of many of them is the Maxwell Theoretical Model. This model uses potential theory to obtain an exact solution for the conductivity of a system with spherical non-interacting particles in a continuous matrix [18]. Since most systems do not have non-interacting spherical particles, this model is not widely applicable to many composite materials without modification. The original model is detailed in Equation 2.8. This equation uses *K* for the thermal conductivity of the composite, ϕ for the volume fraction of constituents, and *k* for the thermal conductivity of the constituents. The subscript *1* indicates the properties of the pure polymer, and *2* indicates the filler properties.

$$K = k_1 \left(\frac{k_2 + 2k_1 + 2\phi_2(k_2 - k_1)}{k_2 + 2k_1 - \phi_2(k_2 - k_1)} \right) \tag{2.8}$$

Bruggeman developed another theoretical model to exactly solve for thermal conductivity using potential theory. This model is based on Maxwell's work and also addresses systems of spherical, non-interacting particles in a continuous matrix; the primary difference in the models derives from assumptions made about the permeability and field strength of the system. Equation 2.9 shows Bruggeman's model [18]. This equation uses the subscript *1* to indicate the properties of the pure polymer, and *2* to indicate the fillers properties. *K* is used for the thermal conductivity of the composite, ϕ

is used for the volume fraction of constituents, and k is used for the thermal conductivity of the constituents.

$$1 - \phi_2 = \frac{k_2 - K}{k_2 - k_1} \cdot \left(\frac{k_1}{K}\right)^{1/3}$$
(2.9)

The Hamilton and Crosser Semi-Theoretical Model has multiple applications. This model is applicable to two-phase systems, multiple-phase systems, and can take the shape of the particle into account. This model is derived from work done by Maxwell and Fricke and is shown in Equations 2.10a-b [18]. These two equations use the subscript *1* to indicate the properties of the pure polymer, *2* to indicate the particle properties, K to indicate the thermal conductivity of the composite, ϕ to indicate the volume fraction of constituents, k to indicate the thermal conductivity of the constituents, and ψ to indicate the sphericity of the particles. The sphericity of the particle is the surface area of a sphere with the same volume as the particle divided by the surface area of the actual particles. The value of ψ is between 0.58 and 1.0 for the investigated data sets [18].

$$K = k_1 \left(\frac{k_2 + (n-1)k_1 + (n-1)\phi_2(k_2 - k_1)}{k_2 + (n-1)k_1 - \phi_2(k_2 - k_1)}\right)$$
(2.10a)

$$n = \frac{3}{\psi}$$
(2.10b)

In Maxwell's model, $n = 3$. This follows from the definition of sphericity above. Hamilton and Crosser correlated large sets of data to derive and confirm Equation 2.10b [19].

McCullough proposed a general method for combining mixture rules for predicting transport properties, such as thermal conductivity, for composite systems [17]. This method uses a generalized equation in combination with traditional mixing rules and

a reference state. This generalized method is for a class of composites that show orthotropic symmetry. There are multiple different sets of equations for this model to deal with various types of composite systems; only the diffuse transport case will be discussed here. The generalized equations are found in Equation 2.11a-d. This general model is based on the standard rule of mixtures. The K_* term is the reference state that changes dependent on the composite system. K_j is the thermal conductivity in the j direction, where $j = 1$ for measurements in the longitudinal direction (the direction of greatest thermal conductivity in an anisotropic material) and where $j = 2$ or 3 for measurements in a direction transverse to $j = 1$. y_i is the shape factor; this quantity is calculated from the orientation and general shape of the particles. K_i is the thermal conductivity of the ith constituent, where 1 stands for the matrix and 2 stands for the filler. ϕ_i is the volume fraction of the ith constituent.

$$K_j = K_* + \frac{\left(\langle K \rangle - K_*\right) \cdot K_* + y_j \cdot \Delta K_1 \cdot \Delta K_2}{\left(1 - y_j\right) \cdot K_* + y_j \cdot \langle \varphi \rangle} \qquad (2.11a)$$

$$\Delta K_i = K_i - K_* \qquad (i = 1, 2) \qquad (2.11b)$$

$$\langle K \rangle = \phi_2 \cdot K_2 + \phi_1 \cdot K_1 \qquad (2.11c)$$

$$\langle \varphi \rangle = \phi_1 \cdot K_2 + \phi_2 \cdot K_1 \qquad (2.11d)$$

Using this form of McCullough's model with some rearrangement leads to the Halpin-Tsai equations [17]. In this set of equations, $K_* = K_1$. The Halpin-Tsai equations are the starting point for the derivation of the Nielsen Model. The Halpin-Tsai equations can be found in Equation 2.12a-c.

$$\frac{K}{k_1} = \frac{1 + \xi \cdot \chi \cdot \phi_2}{1 - \chi \cdot \phi_2} \qquad (2.12a)$$

$$\chi = \frac{K_2 - K_1}{K_1 - \xi \cdot K_1}$$

(2.12b)

$$\xi = \frac{1 - y_i}{y_i}$$

(2.12c)

The Nielsen model [20-21] originates from Albert Einstein's model for the viscosity of a fluid with dispersed spheres. This model was first studied with regards to viscosity, but can also be used to predict the elastic modulus of a two-phase composite. Lewis and Nielsen developed an improved model for the elastic modulus using the Halpin-Tsai equations as a starting point [21]. Nielsen made a couple of nomenclature changes while developing the model; χ became B and ξ became A. In addition, Nielsen added a value to the denominator of the primary equation and termed it ψ. This term was added to take into account the orientation and the packing of the filler in the matrix. Nielsen also changed how the A term was determined. In the Halpin-Tsai equations, the ξ term only took into account the shape of the filler; Nielsen incorporated both the orientation and shape of the filler particles into the A term.

Equations 2.13a-c comprise the Nielsen model for thermal conductivity of a two-phase system (polymer plus one filler).

$$\frac{K}{k_1} = \frac{1 + A \cdot B \cdot \phi_2}{1 - B \cdot \psi \cdot \phi_2}$$

(2.13a)

$$B = \frac{\dfrac{k_2}{k_1} - 1}{\dfrac{k_2}{k_1} + A}$$

(2.13b)

$$\psi \cong 1 + \frac{1 - \phi_m}{\phi_m^2} \cdot \phi_2$$

(2.13c)

In Equation 2.13a-c, K is the thermal conductivity of the composite and k_i is the thermal conductivity of an individual component. The subscript 1 represents the polymer matrix, and the subscript 2 represents the filler. The A parameter takes into account the geometry of the filler, with the primary factor in the geometry being the aspect ratio (length divided by diameter of the filler particle). The A parameter can be theoretically calculated by $A = 1 - k_e$, where k_e is the Einstein coefficient. The A parameter has been determined for some filler types and orientation, which are shown in Table 2.3-1 [11]. The ϕ_m term is the maximum volumetric packing fraction of the filler. Sample values for ϕ_m are located in Table 2.3-2 [11].

Table 2.3-1: Shape Factor 'A' for Common Filler Types [11]

Filler Type	Aspect Ratio	A
Cubes	1	2
Spheres	1	1.5
Random Fibers	2	1.58
Random Fibers	4	2.08
Random Fibers	6	2.80
Random Fibers	10	4.93
Random Fibers	15	8.38
Uniaxially Oriented Fibers	--	2L/D [a]
Uniaxially Oriented Fibers	--	0.5 [b]

[a] Heat flow in direction of fibers
[b] Heat flow in transverse to fiber direction

Table 2.3-2: Maximum Packing Fraction of Selected Fillers [11]

Particle Shape	Packing order	ϕ_m
Spheres	Hexagonal Close	0.7405
Spheres	Face Centered Cubic	0.7405
Spheres	Body Centered Cubic	0.60
Spheres	Simple Cubic	0.524
Spheres	Random Loose	0.601
Spheres	Random Close	0.637
Irregular	Random Close	~0.637
Fibers	Three Dimensional Random	0.52
Fibers	Uniaxial Hexagonal Close	0.907
Fibers	Uniaxial Simple Cubic	0.785
Fibers	Uniaxial Random	0.82

Progelhof et al. [22] reviewed many composite thermal-conductivity models. This review determined that the Nielsen model fit the data the best over the given data range (0 to 30 volume percent) for a two-phase system. This review studied 62-88 micron diameter glass spheres and 62-125 micron diameter magnesium oxide powder in polyethylene.

McGee and McCullough proposed an improvement to the ψ term [21], using natural silica in epoxy resin and glass spheres in epoxy and polyester resin as test systems [23]. Their improved ψ equation, shown in Equation 2.14, is significantly more complicated than the original equation, seen in Equation 2.13c. The equation again uses the subscript *1* for the pure polymer and *2* for the filler, ϕ for the volume fraction, and ϕ_m for the maximum volumetric packing fraction.

$$\psi \cong 1 + \frac{\phi_1}{\phi_m}\left[\phi_m \cdot \phi_2 + (1 - \phi_m) \cdot \phi_1\right] \tag{2.14}$$

The problem with using the Nielsen model in its present form for this research is that it was originally designed for two-phase systems. To extend the model in this form

to multiple-phase systems, one would take the polymer and one of the fillers and compute the thermal conductivity of the composite of these two materials. This composite material and another of the fillers are then used to calculate the thermal conductivity of the polymer and two filler composite, and so on until all fillers have been included in the calculations. The problem manifests when one considers the order in which the fillers are considered; depending on when fillers are added into the calculations, the end thermal conductivity of the composite varies.

Work done by Weber [24] has expanded the Nielsen model into a form more applicable for multiple-filler systems. The primary change in the system of equations occurs in Equation 2.15a, where the contributions from fillers are accounted for in a summation term. Hereafter in this text, unless specifically noted, references to the Nielsen Model will be referring to Equations 2.15a-c. McGee and McCullough's modification to the ψ term results in a modified Nielsen model. This modification, after updating the subscripts for a multiple-filler system, appears in Equation 2.15d; hereafter in this text, unless specifically noted, references to the Modified Nielsen Model will be referring to Equations 2.15a,b,d.

$$\frac{K}{k_1} = \frac{1 + \sum_{i=2}^{n} A_i \cdot B_i \cdot \phi_i}{1 - \sum_{i=2}^{n} B_i \cdot \psi_i \cdot \phi_i} \qquad (2.15\text{a})$$

$$B_i = \frac{k_i/k_1 - 1}{k_i/k_1 + A_i} \qquad (2.15\text{b})$$

$$\psi_i \cong 1 + \frac{1 - \phi_{mi}}{\phi_{mi}^2} \cdot \phi_i \qquad (2.15\text{c})$$

$$\psi_i \cong 1 + \frac{\phi_1}{\phi_{mi}} \left[\phi_{mi} \cdot \phi_i + (1 - \phi_{mi}) \cdot \phi_1 \right] \qquad \qquad (2.15d)$$

K is the thermal conductivity of the composite, and k_i is the thermal conductivity of each constituent. The subscript i represents the constituent where a subscript of 1 stands for the neat polymer matrix and greater subscripts (2, 3,…) represent the different fillers. ϕ_i is the volume fraction of the indicated filler. As in the case of the original model, Nielsen's method of choosing the A_i parameter can be found in Table 2.3-1 and the ϕ_{mi} parameter for various filler geometries can be found in Table 2.3-2.

Section 2.4: Current Bipolar Plate Technology

Numerous materials have been used in the past for bipolar plates for fuel cells. Metallic plates have been utilized but these have several disadvantages, relative to conductive resins, including higher cost and weight, and corrosion. Hence, conductive resins have been developed. Currently, thermosetting matrix materials (epoxies, phenolics, vinyl esters, etc) are used. One design uses 80 wt% synthetic graphite particles (44 to 150 microns in size) in a vinyl ester resin [13]. To produce the thermosetting conductive resins, a high weight percentage of a single type of graphite powder is mixed with a viscous ester liquid polymer and curing agents are added in a batch process. This mixture is transferred to a mold, where the resin is cured (chemical reaction occurs and a solid is formed) at elevated temperatures [10]. On the other hand, when a thermoplastic is heated, it melts (no chemical reaction occurs) and can be used again.

Thermosets have several disadvantages as compared to thermoplastics. First, relatively long molding cycle times (one minute) are needed to cure the thermosets (to allow for the chemical reaction to take place) as compared to 5 to 10 seconds for thermoplastics. Second, thermosets cannot be remelted. Thermoplastic based resins can be recycled; therefore, used plates and any scrap generated in the manufacturing process can be remelted and used to produce new bipolar plates. Third, bipolar plates made using thermosetting resins are relatively thick and heavy, adding to the volume and weight of commercial fuel cells. Thermoplastics can be formed into thinner bipolar plates. The cost of this current thermoset based technology is approximately $8 to $10/ bipolar plate. The Department of Energy has set a target of $2/bipolar plate (or $10/kW) to facilitate affordable integration of fuel cell technology into public transportation [9]. Clearly,

improvements are need.

Lately, some researchers have begun to investigate using various thermoplastic (polypropylene, polyethylene, polyphenylene sulfide, polyphenylene oxide, nylon, etc.) polymers for bipolar plates [9, 14, 17]. Conductive thermoplastics are mixed in an extruder, which can then directly go to a continuous thermoforming stamping process, which reduces manufacturing costs.

Conductive fillers that have been investigated include various carbon and graphite powders, particles, and fibers [14, 17, 19, 25]. Current technology adds as much of a single type of graphite powder as possible to achieve the needed electrical and thermal conductivity, while still allowing the material to flow into the mold [10]. These values vary depending on the specific needs of the fuel cell.

Section 2.5: References

1.	 J. R. Fried, Polymer Science and Technology. Prentice Hall, New Jersey, 1995.

2.	GE Engineering Thermoplastic Product Guide: Material Selection. GE Plastics.

3.	M. P. Stevens, Polymer Chemistry: An Introduction. Oxford University Press, New York, 1999.

4.	 D. Hansen, and G. A. Bernier, "Thermal Conductivity of Polyethylene: The Effects of Crystal Size, Density, and Orientation on the Thermal Conductivity". *Polymer Engineering and Science*, Vol. 12, No. 3, 1972, pp. 204.

5.	J-P. Issi, B. Nysten, A. Jonas, A. Demain, L. Piraux, and B. Poulaert, "Tailoring the Thermal Conductivity of Organic Materials". Thermal Conductivity 21, Plenum Press, 1990, pp 629-646.

6.	 L. Piraux, E. Ducarme, and J-P. Issi, "Thermal Conductivity of Oriented Polyacetylene Films". *Synthetic Metals*, 41-43, 1991, pp 129-132.

7.	D. W. Sundstrom and Y. Lee, "Thermal Conductivity of Polymer Filled with Particulate Solids". *Journal of Applied Polymer Science*, Vol. 16, 1972 pp 3159-3167.

8.	J. E. Parrott, and A. D. Stuckes, Thermal Conductivity of Solids. Pion Limited, London, 1975.

9.	R. Berman, Thermal Conduction in Solids. Claredon, Oxford, 1976.

10.	R. B. Bird, W. E. Stewart, and E. N. Lightfoot, Transport Phenomena. Wiley, New York, 1960.

11.	D. M. Bigg, "Thermally Conductive Polymer Compositions". *Polymer Composites*, Vol. 7, No. 3, 1986, pp. 125.

12. J-P. Issi, "Improved Materials for Thermal Management". Presentation 7-27-92, Wilmington, DE.

13. L-G. Tang, and J. L. Kardos, "A review of methods for improving the interfacial adhesion between carbon fiber and polymer matrix". *Polymer Composites*, Vol. 18, No. 1, 1997.

14. R. E. Hummel, Electronic Properties of Materials, 2nd ed. Springer-Verlag, Berlin, 1993.

15. Y. Agari, and T. Uno, "Thermal Conductivity of Polymer Filled with Carbon Materials: Effect of Conductive Particle Chains on Thermal Conductivity". *Journal of Applied Polymer Science*, Vol. 30, 1985, pp. 2225-2236.

16. Y. Agari, A. Ueda, and S. Nagai, "Thermal Conductivities of Composites in Several Types of Dispersion Systems". *Journal of Applied Polymer Science*, Vol. 42, 1991, pp. 1655-1669.

17. R. McCullough, "Generalized Combining Rules for Predicting Transport Properties of Composite Materials". *Composites Science and Technology*, Vol. 22, 1985.

18. R. C. Progelhof, J. L. Throne, and R. R. Ruetsch, "Methods of Predicting Thermal Conductivity of Composite Systems: A Review". *Tech. Pap., Reg. Tech. Conf. – Soc. Plast. Eng.*, 1975.

19. R. L. Hamilton and O. K. Crosser, "Thermal Conductivity of Heterogeneous Two-Component Systems". *I&EC Fundamentals*, Vol. 1, No. 3, 1962, pp 187-191.

20. L. E. Nielsen, "The Thermal and Electrical Conductivity of Two-Phase Systems".

I&EC Fundamentals, Vol. 13, No. 1, 1974, pp. 17-20.

21.   L. E. Nielsen, and R. F. Landel, Mechanical Properties of Polymers and Composites. 2nd ed., Marcel Dekker, New York, 1994.

22.   R. C. Progelhof, J. L. Throne, and R. R. Ruetsch, "Methods of Predicting Thermal Conductivity of Composite Systems: A Review". *Reg. Tech. Cond. – Soc. Plast. Eng*, 1975, pp. 221-257.

23.   S. McGee and R. L. McCullough, "Combining Rules for Predicting the Thermoplastic Properties of Particulate Filled Polymers, Polyblends, and Foams". *Polymer Composites*, Vol. 2, No. 4, 1981, pp. 149-161.

24.   E. H. Weber, "Development and Modeling of Thermally Conductive Polymer/Carbon Composites", Ph.D. Dissertation, Michigan Technological University, Houghton, MI, 2001.

25.   H.-J. Ott, "Thermal Conductivity of Composite Materials". *Plastic and Rubber* Processing and Applications, Vol. 1, 1981, pp. 9-24.

Chapter 3: Materials and Experimental Procedures

Section 3.1: Materials

Section 3.1.1: Matrix Materials

Section 3.1.1.1: Vectra A950RX LCP

The matrix used for this project was Ticona's Vectra A950RX Liquid Crystal Polymer (LCP), which is a highly ordered thermoplastic copolymer consisting of 73 mole % hydroxybenzoic acid (HBA) and 27 mole % hydroxynaphtholic acid (HNA). This LCP has the properties needed for bipolar plates, namely high dimensional stability up to a temperature of 250°C, extremely short molding times (often 5-10 seconds), exceptional dimensional reproducibility, chemically resistant in acidic environments present in a fuel cell, and a low hydrogen gas permeation rate [1-2]. The properties of this polymer are shown in Table 3.1-1 [1].

Table 3.1-1: Properties of Ticona's Vectra A950RX LCP [1]

Melting Point	280 °C
Tensile Modulus (1mm/min)	10.6 GPa
Tensile Stress at break (5mm/min)	182 MPa
Tensile Strain at break (5mm/min)	3.4%
Flexural Modulus at 23°C	9.1 GPa
Notched Izod Impact Strength at 23°C	95 KJ/m^2
Density at 23 °C	1.40 g/cc
Volumetric Electrical Resistivity at 23°C	10^{15} ohm-cm
Surface Electrical Resistivity	10^{14} ohm
Thermal Conductivity at 23°C	0.2 W/mK (approx.)
Humidity Absorption (23°C/50% RH)	0.03 wt%
Mold Shrinkage-parallel	0.0%
Mold Shrinkage-normal	0.7%
Coefficient. of linear thermal expansion- parallel	0.04 x 10^{-4} /°C
Coefficient. of linear thermal expansion- normal	0.38 x 10^{-4}/°C

Section 3.1.2: Filler Materials

Section 3.1.2.1: Ketjenblack

Carbon black has been used in many different industrial applications for thousands of years. Its two primary uses today are as a reinforcement material for rubber and as a pigmenting material. Approximately 90% of all carbon black produced is used for rubber reinforcement; most of the remainder is used for pigmenting (which includes fillers for polymer systems)[3].

There are two major methods through which carbon black is produced. The first method, which is also the more common of the two, is collecting the residue from the incomplete combustion of hydrocarbons. In a complete combustion of a hydrocarbon, all the carbon molecules leave the system as carbon dioxide. Incomplete combustion does not remove all the carbon molecules from the system, and the carbon residue that remains is the source of the carbon black. The second method of production is the thermal decomposition of hydrocarbons, which leaves a carbon residue as in the previous method. Table 3.1-2 shows the major categories of carbon black, the process of their production, and typical applications. The major process that is used to produce carbon black today is the furnace black process [3]. However, the quality of carbon black varies by process; two processes that produce high-quality carbon black are the acetylene and thermal decomposition processes.

Table 3.1-2: Classification of Manufacturing Processes, Feedstocks, and Uses of Carbon Black [3]

Chemical Process	Production Process	Feedstock	Uses
Thermal-oxidative decomposition			
Closed System (Turbulent flow)	Furnace black process	Aromatic oils based on coal tar or crude oil, natural gas	Tires, non-tire rubber applications, and pigments
	Lampblack process	Aromatic oils based on coal tar or crude oil	Mechanical rubber goods, electrodes, and carbon brushes
Open System (Diffusion flames)	Dequssa gas black process	Coal tar distillates	Mechanical rubber goods, electrodes, and carbon brushes
	(Channel black process) [a]	Natural Gas	Pigments
Thermal decomposition			
Discontinuous	Thermal black process	Natural Gas (Oils)	Specialty applications
Continuous	Acetylene black process	Acetylene	Electric cells and conductive and antistatic rubber and plastic applications

[a] historical process

These two processes have many similarities. They both work by thermal decomposition of a feed material in a reactor. The reactor is heated to a preset temperature while the feed stream is combusting with an air stream. When the reactor comes to temperature, the air stream is shut off while the feed stream continues to flow. At this point, the feed stops combusting to carbon dioxide and water and instead thermally decomposes to carbon black and hydrogen gas. This process continues as long as the feed stream continues to flow. The carbon black particles collect on the side of the reactor, where they begin to aggregate and form highly branched networks of molecules. The acetylene process has several advantages relative to the thermal black process. Its first advantage is that its single feed material, acetylene, allows for much higher purity

and uniformity of product. Its second advantage is that is an exothermic net reaction, meaning that once it is initiated it will continue of its own volition, with a little cooling needed to prevent a runaway reaction. In comparison, the thermal black process will function on a mix of various light hydrocarbons, but this versatility comes at the cost of a more variable product composition. Also, the thermal black process is an endothermic reaction requiring a constant heat input to maintain the reaction [3].

The carbon black used in this work is Ketjenblack EC-600 JD, produced by Akzo Nobel. Table 3.1-3 shows the properties of this material. This carbon black is a specialty product, designed for the purpose of enhancing electrical conductivity in polymer composites. It significantly reduces the electrical resistivity of a composite at a low filler loading. In work by Narkis [4], this carbon black was found to have the largest impact per volume on the resistivity. In addition, its highly branched structure, as depicted in Figure 3.1-1, allows it to contact large volumes of polymer with minimal filler loading [5].

Table 3.1-3: Properties of Akzo Nobel Ketjenblack EC-600 JD Carbon Black [5]

Electrical Resistivity	0.01-0.1 ohm-cm
Aggregate Size	20-100 nm
Specific Gravity	1.8 g/cm^3
Apparent bulk density	100-120 kg/m^3
Ash content, max %	0.1
Moisture, max %	0.5
BET Surface Area	1250 m^2/g
Pore Volume	480-510 cm^3/100g
pH	8-10
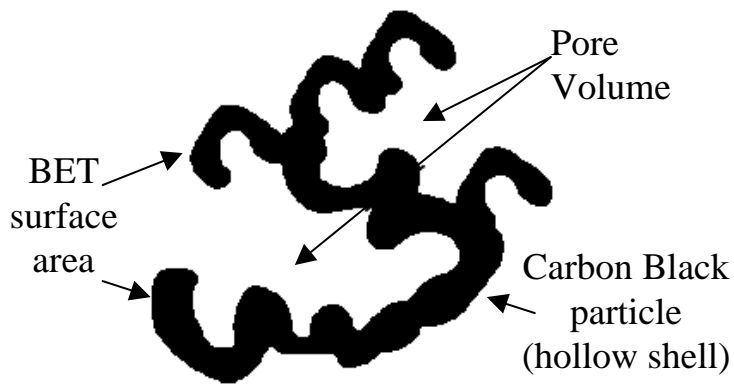
Figure 3.1-1: Carbon Black Illustration [5]

Section 3.1.2.2: Asbury Thermocarb Synthetic Graphite

Synthetic graphite can be created from any material that leaves a carbon residue

upon heating; however, the most common base material is petroleum coke [6,7]. There

are many different grades of synthetic graphite, which is graded by properties including

crystallite orientation, void fraction, size of voids, degree of graphitization, particle sizes,

and particle size distribution. This graphite is normally graphitized at a temperature

between 2500 and 3000°C in an inert atmosphere [7]. This product is intimately

dependent on the choice of feed materials, and its final form depends on the intended end

use. For polymer processing applications, the graphite is typically used in particle form.

Compared to natural graphite, formed under heat and pressure within the earth and then

mined for use, a typical synthetic graphite has the advantages of higher mechanical

strength, lower ash content and more uniform properties [7].

The synthetic graphite that was used in this project is Asbury's Thermocarb^{TM}

TC-300 Specialty Graphite [8-10]. Table 3.1-4 shows the properties of this material.

This material was used in this project due to its high thermal conductivity and its good

results in previous projects [8, 9, 11]. Figure 3.1-2 is a representative SEM micrograph

of this filler.

Table 3.1-4: Properties of Conoco's Thermocarb TC-300 [10]

Filler	Thermocarb Synthetic Graphite
Carbon Content, wt%	99.91
Ash, wt%	<0.1
Sulfur, wt%	0.004
Density, g/cc	2.24
Thermal Conductivity at 23°C, W/mK	600.
Electrical Resistivity at 23°C, ohm-cm	10^{-5}
Particle Shape	acicular
Particle Aspect Ratio	1.7
Sieve Analysis, Microns, wt%	
+600 microns	0.19
+ 500 microns	0.36
+ 425 microns	--
+300 microns	5.24
+ 212 microns	12.04
+180 microns	8.25
+150 microns	12.44
-150 microns	--
+75 microns	34.89
+44 microns	16.17
-44 microns	10.42
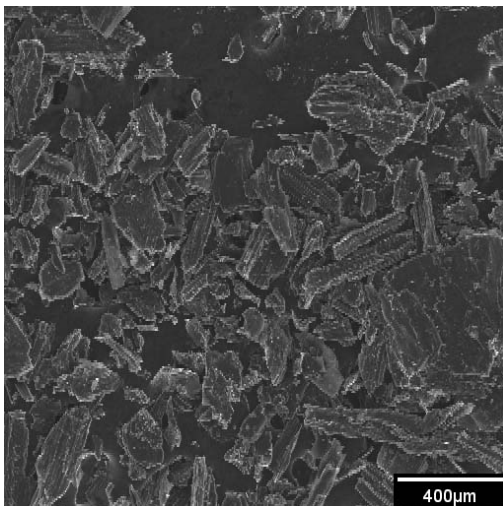
Figure 3.1-2: Thermocarb TC-300 SEM image

Section 3.1.2.3: Asbury Synthetic Graphite 4012

Synthetic graphite is manufactured by high temperature heat treatment of amorphous carbonaceous materials. The primary feed stocks used in the United States for making synthetic graphite are calcined petroleum coke and coal tar pitch, both of which contain highly graphitizable forms of carbon. The manufacturing process consists of various mixing, molding, and baking operations, followed by heat-treating to temperatures between 2500°C and 3000°C. This high temperature is needed to drive the carbon from an amorphous phase to a graphitic phase. The high temperate also helps in burning off impurities that may have been present in the carbon, including metal oxides, sulfur, nitrogen, hydrogen, and all organic components that were part of the original petroleum or coal tar pitch [12]. Table 3.1-5 [10] lists the important properties of this material. Figure 3.1-3 is a representative SEM micrograph of this filler.

Table 3.1-5: Properties of Asbury Synthetic Graphite 4012 [10]

Filler	4012 Synthetic Graphite
Carbon Content, wt%	99.67
Ash, wt%	<0.5
Sulfur, wt%	<0.1
Density, g/cc	2.24
Thermal Conductivity at 23°C, W/mK	600. (approx.)
Electrical Resistivity at 23°C, ohm-cm	10^{-5}
Particle Shape	acicular
Particle Aspect Ratio	1.7
Sieve Analysis, Microns, wt%	
+180 microns	0.22
+150 microns	0.86
-150 microns	--
+75 microns	71.65
+44 microns	24.43
-44 microns	2.82
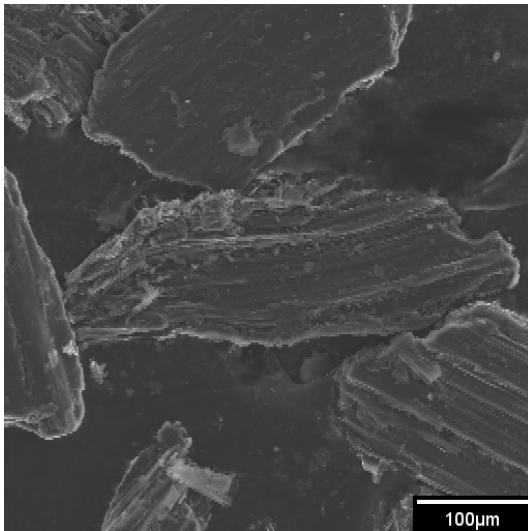
Figure 3.1-3: Asbury Synthetic Graphite 4012 SEM image

Section 3.1.2.4: Asbury Natural Flake Graphite 3160

Flake graphite is a naturally occurring form of graphite. It naturally occurs as discrete flakes with diameters of 50 – 800 microns and thicknesses of 1 – 50 microns thick. Natural flake graphite displays a very high degree of crystallinity; this translates to physical properties of low void fraction, excellent thermal and electrical conductivities, and enhanced molding properties [12]. Table 3.1-6 [10] lists the important properties of this material. Figure 3.1-4 is a representative SEM micrograph of this filler.

Table 3.1-6: Properties of Asbury Natural Flake Graphite 3160 [10]

Filler	3160 Natural Flake Graphite
Carbon Content, wt%	99.30
Ash, wt%	0.7
Sulfur, wt%	<0.1
Density, g/cc	2.24
Thermal Conductivity at 23°C, W/mK	600 (approx.)
Electrical Resistivity at 23°C, ohm-cm	10^{-5}
Particle Shape	flake
Particle Aspect Ratio	4.8
Sieve Analysis, Microns, wt%	
+180 microns	1.9
+150 microns	9.7
-150 microns	--
+75 microns	50.4
+44 microns	21.6
-44 microns	16.4
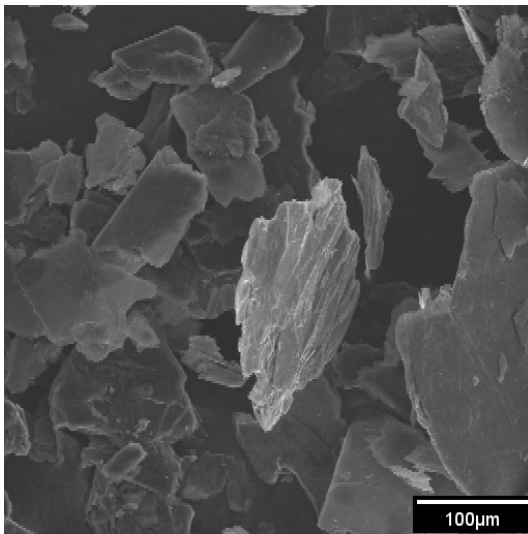
Figure 3.1-4: Asbury Natural Flake Graphite 3160 SEM Image

Section 3.1.2.5: Asbury Calcined Needle Coke F108A

Calcined needle coke is a variety of petroleum coke. It is called needle coke in reference to its structure; it is commonly found as needle-like structures that are clearly visible without magnification and rises from the liquid-crystalline alignment that occurs during the coking procedure. The high degree of orientation is consistent with feedstocks of high aromaticity. Calcined needle coke is typically higher in carbon and lower in ash constituents, such as sulfur and metals, than standard calcined petroleum coke [12]. Table 3.1-7 [10] lists the important properties of this material. Figure 3.1-5 is a representative SEM micrograph of this filler.

Table 3.1-7: Properties of Asbury Calcined Needle Coke F108A [10]

Filler	Calcined Needle Coke F108A
Carbon Content, wt%	99.10
Ash, wt%	0.3
Sulfur, wt%	0.5
Density, g/cc	2.1
Thermal Conductivity at 23°C, W/mK	10 to 20 (approx.)
Electrical Resistivity at 23°C, ohm-cm	10^{-3} (approx.)
Particle Shape	Acicular
Particle Aspect Ratio	2.3
Sieve Analysis, Microns, wt%	
+600 microns	0.13
+ 500 microns	--
+ 425 microns	4.16
+300 microns	19.05
+ 212 microns	42.84
+180 microns	17.56
+150 microns	10.64
-150 microns	5.62
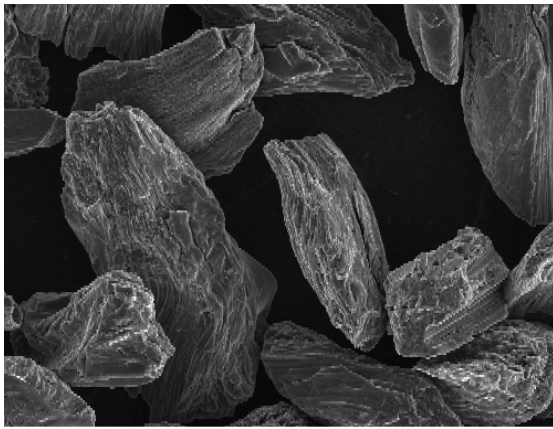
200µm

SEI Filler E 160x

Figure 3.1-5: Asbury Calcined Needle Coke F108A SEM Image

Section 3.1.2.6: Fortafil 243 Carbon Fiber

Akzo Nobel's Fortafil 243 polyacrylonitrile (PAN) based 3.2 mm chopped, surface treated and pelletized carbon fiber was also used to improve the electrical and thermal conductivity of the resin. A proprietary polymer was used as a binder for the pellets that also promoted adhesion with nylon. Table 3.1-8 [13] lists the properties for these fibers. Figure 3.1-6 is a representative SEM micrograph of this filler.

Table 3.1-8: Properties of Akzo Nobel Fortafil 243 PAN based 3.2mm Chopped and Pelletized Carbon Fiber [13]

Tensile Strength	3800 MPa
Tensile Modulus	227 GPa
Electrical	16.7 μohm -m
Thermal	20 W/m K (axial direction)
Bulk Density	356 g/liter
Fiber Diameter	7.3 microns
Filament Shape	Round
Fiber Mean	3.2 mm (entire range is 2.3 mm to 4.1 mm)
Carbon Assay	95%
Binder Content	2.6 wt% proprietary polymer that adheres pellet together and promotes adhesion with nylon matrix
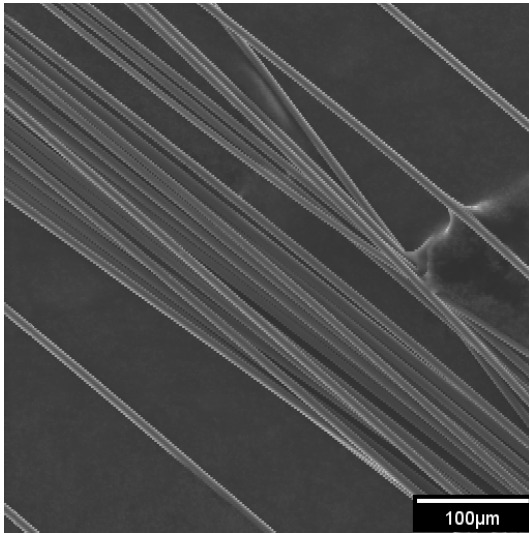
Figure 3.1-6: Fortafil 243 Carbon Fiber SEM Image

Section 3.2: Experimental Design

The experiment was designed in two stages. Stage one was the filler screening stage, where various graphite carbon particles and calcined needle coke could be compared to each other to determine the best one to use for further experimentation. In the screening stage for the graphite and calcined coke particles, loading levels were set at 40, 60 and 70 weight percent (wt%). The carbon black loading levels were set at 2.5, 4, 5, 6, 7.5, 10 and 15 wt%.

The naming convention used for this work is shown below:

EuVwx-y-z

Where:

E = the project description (E = DOE)

u = Filler type (A = carbon black, B = synthetic graphite particles, H= milled pitch-based carbon fiber)

V = Matrix polymer (V for Vectra)

w = Replicate or original (none for original, R for replicate, RR for second replicate, etc.)

x = Weight percent of filler added (5, 10, 15, …)

y = Specimen type (F for flex, T for tensile, TC for thermal conductivity disks)

z = Specimen number

Section 3.3: Methods

Section 3.3.1: Fabrication Methods

Section 3.3.1.1: Drying

For this entire project, the fillers were used as received (not dried). The Vectra A950RX LCP was dried in a Bry Air System indirect heated dehumidifying dryer (dew point of recirculating air = -40°) at ambient temperature. Approximately 300 pounds of Vectra was dried in 20 pound batches at 302°F for 24 hrs. Figure 3.3-1 illustrates the Bry Air dryer used. After drying, the polymer was stored in moisture barrier bags.

Figure 3.3-1: Bry Air Dryer

Section 3.3.1.2: Extrusion

An American Leistritz Extruder Corp. Model ZSE27 27mm co-rotating intermeshing twin-screw extruder was used to create the composite materials for this work. This extruder has a length to diameter ratio of 40:1 with ten independent heating

zones and a water-cooled feed port. An image of the extruder is shown in Figure 3.3-2.

The screw design used for the extrusion runs was chosen with the primary goals of

producing a uniformly mixed composite while minimizing the degradation of the filler.

A diagram of this design can be found in Section 9.1.

Referring to the ten temperature control zones of the extruder, Zone 1 contains the

main feed port where the polymer is always added. This zone is water cooled so the

polymer does not melt and plug the feed port. The polymer is fed by an AccuRate low

range Flexwall gravimetric feeder; an image of this feeder is shown in Figure 3.3-3.

Zones 2 and 3 are closed. Zone 4 is back-vented to the atmosphere allowing for gases

that may have been evolved from melting the polymer, or vapors or gases from the filler

feed in zone 5, to escape. The first side stuffer is located in Zone 5. All fillers used in

this work were added in this zone. Zone 6 is closed, and Zone 7 contains the second side

stuffer (not used in this work). Zone 8 is another closed zone. Zone 9 was vented to the

atmosphere for this work, but it can be set up to pull a vacuum. Zone 10 is another

closed zone. The nozzle used for this project had three 3mm holes through which the

composite material was forced. The nozzle also had a pressure and temperature sensor to

measure properties of the exiting stream.

The side stuffer located in Zones 5 was fed by AccuRate Conisteel loss in weight

feeders. An image of the Accurate Conisteel feeder can be seen in Figure 3.3-4.
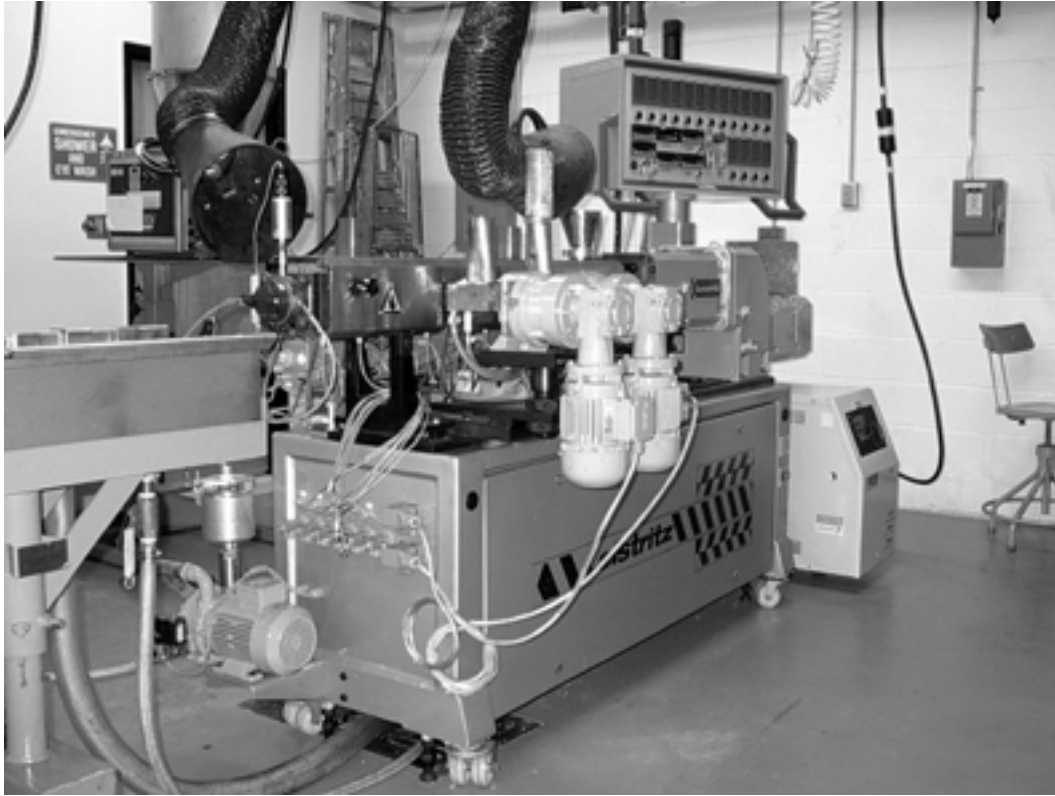
Figure 3.3-2: 27mm Twin Screw American Leistritz Extruder

Figure 3.3-3: AccuRate Flexwall Feeder

Figure 3.3-4: AccuRate Conisteel Feeder

An important element in the extrusion process is the screw design used. This design can have a significant effect on the mixing and degradation of the fillers, which in turn can have a significant effect on the mechanical, thermal and electrical properties of the composites. The screw designs used for this work include screw elements for conveyance and pressure control of the melt and kneading elements for mixing the polymer and filler in a uniform fashion. Over the course of this work, two different screw designs were used, both of the same basic design. Diagrams of the screw designs can be found in Section 9.1. The first three elements in the design were screw elements to convey the polymer pellets into the heating zones and pressurize the melting polymer. The next six elements in this design were kneading elements; four blocks with an increasingly steep thread angle to mix the polymer more and more vigorously as it passes down the extruder and two disks to continue the mixing as the molten polymer approached the first filler entry zone. The next three screw elements were conveyance elements, the first two to elongate the polymer flow and allow an air gap for filler addition and offgas flow and the third to increase the polymer pressure into the next elements.

The next two elements were kneading blocks to integrate the newly added filler into the molten polymer matrix. The two subsequent elements were screw elements; as before, they elongated the flow to allow for introduction of filler at the second side-stuffer and then recompressed the polymer flow for the last set of kneading elements. The next three elements were kneading blocks to integrate the newly added filler into the existing polymer system. The last three elements were screw elements; the first one

elongated the melt one last time to allow vapors to escape before the final two compressive elements forced the melt out of the nozzle.

The three molten strands were forced into the water bath upon leaving the extruder. The composite strands were removed from the water bath while still hot, allowing most of the water to evaporate off. For most composite formulations, no more than two or three feet of the water bath were used. Most of the remaining water was then removed with an air knife. The air stream from the air knife blew directly on the extruder; therefore, a plastic shield was used. The shield minimized the movement of the fillers and the cooling of the extruder. The water bath was 10 ft long, with the air knife located at the end opposite the extruder. After the composite strand passed through the air knife, the strands were pelletized by a ConAir Model 20402HP-14A strand pelletizer. An image of the pelletizer and water bath can be seen in Figure 3.3-5.

Figure 3.3-5: Water Bath and Pelletizer

For each composite formulation, typically ten pounds of pelletized material was produced. The conditions for each extrusion run performed can be found in Section 9.2.

These wet pellets were dried prior to injection molding in vacuum ovens at 302°F for 20 to 24 hours in the Bry Air drier and subsequently stored in moisture barrier bags [14].

Section 3.3.1.3: Injection Molding

For this project, a 4.55 ounce polystyrene shot size Niigata injection-molding machine, model NE85UA$_4$, was used [15]. An image of the injection molder can be seen in Figure 3.3-6. This machine has a 40 mm diameter single screw with a length over diameter ratio of 18:1. The lengths of the feed, compression, and metering sections of the single screw are 396 mm, 180 mm, and 144 mm, respectively. This machine has a maximum injection pressure of 22,610 psig, a maximum screw speed of 320 rpm, and a maximum clamp force of 82.5 US tons. The injection-molding process was completed in full automatic mode. Deltatherm was used to control the temperature of the mold at 190°F [16]. A four-cavity mold was used to injection mold 2.5" diameter by 1/8" thick disk, and 6.5" long by 1/8" thick ASTM tensile bars (end gated only) and 5" long by 1/8" thick by 0.5" wide flex bars [17]. An image of the four-cavity mold can be seen in Figure 3.3-7. A feed hopper dryer was not used although every effort was made to ensure that the dried polymer pellets were exposed to atmospheric conditions for less than one hour. Section 9.3 lists the injection molding conditions for each composite formulation. Zone 4 is the heated zone nearest the feed hopper and zone 1 is the die nozzle heater.

Figure 3.3-6: Niigata Injection Molding Machine
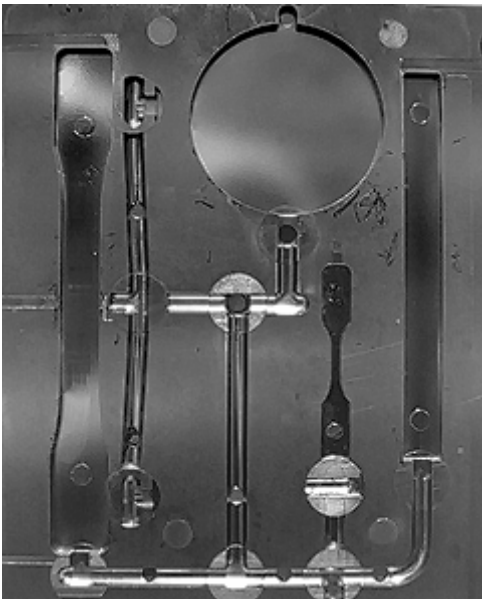
Figure 3.3-7: Four-Cavity Mold

The following procedure was used for the injection molding of the composites [18].

1. The machine was brought up to correct operation temperature for the material to be run. Then Vectra A950RX LCP was run to purge out all of the material that might have been in the injection-molding machine previously.

2. Approximately 4 lbs. of each dried formulation were injection molded into 30 tensile bars, flex bars and 2.5" disks. Conditions were kept as constant as possible, and would only be changed if operational problems were encountered. The only parameter that was changed for every composite formulation was the shot size. This was changed in small increments until a very small amount of flash was present showing that the mold was completely full. The generated samples were stored in low-density polyethylene (LDPE) bags.

3. Once all samples for one formulation were injection molded, the injection-molding machine was operated until it could not fill another shot. The next formulation was then added to the hopper and the next five shots were thrown out as being transition material. During this time, the shot size was optimized for the new material. Once this process was completed, the new composite formulation samples were collected as described in step 2.

4. At the end of each day, the pure polymer was run through the machine until the melted polymer had no more carbon in it. Then polypropylene was used to purge out the high temperature polymer. Polypropylene was also run until the carbon was removed from the injection-molding machine.

Section 3.3.2: Test Methods

Unless specifically mentioned otherwise, all samples tested by the following test methods were conditioned at 50% relative humidity and room temperature for 88 hours prior to testing in accordance with ISO 291 [19].

Section 3.3.2.1: TCA Analysis (Transverse Thermal Conductivity) (ASTM F433-98)

Transverse thermal conductivity of an 1/8" thick by 2" diameter disc-shaped test specimen was measured at 55°C using a Holometrix Model TCA-300 Thermal Conductivity Analyzer, which uses the guarded heat flow meter method (ASTM F433-98) [20-21]. Figure 3.3-8 illustrates this test method, and an image of the equipment can be seen in Figure 3.3-9. The estimated accuracy of this test method is ± 3% [21].
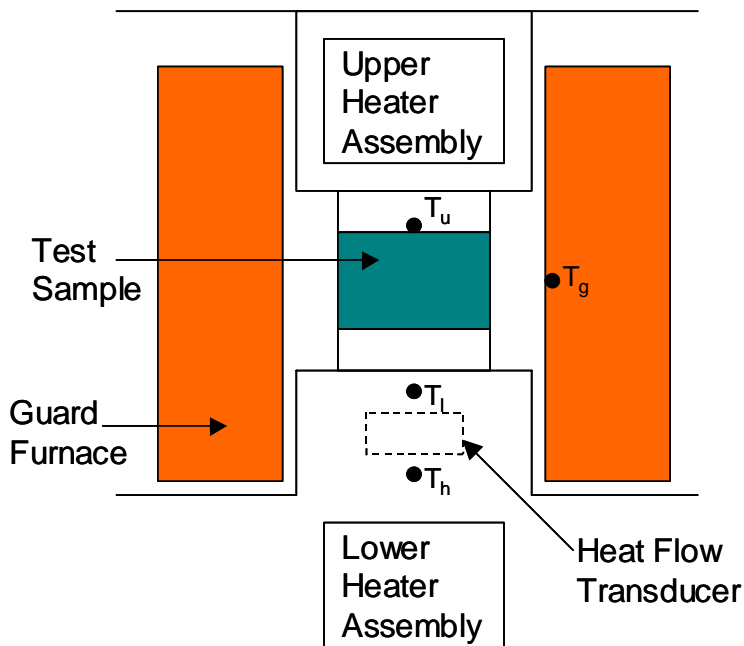
Where:
   T_g = Guard Temperature
   T_u = Upper Heater Assembly Temperature
   T_l = Lower Heater Assembly Temperature
Figure 3.3-8: Diagram of Thermal Conductivity Test Method [21]

Figure 3.3-9: Image of TCA 300

To prepare these samples, the 63.5mm diameter injection molded disks were cut to 50.8mm diameter disks using a water jet cutter. The complete results for each test specimen can be found in Section 9.4.

Section 3.3.2.2: HotDisk Analysis (Specific Heat, Transverse / Longitudinal Thermal Conductivity)

The Mathis Instruments Hot Disk Heat Capacity Cell is a device for measuring the specific heat of a composite material. Three disks, 25mm in diameter and 3.2mm thick, are stacked in an insulated copper cup. A known amount of power is run through the cup for a given time. The change in resistivity of the nickel in the sensor attached to the cup allows for measurement of the temperature rise which, when compared to the data for an empty sample sup, allows for calculation of the specific heat of a compound. Results for specific heat testing can be found in Section 9.5.

The Mathis Instruments Hot Disk Thermal Constants Analyser is an emerging technology that can measure the in-plane and through-plane thermal conductivity of an

anisotropic material in the same test, using the transient plane source technique [22-26].

The sensor used in this test method consisted of a 10 μm thick nickel foil embedded

between two 25.4 μm thick layers of Kapton polyimide film. The nickel foil was wound

in a double spiral pattern with a radius R of 3.189 mm. The thermal conductivities were

measured at 23°C.

Figure 3.3.10 shows how the sensor is positioned between two samples of

composite material. In this experiment, the samples tested were composite disks of

diameter $D = 63.5$ mm and thickness $T = 3.18$ mm. To help ensure that the assumption of

an infinite sample domain was met and that heat was not penetrating completely through

the sample in the axial direction, two of these composite disks were stacked together

above the sensor and two were stacked below it, giving us a sample of double thickness.

This stacking of disks allowed the generation of more reproducible data.

The sensor then had a constant electrical current (variable by sample from 0.03W

– 1.25W) over a short period of time (variable by sample from 2.5s – 40s) passed through.

The generated heat dissipated within the double spiral was conducted through the Kapton

insulating layer and into the surrounding sample, causing a rise in the temperature of the

sensor and the sample.
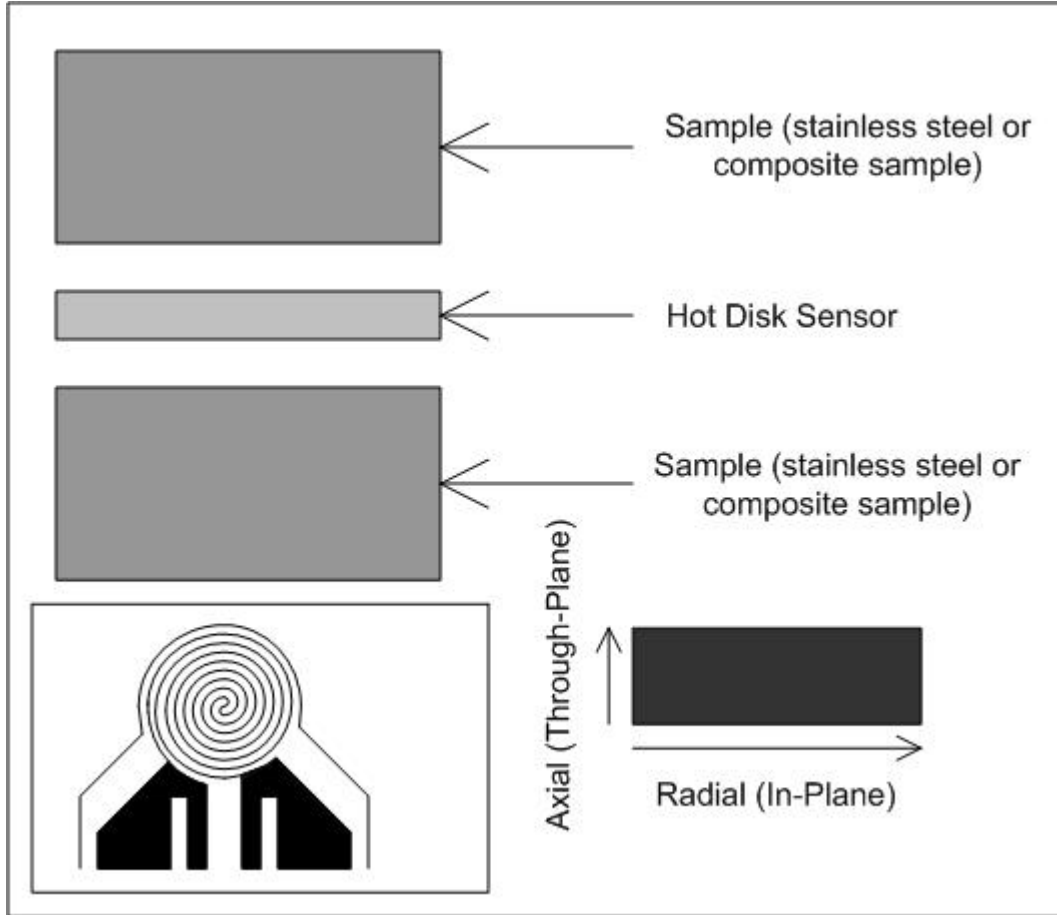
Figure 3.3-10: Schematic of Samples and Sensor. The inset at the lower left shows the double spiral heating element.

From a theoretical standpoint, the double spiral pattern can be approximated as a series of concentric, equally spaced ring sources. The characteristic heat conduction equation, assuming radial symmetry in the sample, is then given as:

$$\left(\rho C_p\right)\frac{\partial T}{\partial t} = k_{in}\frac{1}{r}\left(\frac{\partial}{\partial r}\left(r\frac{\partial T}{\partial r}\right)\right) + k_{thru}\frac{\partial^2 T}{\partial z^2} + \sum_{rings}Q_r\delta(r-r')\delta(z) \tag{3.1}$$

where ρ is the density of the sample (kg/m^3), C_p is the heat capacity of the sample (J/(kg•K)), T is the temperature of the sample (K), t is the time of the measurement (s), k_{in} and k_{thru} are the in-plane and through-plane thermal conductivities of the sample (W/m•K), δ is the Dirac delta function, r' is the radius of one of the ring sources, and Q_r

is the power supplied to that ring per unit length of the ring (W/m). The total power for each ring is proportional to the circumference of the ring $2\pi r'$, such that the total power supplied for all of the rings is Q (W). This total power Q is an input parameter to the Hot Disk Thermal Constants Analyser. The first term in Equation 3.1 represents accumulation of thermal energy, the second term radial (referred to as in-plane in our experiments) heat conduction, the third term axial (referred to as through-plane in our experiments) heat conduction, and the final term is a heat source.

The sample can be approximated as an infinite domain if the experimental time is much less than the characteristic thermal diffusion time. For an anisotropic material in a cylindrical geometry, the experimental time must meet the following two criteria: $t \ll (D/2)^2 /(\alpha_{in})$ and $t \ll T^2 /(\alpha_{thru})$. In these formulas $\alpha = k/(\rho C_p)$, which is the thermal diffusivity of the composite material.

The average transient temperature increase of the sensor is simultaneously measured by recording the change in electrical resistance of the nickel sensor [22-26] according to:

$$\Delta T = \frac{1}{\beta}\left(\frac{R_n}{R_{no}} - 1\right) \tag{3.2}$$

where: ΔT is the change in temperature at time t (K), β is the temperature coefficient of resistance (TCR) of the material (1/K), R_n is the electrical resistance of the nickel at time t (Ω), and R_{no} is the electrical resistance of the nickel at time 0 (Ω). The temperature rise in Equation 3.2 is correlated with the in-plane and through-plane thermal conductivities through the solution of Equation 3.1 as:

$$\Delta T = \frac{P}{\pi^{3/2} R \sqrt{k_{in} k_{thru}}} F(\tau) \tag{3.3}$$

where $F(\tau)$ is a dimensionless time dependent function of $\tau = \sqrt{\alpha_{thru} t / R^2}$ given by an

integral of a double series over the number of rings m:

$$F(\tau) = [m(m+1)]^{-2} \int_0^\tau \sigma^{-2} \left[\sum_{l=1}^m l \sum_{k=1}^m k \exp\left(-\frac{l^2 + k^2}{4m^2 \sigma^2} \right) I_0\left(\frac{lk}{2m^2 \sigma^2} \right) \right] d\sigma \tag{3.4}$$

A more detailed derivation of Equations 3.3 and 3.4 is given by He [27]. The complete

results for the through-plane and in-plane thermal conductivity of each test specimen can

be found in Section 9.6.

The results of this testing, described more fully in chapters 5 and 6, revealed the

following relationship between thermal conductivity and volume fraction of filler:

$$\sqrt{k_{in} k_{thru}} = A e^{B\phi} \tag{3.5}$$

'k_{in}' stands for the in-plane thermal conductivity, 'k_{thru}' stands for the through-plane

thermal conductivity, 'ϕ' stands for the volume fraction of filler in the sample, and A and

B are system-dependent parameters.

Section 3.3.2.3: Density (ASTM D792-98)

The density of specimens from all formulations was determined using ASTM

D792-98, density of plastics by water displacement [28]. The injection-molded parts

were first weighed while dry. The samples were then weighed while submerged in water.

The temperature of the water was noted as well. From these three pieces of data, the

density of the sample was calculated using Equation 3.5. The density was measured on

the thermal conductivity disks after they were tested. The theoretical density was also

calculated for each composite formulation using Equation 3.6. The results for each

sample can be found in Section 9.7. In these equations, 'ρ_i' is the density of the

constituents, ϕ_i is the volume fraction of the constituents, and 'ρ_{Theo}' is the calculated

theoretical density.

$$\rho = \frac{DryWeight}{DryWeight - WetWeight} \cdot \rho_{Water}(T) \tag{3.5}$$

$$\rho_{Theo} = \frac{1}{\sum_i \frac{\phi_i}{\rho_i}} \tag{3.6}$$

Section 3.3.2.4: Solvent Digestion (ASTM D5526-98)

Solvent digestion was used to liberate the fillers from injection-molded parts. The

ASTM D5226-98 [29] method was followed to digest the polymers. The liberated fillers

were used to determine the length and aspect ratio of the fillers after being processed. A

0.2g sample was obtained from the scraps of each transverse thermal-conductivity sample

after they were tested and subsequently cut for use in determination of orientation

discussed in Chapter 3.3.3. This resulted in three solvent digestion samples being run for

each composite formulation.

The solvent digestion procedure is described in the following paragraphs. The

0.2g composite sample was placed in a 2 ounce glass vial with a polytetrafluoroethylene

lid. The sample identification was recorded on the side of the vial. The vials were filled

approximately halfway with diethylenetriamine (DETA). The exact amount of solvent is

not critical since the solvent was pulled through the filler and disposed of in a manner

consistent with regulations. The only constraint on the amount of solvent used is that it

be enough to completely dissolve the 0.2g samples. The samples were allowed to soak in

the solvent until the entire polymer matrix was completely dissolved. These samples

took between four to six hours to dissolve at a minimum temperature of 170°C.

While the samples were dissolving, the filter papers and Petri dishes were

weighed separately using a four-place Denver Instruments A-250 scale and the weights

subsequently recorded. The Petri dishes were labeled to ensure the correct filters were

used for each sample. The filters used were 0.45 μm pore size modified polyvinylidene

fluoride filters produced by Millipore and named Durapore® membrane filters. All

samples used only one filter.

For all steps in this process where a solvent was being used, the proper personal

protection equipment was used (safety glasses, polyurethane gloves, lab coat, long pants,

and closed toed shoes). In addition, all steps that used a solvent were carried out in a

fume hood to minimize exposure to vapors from the solvents.

Once the matrix was completely dissolved, the polymer/filler/solvent solution was

filtered. This was carried out using the apparatus seen in Figure 3.3-11. The apparatus

contained a Fisher Brand 47mm microanalysis filter assembly, vacuum flask, and

vacuum pump. The pre-weighed filter paper was placed in the filtration assembly, and

the shaken solution was poured on the filter. The vacuum pulled the solvent and

dissolved matrix through the filter leaving the filler on the filter paper. The vial and

funnel were rinsed with solvent, to make sure that all of the filler was on the filter paper.

The vacuum was kept on until all standing liquid was removed from the samples. The

filter paper and filler were placed in the pre-weighted and labeled Petri dishes. The Petri

dishes were left open and placed in a hood overnight to allow the remaining solvent to

evaporate. It was quickly found in this process that carbon black would immediately

plug the filter; therefore, only composites filled with carbon fiber and synthetic graphite particles could be run. Once the samples were completely dried, the Petri dish containing the filter paper and filler were weighed.
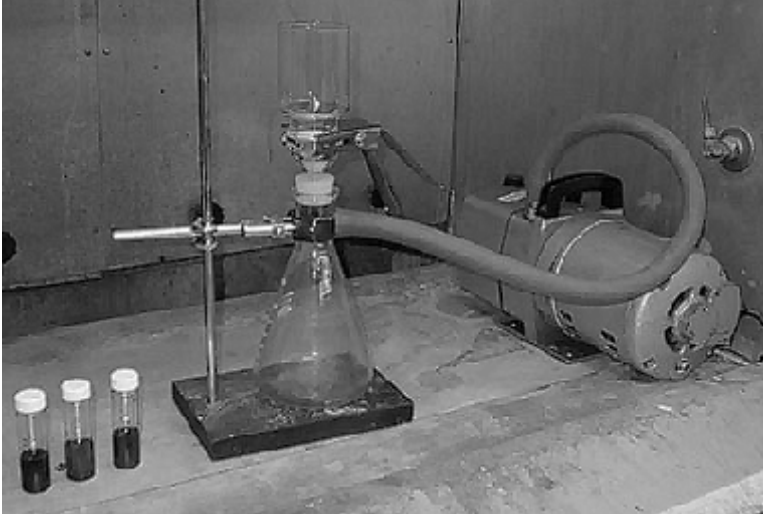
Figure 3.3-11: Solvent Digestion Filtration Apparatus

The weight percent filler was calculated using Equation 3.7.

$$wt\% = \frac{Wt_{Final} - W_{Filter(s)} - W_{PetriDish}}{W_{Composite}}$$

(3.7)

Section 3.3.2.5: Filler Length and Aspect Ratio

The filler liberated from the composites was used to determine the filler length and aspect ratio that was in the injection molded samples. Solvent digestion produced three samples of liberated fibers per formulation. The as-received fillers were also measured to see how the material changed due to extrusion and injection molding.

A diagram of the apparatus used to disperse the fillers can be found in Figure 3.3-12. The filler from each sample was removed from the filter paper using a micro-spatula. Using the micro-spatula, a small amount (typically about 0.01 g) of the filler was placed in the crucible while the one-hole stopper was removed. The amount was small enough

so that a large number of particles were not overlapping in the images. The apparatus was prepared to disperse the filler by replacing the one-hole stopper and placing the flask over the glass slide on the cleaned surface. The fiber was dispersed onto the glass slide using a short burst from a duster can that contained 1,1,1,2-tetrafluoroethane. The nozzle of the duster was placed through the stopper but not into the crucible. Care was taken to clean the apparatus and surface on which the slide was placed between each run.
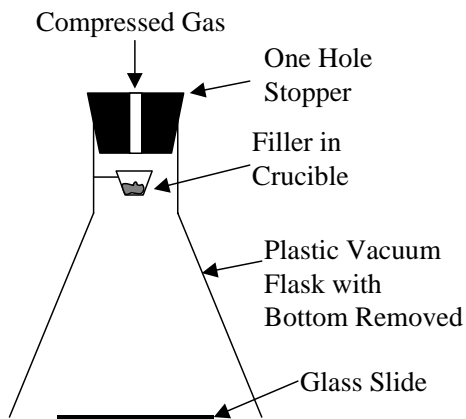
Figure 3.3-12: Fiber Dispersion Apparatus

The glass slide with the dispersed filler was placed on a Prior automatic stage for the microscope setup. An image of this setup can be seen in Figure 3.3-13. The microscope used for the imaging was an Olympus SZH10 optical microscope with an Optronics Engineering LX-750 video camera for digital imaging. The images were collected using an automated series of steps (macro) in Scion Image version 1.62. The macro that was used was originally written by Dr. Larry Sutter and it was modified for this project. All images were collected at 60x magnification.
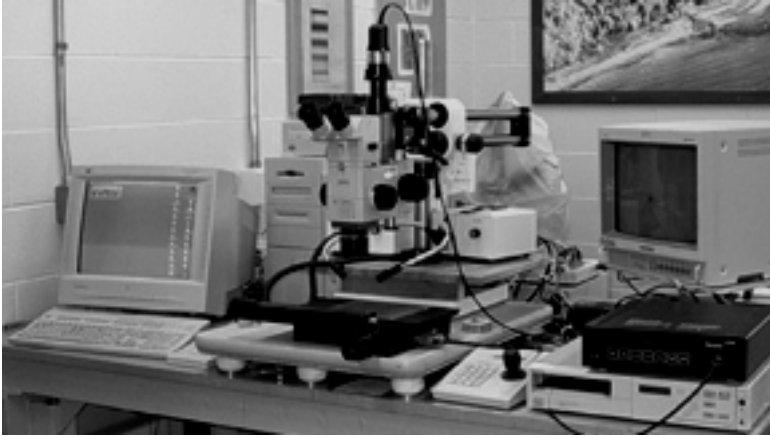
Figure 3.3-13: Image of Microscope Setup used for Filler Length and Aspect Ratio

The resulting images were processed and measured using the academic version of Adobe Photoshop 5.0 and a package of filters called The Image Processing Tool Kit (version 3.0). An action was created so the batch operation could be used for the processing of the images, since between 20 and 85 images were collected for each sample examined. The action contained the following steps:

1. Convert image from RGB to grayscale

2. Fit and remove the background to remove the uneven lighting of the image

3. Automatic leveling of the image, which standardizes the contrast of the image

4. Threshold, this converts the image to a binary image in which all the fillers are in black

5. Feature cutoff and threshold, this removed all the features that came in contact with the edge of image

6. Calibrate, this loaded a predetermined calibration based on the magnification and resolution of the image

7. Measure all, this measured 26 different items of each feature in the image and stored them in a text file that was appended to for each new image

This process was used for all single filler samples. Between 1000 and 6000 particles were measured for each sample.

The length and aspect ratio were measured using an algorithm that measured the maximum and minimum caliper distance of each feature. The caliper length and height of the feature was measured every 11.25°, from this the maximum (length) and minimum (breath) caliper distance were calculated. The aspect ratio is calculated by dividing the length by the breath. This method worked well for all particles except for ones that are long and thin; then it measured only the length accurately. The inaccuracy in the breath measurement comes from the fact that the measurement is made only every 11.25° and the chances of getting the exact smallest dimension of the particle is highly improbable. This issue is compounded by the particle being long so a small deviation will make the particle breath appear even larger. This difficulty led to dividing the length of the fibers by literature diameter to produce the aspect ratio.

Section 3.3.3: Determination of Particle Orientation in the Composite

Section 3.3.3.1: Sample Preparation

Four 0.5" by 0.5" squares were cut out of the center of each of the thermal conductivity samples to generate the through-plane samples studied. Three portions of matchsticks used in ER testing were used to generate the in-plane samples studied. The epoxy mixture was carefully poured over the samples, and they were carefully pushed down. The epoxy used, Epoxide Cold Mounting Resin and Hardener, was a two-part epoxy purchased from Mager Scientific. The epoxy was mixed by weight in a five parts

resin to one part hardener ratio. The epoxy plugs were allowed to cure overnight at room temperature and were subsequently removed from the sample holders.

Section 3.3.3.2: Polishing

After curing, the epoxy plugs were polished using a multi-step process. The polishing was done using a Buehler Ecomet 4 Grinder/Polisher with an Automet 2 Power Head. A ten-sample holder was used to hold the samples. An image of this apparatus can be seen in Figure 3.3-14. The samples were washed in an ultrasonic bath after each polishing step to remove the polishing media. The procedures that were used for polishing are shown in Tables 3.3-1 and 3.3-2. These processes were developed by Buehler's technical service department [30-31]. The process as described in Table 3.3-1 was used on all formulations except for the EHV family.

Figure 3.3-14: Polishing Apparatus

Table 3.3-1: Polishing Procedure [30]

	Polishing Media	Time	RPM	Polishing Cloth	Direction	Force Per Sample	Lubricant
1	320 Grit SiC	30 sec	250	None	Contra	4 lbs.	Water
2	9 μm Mono Crystalline Diamond	4 min	150	Ultra-Pol™*	Contra	5 lbs.	None
3	3 μm Mono Crystalline Diamond	4 min	120	Texmet® 1000*	Co-Current	6 lbs.	None
4	0.05μm Deagglomerated Alumna Suspension	3 min	120	Mastertex®*	Contra	3 lbs.	None

Table 3.3-2: Polishing Procedure [31]

	Polishing Media	Time	RPM	Polishing Cloth	Direction	Force Per Sample	Lubricant
1	240 Grit SiC	15 min	250	None	Contra	5 lbs.	Water
2	320 Grit SiC	55 min	250	None	Contra	5 lbs.	Water
3	400 Grit SiC	70 min	250	None	Contra	5 lbs.	Water
4	600 Grit SiC	45 min	250	None	Contra	5 lbs.	Water
5	800 Grit SiC	45 min	250	None	Contra	5 lbs.	Water
6	3 μm Mono Crystalline Diamond	30 min	120	Texmet® 1000*	Comp	5 lbs.	Green Solution
7	0.05μm Deagglomerated Alumna Suspension	20 min	120	Mastertex®*	Comp	4 lbs.	White Solution

Section 3.3.3.3: Optical Imaging Methods

The polished samples were imaged using an Olympus BX60 microscope at 100x and 200x magnification. An image of the microscope can be seen in Figure 3.3-15. The images were collected using Scion Image Version 1.62. The images were taken across

the thickness of the sample, which was the direction of conduction that was measured in

the transverse thermal-conductivity test. These images were pieced together to get a

large composite image for analysis.
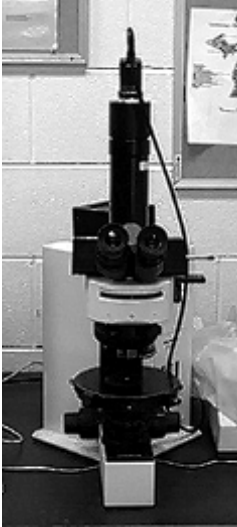
Figure 3.3-15: Olympus BX60 Microscope
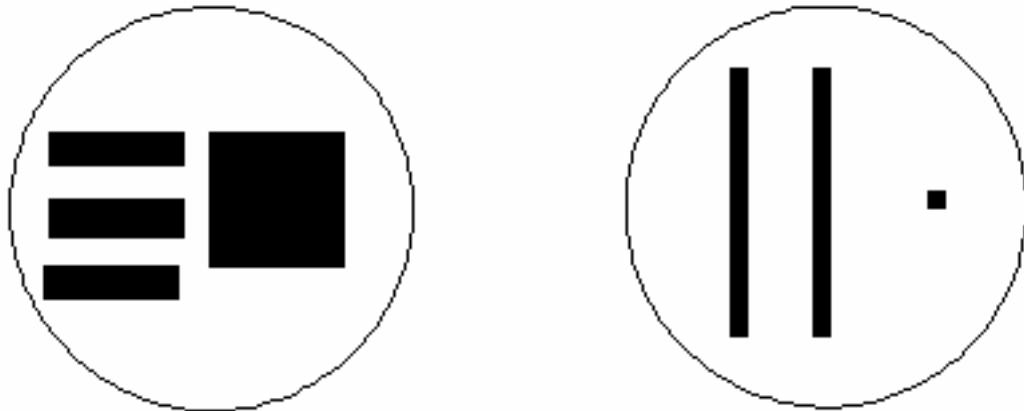
Figure 3.3-16: Top View of Sample Pucks used in Image Analysis (Through-Plane and In-Plane)

Section 3.3.3.4: Image Processing

The image processing was carried out using the Image Processing Tool Kit and Adobe Photoshop®. The first step in the image processing was to take each of the sixteen images and remove the color and then fit and remove the background variation. This step turned each image into an 8 bit gray scale image and leveled the uneven lighting. The next step was to paste each of the sixteen images into one composite image making sure all the image edges matched. The image was then thresholded to produce a binary image with the fillers being black. Next, a Euclidean distance map (EDM) open operation was done to remove small artifacts in the image and better separate the fillers from the matrix. The EDM open operation shrunk each feature by a set number of pixels then dilated them by the same number of pixels. The EDM version of "open" command kept the shape of the particle better then the standard morphological open. A "cutoff" operation was then completed to remove all features touching the edge and remove features smaller than 50 pixels.

Section 3.3.3.5: Image Analysis and Measurements

The moment angle was measured for each filler particle as a measure of the orientation. This measurement gives some insight into the orientation of the fillers in the composites. The angle was measured from the direction of heat conduction. The angle of the particle was measured using a method similar to fitting a line to a set of data [32]. It was calculated using the Equations 3.8a-i [32]. The summations of the location of each pixel in each particle are calculated in Equations 3.8a-e. The moment around the x and y-axes are calculated in Equations 3.8f-h. The angle of minimum momentum or moment angle is calculated in Equation 3.8i. This method uses each pixel in a particle as a

separate data point. This method is a robust method because it does not fit an ellipse to the outside of the particle and uses the main axes calculate the angle. In the ellipse method, a single pixel can cause the angle to be substantially different from the actual angle. The moment angle method is a much more robust method because if a single pixel or two stick out on the edge of the feature the angle does not change significantly. The moment angles from each feature were measured using PhotoShop® and the Image Processing Tool Kit®. The results from this analysis can be found in Section 9.8. Micrographs of through-plane and in-plane samples can be found in Appendices I and J respectively.

$$S_x = \sum x_i \tag{3.8a}$$

$$S_y = \sum y_i \tag{3.8b}$$

$$S_{xx} = \sum x_i^2 \tag{3.8c}$$

$$S_{yy} = \sum y_i^2 \tag{3.8d}$$

$$S_{xy} = \sum x_i \cdot y_i \tag{3.8e}$$

$$M_{xx} = S_{xx} - \frac{S_x^2}{Area} \tag{3.8f}$$

$$M_{yy} = S_{yy} - \frac{S_y^2}{Area} \tag{3.8g}$$

$$M_{xy} = S_{xy} - \frac{S_x \cdot S_y}{Area} \tag{3.8h}$$

$$\theta = \tan^{-1}\left\{ \frac{M_{xx} - M_{yy} + \sqrt{(M_{xx} - M_{yy})^2 + 4 \cdot M_{xy}^2}}{2 \cdot M_{xy}} \right\} \tag{3.8i}$$

Section 3.4: References

1.   Ticona Vectra Liquid Crystal Polymer (LCP) Product Information, Ticona, Summit, NJ, 07901, 2000.

2.   Chiou, J. S.; Paul, D. R. Journal of Polymer Science Part B: Polymer Physics, 1987, 25, 1699.

3.   J.-B. Donnet, R. C. Bansal, M.-J. Wang, Carbon Black, 2nd. Marcel Dekker, New York, 1993.

4.   The Freedonia Group, Inc., "Conductive Polymers". Cleveland, OH 44143-2326, 2000.

5.   Akzo Nobel Electrically Conductive Ketjenblack Product Literature, Akzo Nobel.

6.   The Industrial Graphite Engineering Handbook. Union Carbide Corp, NY, 1970.

7.   L. C. F. Blackman, Modern Aspects of Graphite Technology. Academic Press, NY, 1970.

8.   J.A. King, K. W. Tucker, B. D. Vogt, E. H. Weber, and C. Quan, "Conductive High Temperature Nylon". *Journal of Composite Materials,* Vol. 34, No. 24, 2000, pp. 2038-2060.

9.   J. A. King, K. W. Tucker, J. D. Meyers, E. H. Weber, M. L. Clingerman, and K. R. Ambrosius, "Factorial Design Approach Applied to Electrically and Thermally Conductive Nylon 6,6". *Polymer Composites*, Vol. 22, No. 1, 2001, pp. 142-154.

10.   Asbury Carbons Product Information, Asbury, NJ, 08802 (2004).

11.   J. A. King, K. W. Tucker, B. D. Vogt, E. H. Weber, and C. Quan, "Electrically and Thermally Conductive Nylon 6,6". *Polymer Composites*, Vol. 20, No. 5, 1999.

12.   www.asbury.com, Materials Chapter, accessed 4/20/2006.

13   Akzo Nobel, "Fortafil Carbon Fibers", Fortafil Fibers, Inc., 8870 Cedar Springs Lane, Suite 8, Knoxville, TN 37923.

14.   E. H. Weber, M. L. Clingerman, and J. A. King, "Thermally Conductive Nylon 6,6 and Polycarbonate Based Resin. Part 1: Synergistic Effects of Carbon Fillers", Journal of Applied Polymer Science, Vol. 88, pp. 112-122, 2003.

15.   Niigata Engineering Co. Ltd., Nagaoka Works, Model NE85UA4, Machine No. 50031F. Nagaoka Works, Niigata, Japan.

16.   Deltatherm Model A410, Serial No. 12003, 4500 Watts/Heater, Delta T Systems Inc., Richfield, WI 53076, phone 800-733-4204.

17.   Four Cavity Mold, Master Precision Molds, Inc., Greenville, MI, Phone No. 800-632-8912.

18.   Zytel® nylon resin: Product and Property Guide. DuPont.

19.   International Organization for Standardization (ISO). Plastics – Standard Atmospheres for Conditioning and Testing; ISO 291; 1997, 1998.

20.   "Evaluating Thermal Conductivity of Gasket Materials", ASTM Standard F433 - 77 Reapproved 1993, American Society for Testing and Materials, Philadelphia, Pennsylvania, 1996.

21. Holometrix Model TCA - 300 Thermal Conductivity Analyzer using Guarded Heat Flow Meter Method, 25 Wiggins Avenue, Bedford, Massachusetts.

22. Gustavsson, M.; Karawacki, E.; Gustafsson, S. E. Rev. Sci. Instrum., 1994, 65 (12), 3856-3859.

23. Log, T.; Gustafsson, S. E. Fire and Materials, 1995, 19, 43-49.

24. Bohac, V.; Gustavsson, M. K.; Kubicar, L.; Gustafsson, S. E. Rev. Sci. Instrum., 2000, 71(6), 2452-2455.

25. Hot Disk Thermal Constants Analyser Instruction Manual, Mathis Instruments, Ltd., Fredericton, New Brunswick, Canada, 2001.

26. Transient Plane Source – Gustafsson Hot Disk Technique, Standards for Contact Transient-Measurements of Thermal Properties, National Physical Laboratory, United Kingdom, accessed February 2006 at http://www.npl.co.uk/thermal/ctm/

27. He, Y. Thermochim. Acta, 2005, 436, 122-129.

28. "Specific Gravity and Density of Plastics by Displacement", ASTM Standard D792 - 66 (Re-approved 1975), American Society for Testing and Materials, Philadelphia, Pennsylvania, 1986.

29. "Standard Practice for Dissolving Polymer Materials", ASTM Standard D5226 - 98, American Society for Testing and Materials, Philadelphia, Pennsylvania, 1998.

30. George Blann from Buehler, Letter to J. King, January 25, 2001.

31. Buehler Corporation, Correspondence with J. King, Summer 2006.

32.   J. C. Russ, <u>The Image Processing Handbook</u>, 3rd ed. CRC and IEEE Press, Boca

        Raton, 1999.

Chapter 4:   Carbon Black and Carbon Particle Studies

The first thing to be done in this work was to characterize the thermal

conductivity of composites using the preselected carbon black and to determine which

carbon particle (hereinafter, in this chapter, 'carbon particle' applies to synthetic graphite,

natural flake graphite, and calcined needle coke particles) would be used for further study.

Section 4.1: Materials

The matrix material for all composites discussed in this chapter was Vectra

A950RX LCP; the filler materials being tested were Ketjenblack EC-600 JD, Thermocarb

TC-300, Asbury SG 4012, Asbury NFG 3160, and Asbury Calcined Needle Coke F108A.

More information on these materials is provided in Chapters 3.1.1.1 and 3.1.2.1 – 3.1.2.5

of this dissertation.

Section 4.2: Experimental Method

The studies of the carbon black composites and the carbon particle composites were designed to give two different types of information. The carbon black study was meant to give a wide range of data points for the generation of thermal conductivity vs. filler loading curves; as such, seven composites ranging from 2.5wt% - 15% carbon black were generated. The carbon particle study was meant to help choose between the carbon particles for continued study. As the carbon particle was intended to be a large part of the final composite product, three composites for each particle were generated using fairly high filler loadings between 40 – 70wt%. Table 4.2-1 shows the weight and volume percent loading levels for the fillers in this study.

Table 4.2-1: Single Filler Loading Levels in Vectra A950RX

Filler	Filler Concentrations
Ketjenblack EC-600 JD	Wt%: 2.5, 4.0, 5.0, 6.0, 7.5, 10.0, 15.0 Vol%:1.9, 3.1, 3.9, 4.7, 6.0, 8.0, 12.1
Thermocarb TC-300 Synthetic Graphite	Wt%: 40.0, 60.0, 70.0 Vol%: 29.3, 48.4, 59.3
4012 Synthetic Graphite	Wt%: 40.0, 60.0, 70.0 Vol%: 29.3, 48.4, 59.3
3160 Natural Flake Graphite	Wt%: 40.0, 60.0, 70.0 Vol%: 29.3, 48.4, 59.3
Calcined Needle Coke F108A	Wt%: 40.0, 60.0, 70.0 Vol%: 30.8, 50.2, 61.4

Section 4.3: Sample Fabrication

The fillers were used as-received for this study; the matrix material was dried as described in Chapter 3.3.1.1. The composite materials were blended, extruded and pelletized as described in Chapter 3.3.1.2 using the first screw design as shown in Section 9.1. The pellets were then injection molded as described in Chapter 3.3.1.3.

Section 4.4: Sample Testing

All samples were conditioned as described in Chapter 3.3.2 prior to the thermal conductivity testing. Four samples from each formulation were then tested as described in Chapter 3.3.2.1. In addition, filler orientation testing was performed on samples containing the carbon particles as described in Chapter 3.3.3. The carbon black particles were too small to be seen by optical microscopy.

Section 4.5: Results

Figure 4.5-1 summarizes all of the thermal conductivity data collected in this study.
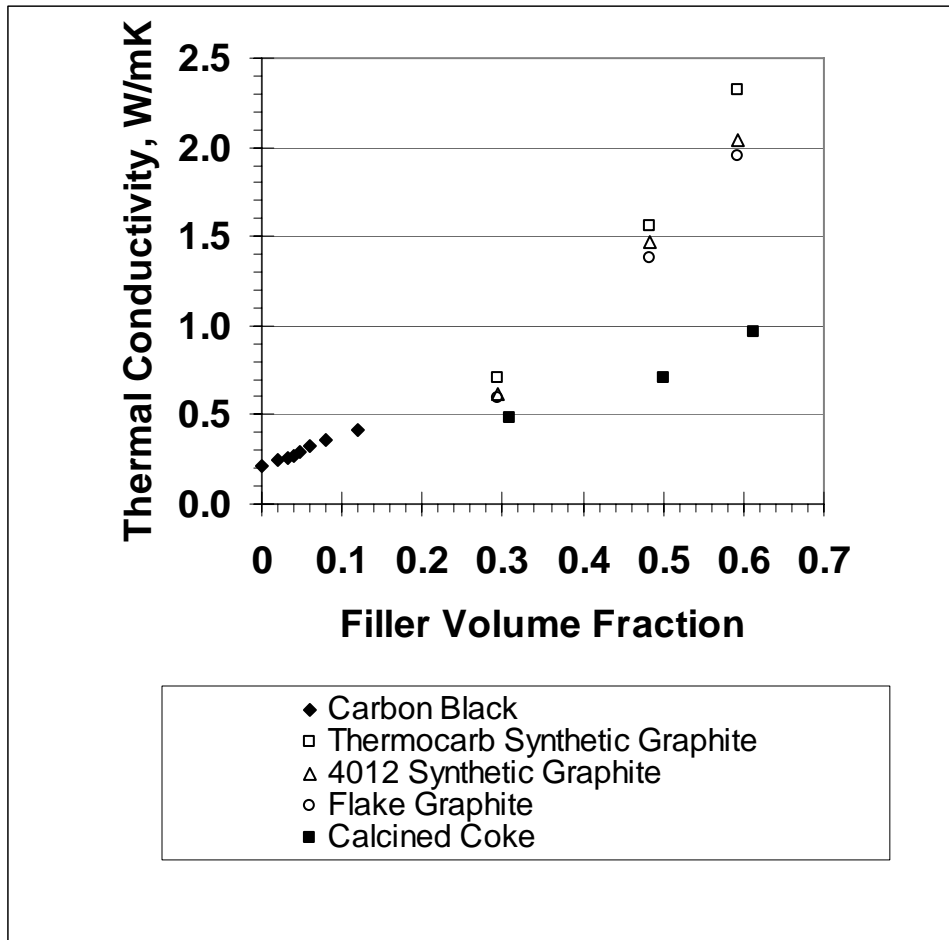
Figure 4.5-1: Through-Plane Thermal Conductivity Results

Section 4.5.1: Thermal Conductivity Results

Figure 4.5-1 shows the mean through-plane thermal conductivity of the composites plotted as a function of the volume fraction of filler in the composite. These formulations are the same as those listed in Table 4.2.-1. The mean thermal conductivity of the matrix material, neat Vectra A950RX LCP, was 0.22 W/mK. In these

measurements, the standard deviation was typically less than 5% of the mean value. The

full data can be seen in Section 9.4.

Section 4.5.1.1: Carbon Black Thermal Conductivity Results

As shown above in Figure 4.1, the carbon black composite thermal conductivity

ranged from 0.22 W/mK at 0 vol% filler to 0.42 W/mK at 12.1 vol% filler. The thermal

conductivity appears to be following a linear trend for the data gathered. Extrusion of

this composite at 12.1 vol% filler was very difficult with the equipment used due to the

entangling nature of the carbon black particles; as such, it was decided to stop the study

there. If other varieties of carbon are to be added to a multi-filler system, the loading

level of the carbon black will have to be greatly reduced for processing concerns.

Section 4.5.1.2: Carbon Particle Thermal Conductivity Results

The results of the thermal conductivity screening study provided useful

information. The first item to note is with regards to the calcined needle coke, which

showed a much lower thermal conductivity (0.5 – 1.0 W/mK) than the synthetic graphites

and the natural flake graphite that were tested. This was attributed to the difference in

chemical structure between these materials. Calcined needle coke and graphite both

show excellent planar orientation; however, the orbital overlap between planes in

calcined needle coke is much less symmetrical than that in graphite, which lowers the

thermal conductivity in that direction dramatically. The second item of note is how the

Thermocarb TC-300 synthetic graphite has a consistently higher thermal conductivity

than the other two graphites (0.75 – 2.35 W/mK, compared to 0.6 – 2.0 W/mK) and,

further, that the difference increases with loading level. Thermocarb TC-300 has a very

high degree of crystallinity and a lower percentage of impurities, as discussed in Chapter

3.1.1.2. These factors are probably the reason for the increased thermal conductivity relative to the other carbon particles.

Section 4.5.2: Filler Orientation Results

The data of interest in the filler orientation study was the angle between the filler and the direction of conductivity measurement. In this study, an angle of 0° signifies that the filler particles are aligned parallel to the direction of measurement; an angle of 90° signifies that the filler particles are aligned perpendicular to the direction of measurement. Figure 4.5-2 is a representative sample. It is clearly shown that the filler particles are more oriented transverse to the direction of measurement of conductivity. The mean filler angle was 52°; this result agrees with previous studies [1]. The full data for this study can be seen in Section 9.8.

Figure 4.5-2: Through –Plane Thermal Conductivity Sample Containing 40 wt% Calcined Needle Coke F108A in Vectra A950RX at 100X Magnification

Section 4.6: Summary

The data gathered in this study helped in determining which carbon particle would be used in continuing work for this project. The clear difference in thermal conductivity between the Thermocarb and the other carbon particles that were tested is of utmost importance in an application where the goal is a dramatic increase of thermal conductivity in a carbon-polymer composite. The data from the carbon black study is useful for characterizing the material as well as for understanding the processing concerns of this particular composite.

Section 4.7: References

1.   J. A. Heiser and J. A. King, *Polym. Compos*, **25**, 186 (2004).

Chapter 5: Thermocarb TC-300 Study

Having determined that Asbury Carbon's Thermocarb TC-300 had the most

desirable thermal conductivity properties of the synthetic graphites, natural flake graphite

and calcined needle coke examined in the screening study, a second study was performed

on this material over a wider range of filler loadings to better understand how the thermal

conductivity varied with filler loading.

Section 5.1: Materials

The matrix material for all composites discussed in this chapter was Vectra

A950RX LCP; the filler material being tested was Thermocarb TC-300. More

information on these materials is provided in Chapter 3.1.1.1 and Chapter 3.1.2.2 of this

dissertation.

Section 5.2: Experimental Method

The primary purpose of this study was to provide a wide range of data points for
the generation of thermal conductivity vs. filler loading curves. With this in mind,
fourteen composites ranging from 10wt% - 75wt% (6.5 vol% - 65.2 vol%) synthetic
graphite were generated. Table 5.2-1 shows the weight and volume percent loading
levels for the filler in this study.

**Table 5.2-1: Single Filler Loading Levels of Thermocarb TC-300 in Vectra A950RX
LCP**

Filler wt %	Filler vol%
0.0	0.0
10.0	6.5
15.0	9.9
20.0	13.5
25.0	17.2
30.0	21.1
35.0	25.2
40.0	29.3
45.0	33.8
50.0	38.5
55.0	43.3
60.0	48.4
65.0	53.7
70.0	59.3
75.0	65.2

A secondary purpose of this study was to elaborate upon a previously developed model [1]
for thermal conductivity that predicted the in-plane thermal conductivity of a composite
material using the volume percent of filler and the through-plane thermal conductivity of
the composite material.

Section 5.3: Sample Fabrication

The fillers were used as-received for this study; the matrix material was dried as described in Chapter 3.3.1.1. The composite materials were extruded and pelletized as described in Chapter 3.3.1.2. The pellets were then injection molded as described in Chapter 3.3.1.3. Extrusion and injection molding information can be found in Appendices B and C respectively.

Section 5.4: Sample Testing

All samples were conditioned as described in Chapter 3.3.2 prior to the thermal conductivity testing. Six samples from each formulation were tested as described in Chapter 3.3.2.1. Three different samples from each formulation were tested as described in Chapter 3.3.2.2. In addition, filler orientation testing was performed as described in Chapter 3.3.3.

Section 5.5: Results

There were three important results generated from this study. The first result was the data set showing the relationship between thermal conductivities and filler loading for this composite. The second result was the generation of a predictive model for in-plane thermal conductivity that may be applicable to other filled systems. The third result was confirmation that these samples all had similar filler orientations and as such had similar heat transfer mechanisms.

Section 5.5.1: Thermal Conductivity Results

The through-plane thermal conductivity of the composites was measured using the two test methods mentioned above. Figure 5.5-1 shows the through-plane thermal conductivity as measured by the methods described in Chapter 3.3.2.1, while Figures 5.5-2 and 5.5-3 show the through-plane thermal conductivity and in-plane thermal conductivity as measured by the methods described in Chapter 3.3.2.2. As can be seen from the figures, the through-plane thermal conductivity rises in a mostly linear fashion, but the in-plane thermal conductivity begins exhibiting exponential behavior at approximately 35 vol% filler.
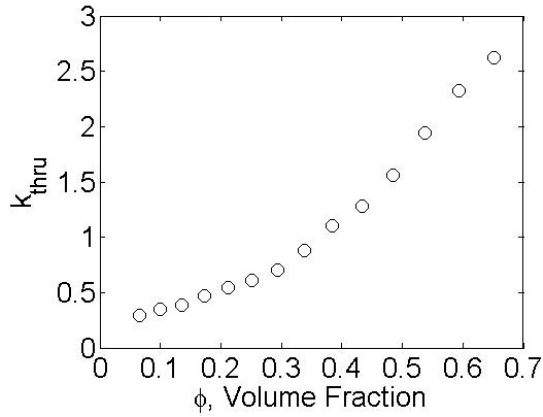
Figure 5.5-1: Through-Plane Thermal Conductivity (W/mK) vs. Volume Fraction Filler for Synthetic Graphite / Vectra Composite, TCA
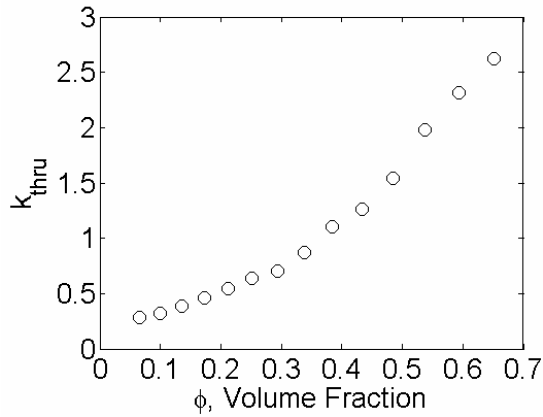
Figure 5.5-2: Through-Plane Thermal Conductivity (W/mK) vs. Volume Fraction Filler for Synthetic Graphite / Vectra Composite, HotDisk
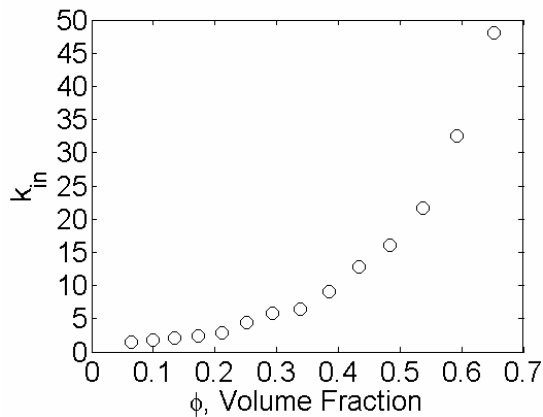
Figure 5.5-3: In-Plane Thermal Conductivity (W/mK) vs. Volume Fraction Filler for Synthetic Graphite / Vectra Composite, HotDisk

Table 5.5-1 displays the mean, standard deviation, and number of samples tested for the through-plane thermal conductivity as measured by the TCA-300 as well as the through-plane and in-plane thermal conductivities as measured by the Hot Disk transient plane source method. There is good agreement between the test methods for the through-plane thermal conductivity results. As expected, the in-plane thermal conductivity was higher than the through-plane thermal conductivity in all cases. The ratio of the in-plane thermal conductivity to the through-plane thermal conductivity varied from 5 to 18 and generally increased as the volume fraction of filler (ϕ) increased. Full results from the TCA-300 and Hot Disk conductivity testing can be found in Appendices D and F.

Table 5.5-1: Thermal Conductivity Results

	Through-Plane Thermal Conductivity (TCA-300)	Through-Plane Thermal Conductivity (Hot Disk)	In-Plane Thermal Conductivity (Hot Disk)
Formulation	W/mK	W/mK	W/mK
Neat Vectra A950RX LCP	0.2169 ± 0.0068 n=4	~ 0.22 (TCA)	~ 0.22 (TCA)
Synthetic Graphite Filler			
10 wt%	0.2935 ± 0.010 n=4	0.284 ± 0.001 n=3	1.426 ± 0.045 n=3
15 wt%	0.3494 ± 0.013 n=4	0.323 ± 0.001 n=3	1.853 ± 0.050 n=3
20 wt%	0.3869 ± 0.012 n=5	0.385 ± 0.010 n=3	2.029 ± 0.055 n=3
25 wt%	0.4699 ± 0.012 n=5	0.459 ± 0.022 n=3	2.433 ± 0.142 n=3
30 wt%	0.5464 ± 0.019 n=4	0.545 ± 0.015 n=3	2.938 ± 0.063 n=3
35 wt%	0.6106 ± 0.021 n=5	0.635 ± 0.021 n=3	4.403 ± 0.594 n=3
40 wt%	0.7064 ± 0.010 n=4	0.702 ± 0.078 n=5	5.881 ± 0.651 n=5
45 wt%	0.8804 ± 0.043 n=5	0.874 ± 0.005 n=3	6.441 ± 0.284 n=3
50 wt%	1.1081 ± 0.031 n=4	1.101 ± 0.010 n=3	9.020 ± 0.025 n=3
55 wt%	1.2851 ± 0.027 n=4	1.265 ± 0.010 n=3	12.80 ± 0.622 n=3
60 wt%	1.5586 ± 0.074 n=8	1.545 ± 0.044 n=3	16.03 ± 0.301 n=3
65 wt%	1.9426 ± 0.113 n=7	1.982 ± 0.052 n=3	21.60 ± 0.606 n=3
70 wt%	2.3225 ± 0.085 n=7	2.318 ± 0.049 n=3	32.55 ± 1.221 n=3
75 wt%	2.6251 ± 0.097 n=5	2.624 ± 0.076 n=3	48.07 ± 1.850 n=3

Section 5.5.2: Thermal Conductivity Model Results

After analysis of the thermal conductivity data generated in this study, an exponential correlation between the square root of the product of the in-plane and through-plane thermal conductivities and the volume percent of filler was observed. This correlation is given by:

$$\sqrt{k_{in}k_{thru}} = 0.4638e^{4.9256\phi} \qquad (5.1)$$

where k_{in} and k_{thru} have units of (W/mK). Rearranging for k_{in} yields the following predictive equation:

$$k_{in} = \frac{(0.4638e^{4.9256\phi})^2}{k_{thru}} = \frac{0.2151e^{9.8512\phi}}{k_{thru}} \qquad (5.2)$$

This is an important result. The three variable parameters in this equation are ϕ, k_{thru} and k_{in}. ϕ is a known quantity and varies by composite. k_{thru} can be calculated using a modified Nielsen model [2]. However, literature data for k_{in} in carbon-polymer systems is not readily available. A predictive equation for k_{in} allows for much more efficient experimentation, as sample generation for specific thermal conductivities will involve much less trial and error. Figure 5.5-4 shows the experimental data plotted along with the predicted results of the model. The experimental data fits the model results quite well.
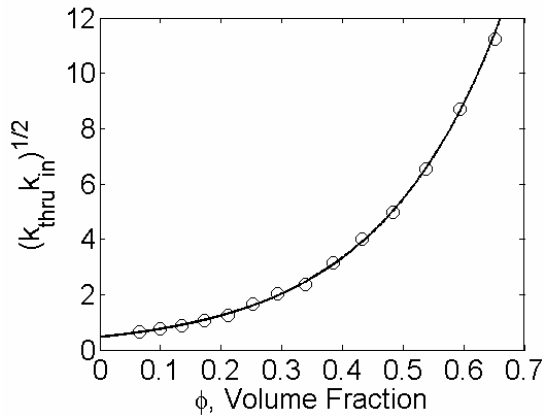
Figure 5.5-4: Combined Thermal Conductivity (W/mK) vs. Volume Fraction Filler for Synthetic Graphite / Vectra Composite (Exponential Fit)

Section 5.5.3: Filler Orientation Results

The data of interest in the filler orientation study was the angle between the filler and the direction of conductivity measurement. In this study, an angle of 0° signifies that the filler particles are aligned parallel to the direction of measurement; an angle of 90° signifies that the filler particles are aligned perpendicular to the direction of measurement. The images gathered show that the filler particles are more oriented transverse to the direction of measurement of conductivity. The mean filler angle was 52°; this result agrees with previous studies [3]. The full data for this study can be seen in Section 9.8.

Section 5.6: Summary

A greater understanding of the thermal conductivity properties of Asbury Carbon's Thermocarb TC-300 and, more importantly, how the filler loading affected the thermal properties of the composite, was obtained. An important result is that at ~35 vol% filler, the thermal conductivities begin to follow an exponential trend. This trend is more pronounced in the in-plane thermal conductivity trend. This data was used to develop a predictive model for the in-plane thermal conductivity which, in concert with the known volume percent of filler and the known or calculated through-plane thermal conductivity of the composite, aids experimental design in targeting desired thermal conductivity values. Additionally, filler orientation studies of the samples showed that the entire family of composites had similar filler orientation properties and therefore had similar thermal conduction properties.

Section 5.7: References

1.   Keith, J. M.; Hingst, C. D.; Miller, M. G.; King, J. A.; Hauser, R. A. Polym.

        Compos., 2006, 27, 1-7.

2.   Weber, E. H.; Clingerman, M. L.; King, J. A. J. Appl Polym. Sci., 2003, 88, 123-

        130.

3.   J. A. Heiser and J. A. King, *Polym. Compos*, **25**, 186 (2004).

Chapter 6:   Fortafil 243 Carbon Fiber Study

The emphasis of this study was to characterize the thermal conductivity of composites using the preselected carbon fiber, Fortafil 243 carbon fiber.

Section 6.1: Materials

The matrix material for all composites discussed in this chapter was Vectra A950RX LCP; the filler material being tested was Fortafil 243 carbon fiber. More information on these materials is provided in Chapter 3.1.1.1 and Chapter 3.1.2.6 of this dissertation.

Section 6.2: Experimental Method

The primary purpose of this study was to provide a wide range of data points for the generation of thermal conductivity vs. filler loading curves. With this in mind, thirteen composites ranging from 5wt% - 60wt% (4.1 vol% - 54.7 vol%) carbon fiber were generated. Table 6.2-1 shows the weight and volume percent loading levels for the filler in this study.

Table 6.2-1: Single Filler Loading Levels of Fortafil 243 Carbon Fiber in Vectra A950RX LCP

Filler wt %	Filler vol%
0.0	0.0
5.0	4.1
7.5	6.1
10.0	8.2
15.0	12.4
20.0	16.8
25.0	21.2
30.0	25.5
35.0	30.2
40.0	34.9
45.0	39.7
50.0	44.6
55.0	49.6
60.0	54.7

A secondary purpose of this study was to elaborate upon a previously developed model [1] for thermal conductivity that predicted the in-plane thermal conductivity of a composite material using the volume percent of filler and the through-plane thermal conductivity of the composite material.

Section 6.3: Sample Fabrication

The fillers were used as-received for this study; the matrix material was dried as described in Chapter 3.3.1.1. The composite materials were extruded and pelletized as described in Chapter 3.3.1.2. The pellets were then injection molded as described in Chapter 3.3.1.3. Extrusion and injection molding conditions can be found in Appendices B and C.

Section 6.4: Sample Testing

All samples were conditioned as described in Chapter 3.3.2 prior to the thermal conductivity testing. Six samples from each formulation were tested as described in Chapter 3.3.2.1. Three different samples from each formulation were tested as described in Chapter 3.3.2.2.

Section 6.5: Results

There were two important results generated from this study. The first result was the data set showing the relationship between thermal conductivities and filler loading for this composite. The second result was the generation of a predictive model for in-plane thermal conductivity that may be applicable to other filled systems.

Section 6.5.1: Heat Capacity Results

To obtain the heat capacity of the composite material, the following formula was used as a benchmark to compare experimental data to:

$$\sum_{i=1}^{2} M_i \times Cp_i \qquad (6.1)$$

In this equation, M is the volume fraction of the material, Cp is the specific heat of the material, $i=1$ denotes the Vectra and $i=2$ denotes the Fortafil 243 carbon fiber. The formula results showed good agreement with experimental data. Experimental data and full formula results can be found in Section 9.5.

Section 6.5.2: Thermal Conductivity Results

The through-plane thermal conductivity of the composites was measured using the two test methods mentioned above. Figure 6.5-1 shows the through-plane thermal conductivity as measured by the methods described in Chapter 3.3.2.1, while Figures 6.5-2 and 6.5-3 show the through-plane thermal conductivity and in-plane thermal conductivity as measured by the methods described in Chapter 3.3.2.2. As can be seen from the figures, the through-plane thermal conductivity rises in a mostly linear fashion, but the in-plane thermal conductivity begins exhibiting exponential behavior at approximately 30vol% filler.
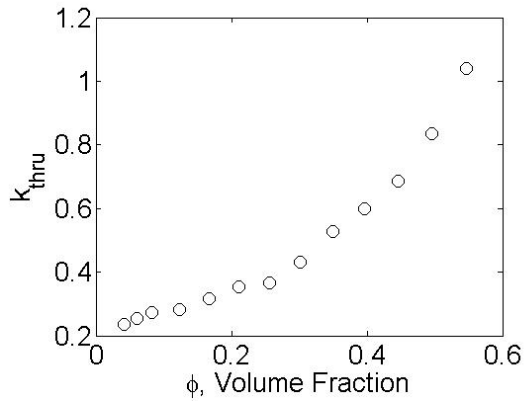
Figure 6.5-1: Through-Plane Thermal Conductivity (W/mK) vs. Volume Fraction Fortafil 243 Carbon Fiber, TCA
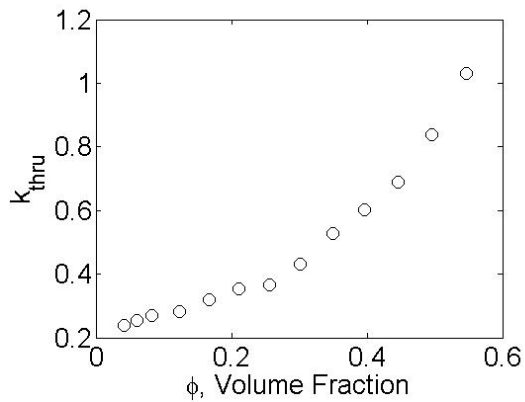
Figure 6.5-2: Through-Plane Thermal Conductivity (W/mK) vs. Volume Fraction Fortafil 243 Carbon Fiber, HotDisk
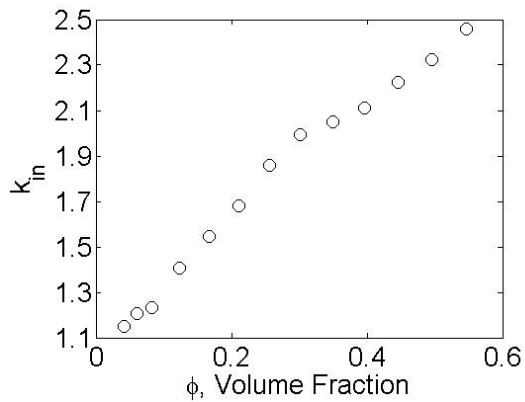
Figure 6.5-3: In-Plane Thermal Conductivity (W/mK) vs. Volume Fraction Fortafil 243 Carbon Fiber, HotDisk

Table 6.5-1 displays the mean, standard deviation, and number of samples tested for the through-plane thermal conductivity as measured by the TCA-300 as well as the through-plane and in-plane thermal conductivities as measured by the Hot Disk transient plane source method. There is good agreement between the test methods for the through-plane thermal conductivity results. As expected, the in-plane thermal conductivity was higher than the through-plane thermal conductivity in all cases. The ratio of the in-plane thermal conductivity to the through-plane thermal conductivity varied from 2.3 to 5.1 and generally decreased as the volume fraction of filler (ϕ) increased. This ratio is lower than observed in the Thermocarb as discussed in Chapter 5; the Thermocarb is a more pure form of carbon than the Fortafil carbon fiber, which partially explains this behavior. Full conductivity data and results can be found in Appendices D and F.

Table 6.5-1: Thermal Conductivity Results

	Through-Plane Thermal Conductivity (TCA-300)	Through-Plane Thermal Conductivity (Hot Disk)	In-Plane Thermal Conductivity (Hot Disk)	In-Plane to Through-Plane Ratio (Hot Disk)
Formulation	W/mK	W/mK	W/mK	unitless
Neat Vectra A950RX LCP	0.217 ± 0.007n=4	~ 0.22 (TCA)	~ 0.22 (TCA)	1.0
Fortafil 243 Carbon Fiber				
5 wt%	0.237 ± 0.006 n=6	0.238 ± 0.002 n=5	1.148 ± 0.030 n=5	4.8
7.5 wt%	0.256 ± 0.004 n=6	0.255 ± 0.002 n=5	1.208 ± 0.034 n=5	4.7
10 wt%	0.272 ± 0.006 n=6	0.271 ± 0.005 n=5	1.234 ± 0.052 n=5	4.6
15 wt%	0.282 ± 0.008 n=6	0.282 ± 0.004 n=5	1.407 ± 0.012 n=5	5.0
20 wt%	0.316 ± 0.010 n=6	0.320 ± 0.004 n=5	1.548 ± 0.026 n=5	4.8
25 wt%	0.352 ± 0.006 n=6	0.353 ± 0.000 n=5	1.680 ± 0.026 n=5	4.8
30 wt%	0.366 ± 0.009 n=6	0.365 ± 0.003 n=5	1.857 ± 0.028 n=5	5.1
35 wt%	0.430 ± 0.025 n=6	0.432 ± 0.004 n=5	1.996 ± 0.005 n=5	4.6
40 wt%	0.527 ± 0.014 n=6	0.527 ± 0.003 n=5	2.050 ± 0.036 n=5	3.9
45 wt%	0.599 ± 0.033 n=6	0.602 ± 0.006 n=5	2.109 ± 0.015 n=5	3.5
50 wt%	0.687 ± 0.034 n=4	0.688 ± 0.004 n=5	2.239 ± 0.037 n=5	3.3
55 wt%	0.836 ± 0.044 n=3	0.838 ± 0.009 n=20	2.324 ± 0.069 n=20	2.8
60 wt%	1.039 ± 0.018 n=5	1.030 ± 0.023 n=10	2.459 ± 0.057 n=10	2.4

Section 6.5.3: Thermal Conductivity Model Results

After analysis of the thermal conductivity data generated in this study, an exponential correlation between the square root of the product of the in-plane and through-plane thermal conductivities and the volume percent of filler was observed. This correlation is given by:

$$\sqrt{k_{in}k_{thru}} = 0.4835e^{2.1619\phi} \tag{6.2}$$

where k_{in} and k_{thru} have units of (W/mK). Rearranging for k_{in} yields the following predictive equation:

$$k_{in} = \frac{(0.4835e^{2.1619\phi})^2}{k_{thru}} = \frac{0.2338e^{4.3238\phi}}{k_{thru}} \tag{6.3}$$

As discussed in Chapter 5.4.2, this result is important as it allows for further development of a predictive model for the thermal conductivity of composites [2]. Figure 6.5-4 shows the experimental data plotted along with the predicted results of the model. The experimental data fits the model results quite well.
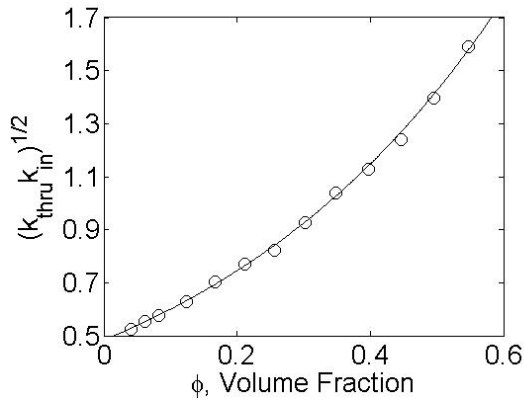
Figure 6.5-4: Combined Thermal Conductivity (W/mK) vs. Volume Fraction Fortafil 243 Carbon Fiber (Exponential Fit)

Section 6.6: Summary

A greater understanding of the thermal conductivity properties of Fortafil 243

carbon fiber and, more importantly, how the filler loading affected the thermal properties

of the composite, was obtained. An important result is that at ~30 vol% filler, the

thermal conductivities begin to follow an exponential trend. This trend is more

pronounced in the in-plane thermal conductivity trend. This data was used to develop a

predictive model for the in-plane thermal conductivity which, in concert with the known

volume percent of filler and the known or calculated through-plane thermal conductivity

of the composite, aids experimental design in targeting desired thermal conductivity

values.

Section 6.7: References

1. Keith, J. M.; Hingst, C. D.; Miller, M. G.; King, J. A.; Hauser, R. A. Polym. Compos., 2006, 27, 1-7.

2. Weber, E. H.; Clingerman, M. L.; King, J. A. J. Appl Polym. Sci., 2003, 88, 123-130.

Chapter 7:   Modeling

After the thermal conductivity data for the selected fillers was collected, it was

subjected to assorted modeling procedures to see if a mathematical model could be

extracted from the results. These mathematical models, if found, would allow for

predictive analysis of composite mixtures, allowing for optimization of product to some

degree before many materials and hours are expended to come to the same conclusion. In

chapters 5 and 6, exponential trendlines were fit to the data for combined thermal

conductivity (the positive square root of the product of through-plane and in-plane

thermal conductivities of a composite material) versus volume fraction of filler. One of

the parameters in these trendline equations is the through-plane thermal conductivity, of

which there are several predictive models available. This chapter is a discussion of the

most prevalent of these models.

Section 7.1: Basic Modeling

All of the following models require the thermal conductivity of the constituents.

Table 7.1-1 is a compilation of these values from tables in Chapter 3 [1-4].

Table 7.1-1: Thermal Conductivity of Constituents [1-4]

Material	Thermal Conductivity (W/mK)
Vectra A950RX Liquid Crystal Polymer	0.22
Ketjenblack EC-600 JD Carbon Black	2.1
Thermocarb TC-300 Synthetic Graphite	600
Fortafil 243 Carbon Fiber	20

In the following models, all subscripts of '1' are referring to the properties of the matrix material; all subscripts of '2' are referring to the properties of the filler material. In addition, all references to 'K' refer to the thermal conductivity of the composite; all references to 'k' refer to the thermal conductivity of a single component; 'ϕ_1' and 'ϕ_2' refer to the volume fractions of the components (which sum to 1). The Nielsen model discussed in Section 7.2 has some additional nomenclature which will be discussed in that section.

Basic thermal conductivity models take into account physical properties of the materials and, using only those properties, give a resulting value for the thermal conductivity of the composite material. There are no adjustable parameters in these models – the data is what it is. Three basic thermal conductivity models were examined in this work and will be discussed.

Section 7.1.1: Rule of Mixtures

The Rule of Mixtures model, sometimes called the series model, can be expressed as follows in the case of a two-component (matrix and one filler) system:

$$K = \phi_1 k_1 + \phi_2 k_2 \qquad (7.1)$$

This model works reasonably well to predict thermal conductivity in continuous fiber, well-aligned composites; previous work has shown that this model tends to overpredict thermal conductivity in short-fiber and/or particulate filler composites [5-6].

Section 7.1.2: Inverse Rule of Mixtures

The Inverse Rule of Mixtures model, sometimes called the parallel model, can be expressed as follows in the case of a two-component (matrix and one filler) system:

$$\frac{1}{K} = \frac{\phi_1}{k_1} + \frac{\phi_2}{k_2} \qquad (7.2)$$

This model also works reasonably well to predict thermal conductivity in continuous fiber, well-aligned composites; previous work has shown that this model tends to underpredict thermal conductivity in short-fiber and/or particulate filler composites [5-6].

Section 7.1.3: Geometric Rule of Mixtures

The Geometric Rule of Mixtures model, sometimes called the geometric mean model, can be expressed as follows in the case of a two-component (matrix and one filler) system:

$$K = k_1^{\phi_1} k_2^{\phi_2} \qquad (7.3)$$

This model is better at predicting thermal conductivity in short-fiber and/or particulate filler composites than the two aforementioned models [5-6].

Section 7.1.4: Basic Modeling Results

Graphical results will be presented and discussed here – full data for these test cases can be found in Section 9.11. Two error analysis terms were calculated for these and the Nielsen models:

$$\varepsilon = \frac{\sum_i (y_i - y_{\text{mod},i})^2}{\sum_i y_i^2} \tag{7.4}$$

$$SS = \sum_i (y_i - y_{\text{mod},i})^2 \tag{7.5}$$

'ε' is a standardized lack of fit term; 'y_i' is an experimental through-plane thermal conductivity result; '$y_{\text{mod},i}$' is the corresponding model-predicted through-plane thermal conductivity result; 'i' is the summation variable which ranges from 1 to the total number of formulations; 'SS' is shorthand for Sum of Squares, which is the sum of the squares of the difference between the experimental value and predicted value of the thermal conductivity of a composite. A result of 0 for either of these equations indicates a perfect fit of the model to the data.

Section 7.1.4.1: Carbon Black Basic Model Results

As shown in Table 7.1-2, the Rule of Mixtures model was the best match to the experimental data, outperforming the other basic models tested by an order of magnitude in terms of minimizing the sum of squares and standardized lack of fit terms. As expected, the Rule of Mixtures tended to overpredict the thermal conductivity of the composite while the Inverse Rule of Mixtures tended to underpredict the thermal

conductivity of the composite. In this case, the Geometric Rule of Mixtures

underpredicted the thermal conductivity of the composite. The Rule of Mixtures gave the

closest predictive fit when compared with experimental data.

Table 7.1-2: Error Analysis - Basic Mixing Rules, Carbon Black Composite

	Rule Of Mixtures	Inverse Rule Of Mixtures	Geometric Rule Of Mixtures
EAV SS	0.002643	0.059687	0.034871
EAV ε	0.003577	0.080772	0.047189

Figure 7.1-1 is a graphical comparison of the model results to the experimental data.
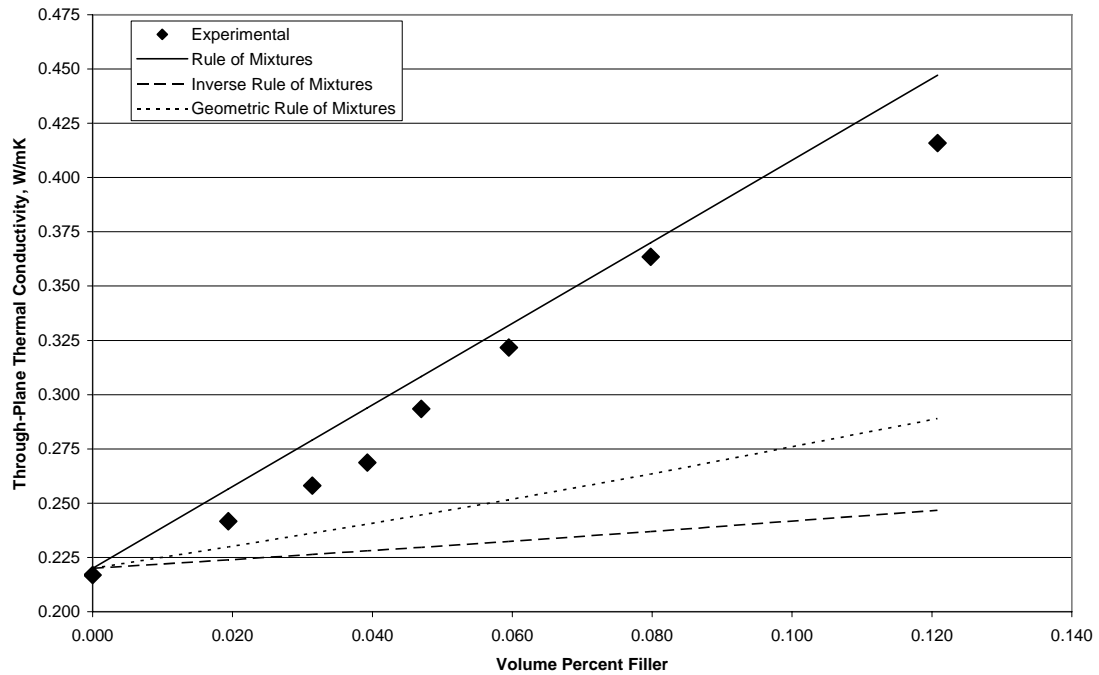
Figure 7.1-1: Basic Mixing Rule Model Results – Carbon Black Composites

Section 7.1.4.2: Synthetic Graphite Basic Model Results

As shown in Table 7.1-3, the Inverse Rule of Mixtures model was the best match to the experimental data, outperforming the other basic models tested by several orders of magnitude in terms of minimizing the sum of squares and standardized lack of fit terms. As expected, the Rule of Mixtures tended to overpredict the thermal conductivity of the composite while the Inverse Rule of Mixtures tended to underpredict the thermal conductivity of the composite. In this case, the Geometric Rule of Mixtures overpredicted the thermal conductivity of the composite.

Table 7.1-3: Error Analysis - Basic Mixing Rules, Synthetic Graphite Composite

	Rule Of Mixtures	Inverse Rule Of Mixtures	Geometric Rule Of Mixtures
EBV SS	714497	12.6547	2048.31
EBV ε	29846.9	0.528627	85.5646

Figures 7.1-2 and 7.1-3 are graphical comparisons of the model results to the experimental data. They share the same data; however, the Rule of Mixtures model is omitted from Figure 7.3 to allow a better look at how the other two models approximate the experimental data.
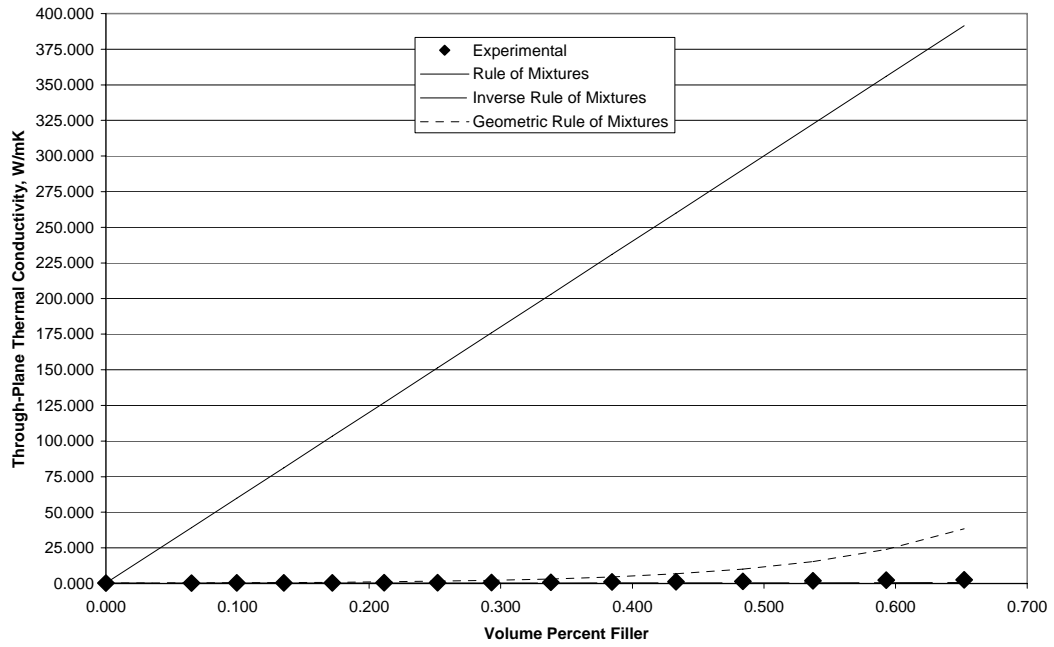
Figure 7.1-2: Basic Mixing Rule Model Results – Synthetic Graphite Composites
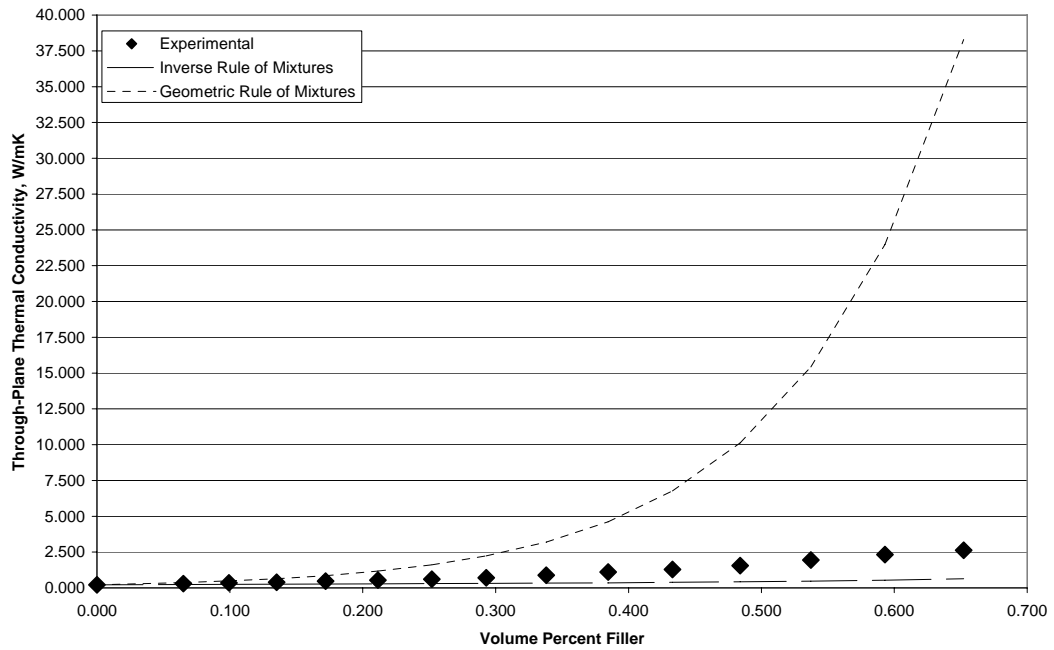
Figure 7.1-3: Selected Basic Mixing Rule Model Results – Synthetic Graphite Composites

Section 7.1.4.3: Carbon Fiber

As shown in Table 7.1-4, the Inverse Rule of Mixtures model was the best match to the experimental data, outperforming the other basic models tested by varying orders of magnitude in terms of minimizing the sum of squares and standardized lack of fit terms. As expected, the Rule of Mixtures tended to overpredict the thermal conductivity of the composite while the Inverse Rule of Mixtures tended to underpredict the thermal conductivity of the composite. In this case, the Geometric Rule of Mixtures overpredicted the thermal conductivity of the composite.

Table 7.1-4: Error Analysis - Basic Mixing Rules, Carbon Fiber Composite

	Rule Of Mixtures	Inverse Rule Of Mixtures	Geometric Rule Of Mixtures
EHV SS	448.065	0.679135	6.02546
EHV ε	119.638	0.181337	1.60887

Figures 7.1-4 and 7.1-5 are graphical comparisons of the model results to the experimental data. They share the same data; however, the Rule of Mixtures model is omitted from Figure 7.1-5 to allow a better look at how the other two models approximate the experimental data.
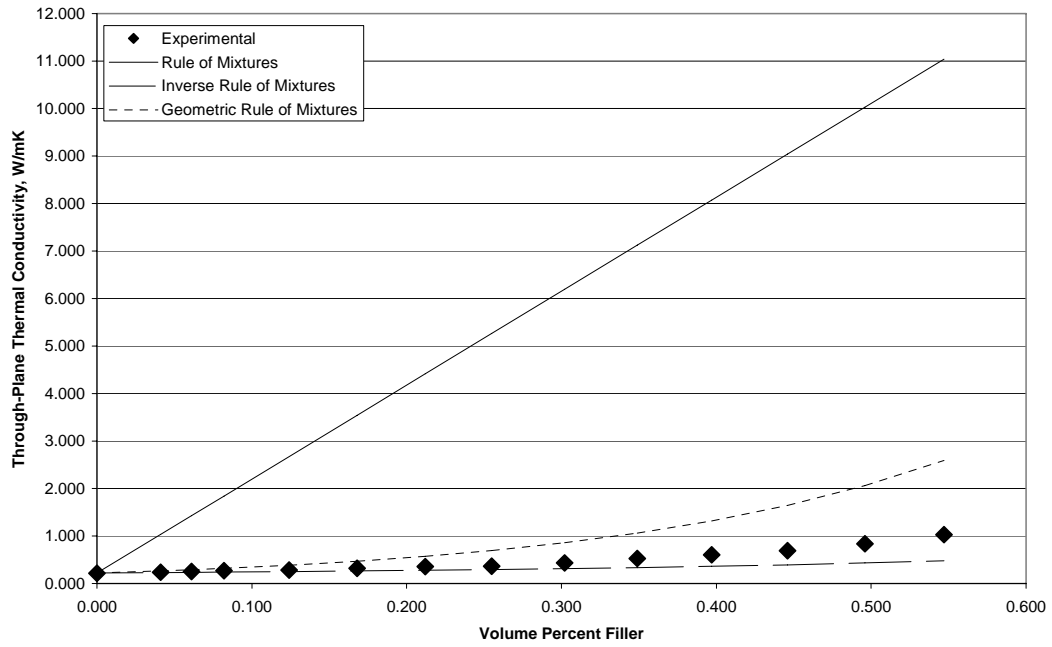
Figure 7.1-4: Basic Mixing Rule Model Results – Carbon Fiber Composites
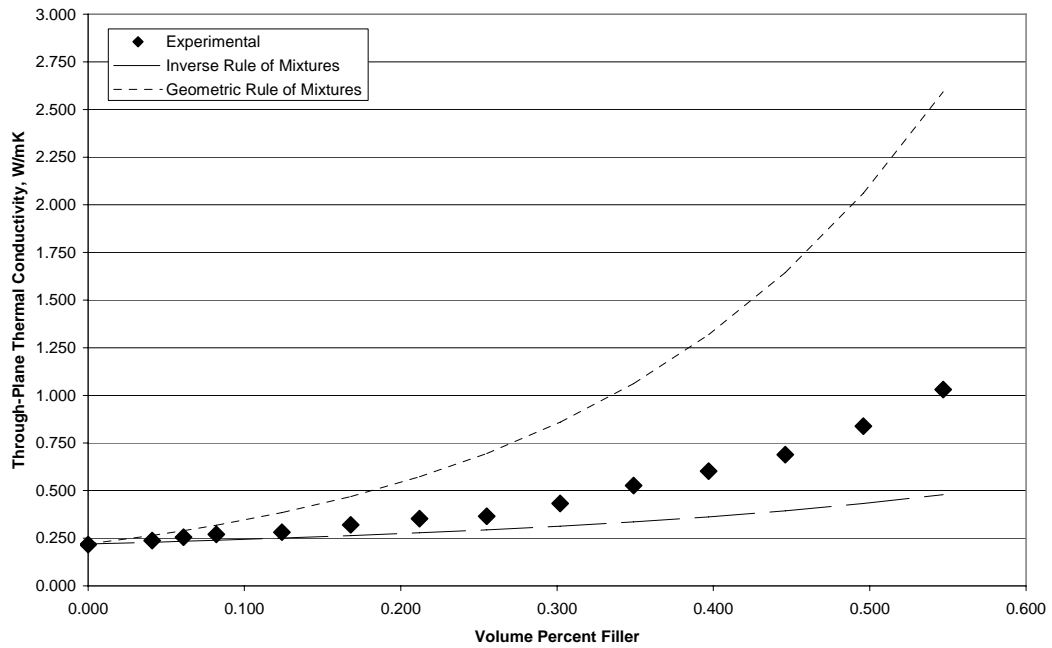
Figure 7.1-5: Selected Basic Mixing Rule Model Results – Carbon Fiber Composites

7-9

Section 7.2: Nielsen's Model and Variants

The advanced model used in this work is Nielsen's Model. A review of thermal conductivity models by Progelhof et al [7] was the impetus for the selection of the Nielsen Model in work by Weber et al [5-6]. It was decided to continue with this model for this work to see how well the model adapted to higher volume fractions of filler than was studied by Weber et al [5-6].

The base equations for the Nielsen Model are as follows:

$$\frac{K}{k_1} = \frac{1 + AB\phi_2}{1 - B\psi\phi_2} \tag{7.6a}$$

$$A = k_E - 1 \tag{7.6b}$$

$$B = \frac{\frac{k_2}{k_1} - 1}{\frac{k_2}{k_1} + A} \tag{7.6c}$$

$$\psi \cong 1 + \frac{1 - \phi_m}{\phi_m^2}\phi_2 \tag{7.6d}$$

'A' is a function of the aspect ratio and orientation of the filler and is related to the generalized Einstein coefficient, 'k_E'. 'B' is a factor that accounts for the relative thermal conductivity of the two components. 'ψ' is a factor that accounts for the maximum packing fraction of the filler, 'ϕ_m'. The term '$\psi\phi_2$' approaches 1.0 when $\phi_2 = \phi_m$.

McGee and McCullough [8] proposed a variant equation to determine ψ:

$$\psi \cong 1 + \frac{\phi_1}{\phi_m}\left[\phi_m\phi_2 + (1 - \phi_m)\phi_1\right] \tag{7.6e}$$

Equations 7.6a-c and 7.6e comprise the Modified Nielsen Model.

Work by Weber et al [5-6] hinted at the potential for further optimizing the accuracy of the Nielsen Model and Modified Nielsen Model by varying the 'A' and 'ϕ_m'

parameters to enhance the fit of the model to the data. This previous work determined

that the best course of action was to optimize the 'A' parameter and to leave the 'ϕ_m' term

as tabulated; as such, two cases of the Nielsen Model and Modified Nielsen Model were

run – one with the tabulated values for 'A' and one with 'A' solved for to minimize the

sum of squares error term. These are given the following names: Nielsen Model for the

literature 'A' value and the original 'ψ' term, Modified Nielsen Model for the literature

'A' value and the modified 'ψ' term, Optimized Nielsen Model for the literature 'A'

value and the original 'ψ' term, and the Optimized Modified Nielsen Model for the

optimized 'A' value and the modified 'ψ' term.

Table 7.2-1 is a listing of 'A' and 'ϕ_m' parameters used and/or determined in this

work. In the optimized cases, this 'A' parameter is a calculated value, in the non-

optimized cases, it is a literature value [9-10].

Table 7.2-1: Nielsen Model Parameters [9-10]

Carbon Filler	Literature 'ϕ_m'	Literature 'A'	Optimized Nielsen Model 'A'	Optimized Modified Nielsen Model 'A'
Ketjenblack EC-600 JD Carbon Black	0.637	1.5	47.3142	41.5020
Thermocarb TC-300 Synthetic Graphite	0.637	1.58	0.0000	1.8538
Fortafil 243 Carbon Fiber	0.520	4.29	0.0000	0.0754

Section 7.3: Nielsen's Model and Variants Results

Section 7.3.1: Carbon Black Advanced Model Results

Table 7.3-1 is a summary of the results of the four modeling cases performed on the carbon black composite. The Modified Nielsen Model performed better than the Nielsen Model with or without optimization, though not appreciably so. The optimization enhanced the degree of fit of the model to the data by approximately a factor of 5 in both cases. However, in optimization the value of 'A' ballooned from the literature value of 1.5 to experimental values of 47.3 and 41.5 (unmodified and modified cases, respectively).

Table 7.3-1: Error Analysis - Nielsen's Model, Carbon Black Composites

	Nielsen's Model	Optimized Nielsen's Model
EAV SS	0.039807	0.000701
EAV ε	0.053869	0.000948
	Modified Nielsen's Model	Optimized Modified Nielsen's Model
EAV SS	0.032807	0.000691
EAV ε	0.044397	0.000935

Figure 7.3-1 is a graphical comparison of the model results to the experimental data. The unoptimized models tend to underpredict the thermal conductivity of the composite; the optimized models follow it more closely.
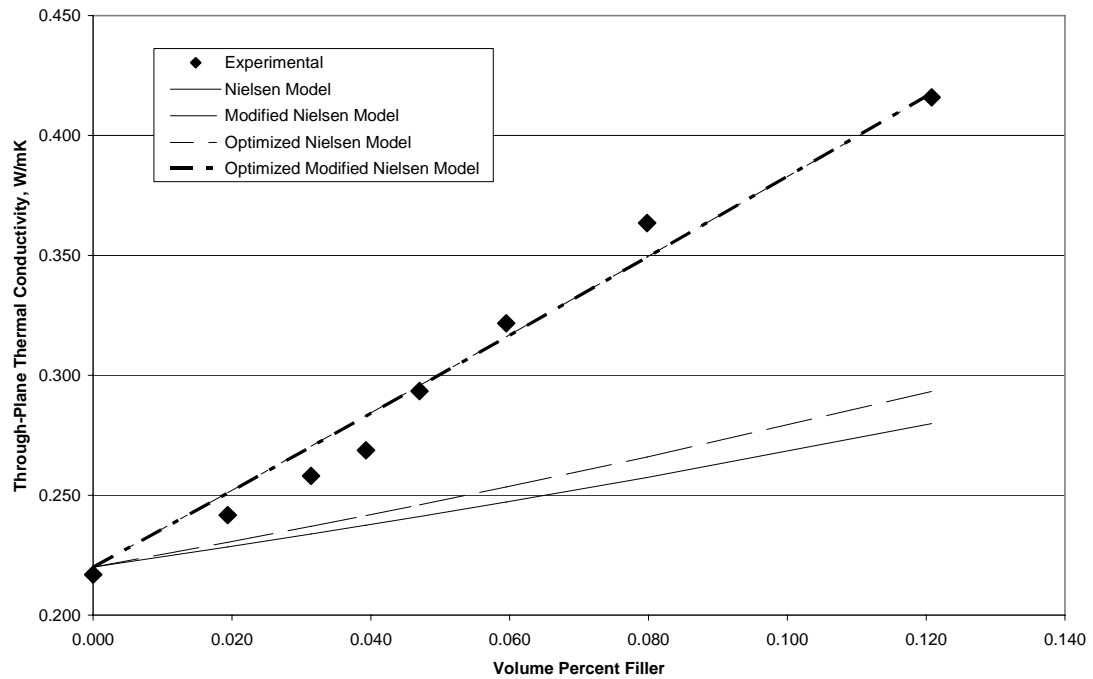
Figure 7.3-1: Advanced Model Results – Carbon Black Composites

Section 7.3.2: Synthetic Graphite Advanced Model Results

Table 7.3-2 is a summary of the results of the four modeling cases performed on the synthetic graphite composite. The Modified Nielsen Model performed appreciably better than the Nielsen Model with or without optimization. A large part of this can be traced to a failing of the Nielsen Model – the method of calculation of 'ψ' leads to a prediction of a negative thermal conductivity at the 75 wt% composite, which introduces a large (by comparison to the other points) difference between experimental and theoretical values, which is then squared. More than 95% of the value of the sum of squares value in the Nielsen Model cases can be attributed to this last data point. The optimization enhanced the degree of fit of the model to the data by approximately a factor of 3 in the case of Nielsen's Model and 1.2 in the case of the Modified Nielsen's Model

in both cases. In optimization the value of 'A' from the literature value of 1.5 to

experimental values of 0 and 1.8538 (unmodified and modified cases, respectively). The

result of 0 in the unmodified case can be attributed to the negative result it produces at 75

wt% filler.

Table 7.3-2: Error Analysis - Nielsen's Model, Synthetic Graphite Composites

	Nielsen's Model	Optimized Nielsen's Model
EBV SS	284.010	91.8511
EBV ε	11.8640	3.83693
	Modified Nielsen's Model	Optimized Modified Nielsen's Model
EBV SS	0.723381	0.597762
EBV ε	0.030218	0.024971

Figure 7.3-2 is a graphical comparison of the model results to the experimental

data. All of the models tend to underpredict the thermal conductivity of the composite

until high filler loadings; the optimized models follow it more closely.
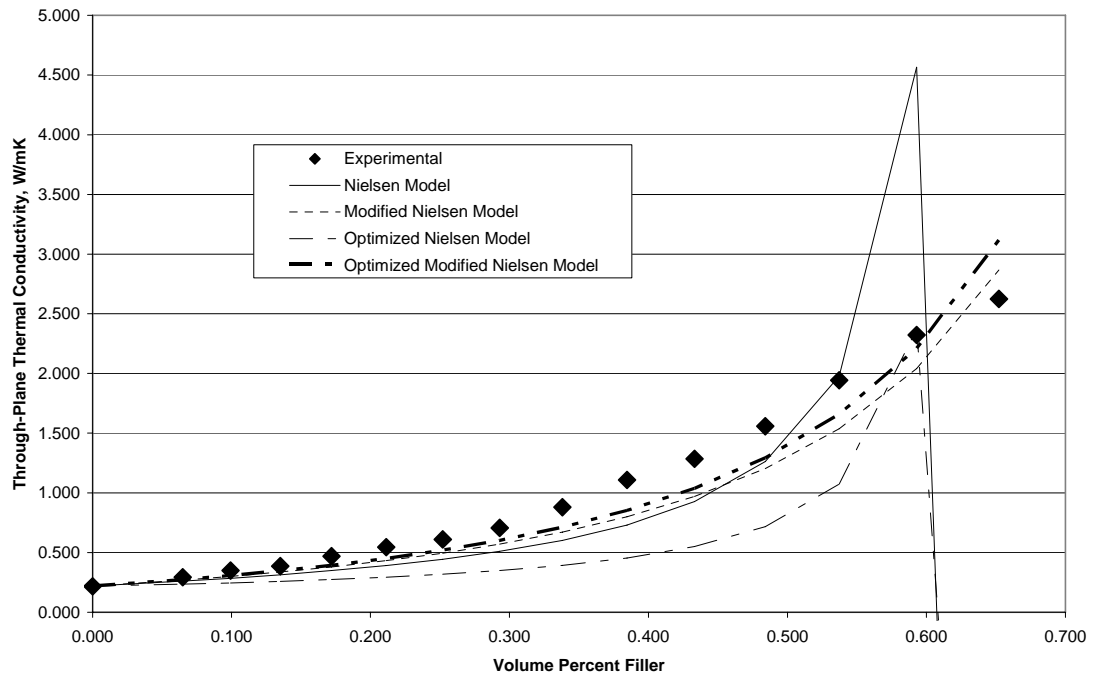
Figure 7.3-2: Advanced Model Results – Synthetic Graphite Composites

Section 7.3.3: Carbon Fiber Advanced Model Results

Table 7.3-3 is a summary of the results of the four modeling cases performed on

the synthetic graphite composite. The Modified Nielsen Model performed appreciably

better than the Nielsen Model with or without optimization. A large part of this can be

traced to a failing of the Nielsen Model – the method of calculation of 'ψ' leads to a

prediction of a negative thermal conductivity at the 60 wt% composite, which introduces

a large (by comparison to the other points) difference between experimental and

theoretical values, which is then squared. More than 95% of the value of the sum of

squares value in the Nielsen Model cases can be attributed to this last data point. The

optimization enhanced the degree of fit of the model to the data by approximately a factor

of 35 in the case of Nielsen's Model and 3600 in the case of the Modified Nielsen's

Model in both cases. In optimization the value of 'A' from the literature value of 4.29 to

experimental values of 0 and 0.0754 (unmodified and modified cases, respectively). The

result of 0 in the unmodified case can be attributed to the negative result it produces at 60

wt% filler.

Table 7.3-3: Error Analysis - Nielsen's Model, Carbon Fiber Composites

	Nielsen's Model	Optimized Nielsen's Model
EHV SS	799.730	23.0534
EHV ε	213.537	6.15553
	Modified Nielsen's Model	Optimized Modified Nielsen's Model
EHV SS	5.80270	0.001609
EHV ε	1.54939	0.000430

Figure 7.3-3 is a graphical comparison of the model results to the experimental

data. The unoptimized models tend to overpredict the thermal conductivity of the

composite; the optimized models follow it more closely. Note that the Optimized

Nielsen's Model begins to lose fit and overpredict at ~45 vol% (50 wt%).
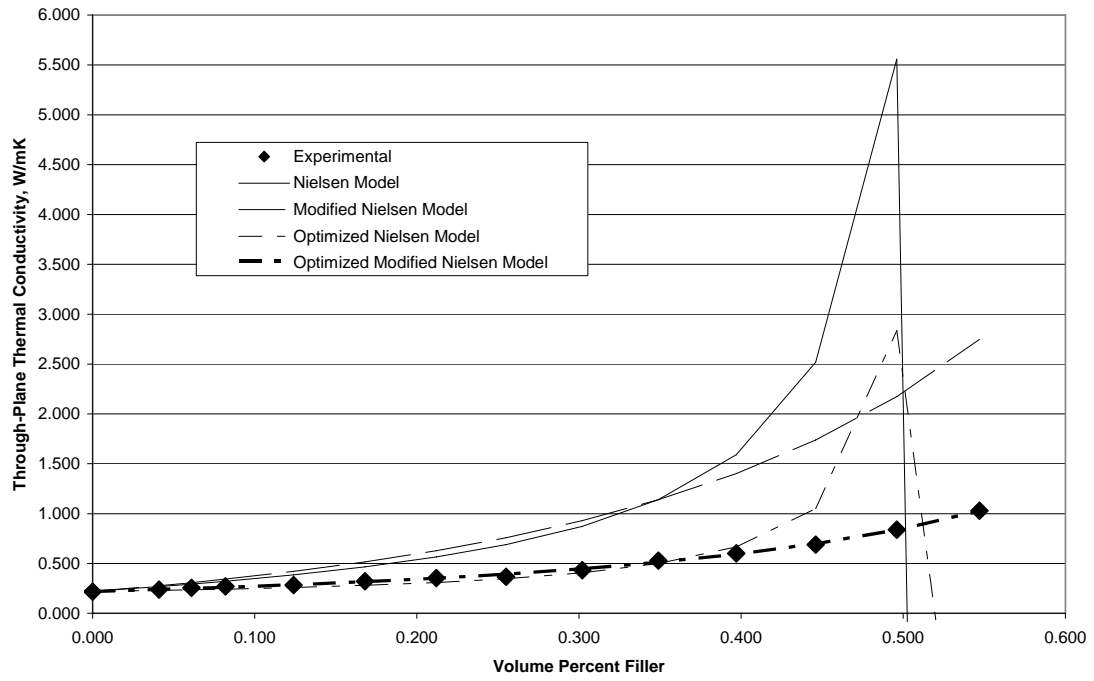
Figure 7.3-3: Advanced Model Results – Carbon Fiber Composites

Section 7.4: Modeling Summary

Looking at the basic models, the Rule of Mixtures provided the best model fit to the experimental data obtained from the carbon black composites, while the Inverse Rule of Mixtures provided the best model fit to the experimental data obtained from the synthetic graphite and carbon black composites. However, none of these fits were comparable to that provided by the Optimized Modified Nielsen Model, which was the best model fit to the experimental data in all cases. The unmodified Nielsen Model cases broke down when the volume fraction of filler surpassed the theoretical maximum packing fraction for that filler; this may be a good area for exploration in future work to determine whether or not the theoretical maximum packing fractions are valid for the materials being used.

Section 7.5: References

1. Ticona Vectra Liquid Crystal Polymer (LCP) Product Information, Ticona, Summit, NJ, 07901, 2000.

2. Akzo Nobel Electrically Conductive Ketjenblack Product Literature, Akzo Nobel.

3. Asbury Carbons Product Information, Asbury, NJ, 08802 (2004).

4. Akzo Nobel, "Fortafil Carbon Fibers", Fortafil Fibers, Inc., 8870 Cedar Springs Lane, Suite 8, Knoxville, TN 37923.

5. E. H. Weber, M. L. Clingerman, and J. A. King, "Thermally Conductive Nylon 6,6 and Polycarbonate Based Resin. Part 1: Synergistic Effects of Carbon Fillers", Journal of Applied Polymer Science, Vol. 88, pp. 112-122, 2003.

6. E. H. Weber, M. L. Clingerman, and J. A. King, "Thermally Conductive Nylon 6,6 and Polycarbonate Based Resin. Part 2: Modelling", Journal of Applied Polymer Science, Vol. 88, pp. 123-130, 2003.

7. R. C. Progelhof, J. L. Throne, and R. R. Ruetsch, "Methods of Predicting Thermal Conductivity of Composite Systems: A Review". *Reg. Tech. Cond. – Soc. Plast. Eng*, 1975, pp. 221-257.

8. R. McCullough, "Generalized Combining Rules for Predicting Transport Properties of Composite Materials". *Composites Science and Technology*, Vol. 22, 1985.

9. L. E. Nielsen, "The Thermal and Electrical Conductivity of Two-Phase Systems". *I&EC Fundamentals*, Vol. 13, No. 1, 1974, pp. 17-20.

10. Bigg, D. M. Polym Compos 1986, 7, 125.

Chapter 8:   Summary and Future Work

Section 8.1: Impact of Carbon Black on Thermal Conductivity

As discussed in Chapter 4, 0 – 15wt% Ketjenblack EC-600 JD was added to

Vectra A950RX LCP; the thermal conductivity of the resulting composites was measured

in the through-plane direction. The through-plane thermal conductivity varied from 0.22

W/mK at the minimum loading to 0.42 W/mK at the maximum loading. This increase in

through-plane thermal conductivity was the greatest of the three single-filler composites

studied over the 0 – 15wt% range; however, as noted earlier, testing of higher wt%

loadings of this filler was not possible. This is due to the very large increase in viscosity

that this filler imparts to the composite material, even at very low filler loadings.

Section 8.2: Impact of Carbon Particle on Thermal Conductivity

Four carbon particles (two synthetic graphites, one natural flake graphite and one

calcined needle coke) were screened at 40, 60 and 70 wt% loadings in Vectra A950RX

LCP; the thermal conductivity of the resulting composites was measured in the through-

plane direction. The results of this screening study are discussed in Chapter 4; it was

noted that at every loading level, Thermocarb TC-300 Synthetic Graphite had the greatest

effect on increasing the through-plane thermal conductivity of the composite. On the

basis of these results, a second study was conducted using 0 – 75 wt% Thermocarb in

Vectra; the thermal conductivity of the resulting composites was measured in both the

through-plane and in-plane directions. The full results of this study are discussed in

Chapter 5; in summary, the through-plane thermal conductivity ranged from 0.22 W/mK

at 0 wt% filler loading to 2.624 W/mK at 75 wt% filler loading, while the in-plane

thermal conductivity ranged from 0.22 W/mK at 0 wt% filler loading to 48.07 W/mK at 75 wt% filler loading. These effects are the largest positive improvement shown to thermal conductivity for any of the fillers studied.

Section 8.3: Impact of Carbon Fiber on Thermal Conductivity

Fortafil 243 Carbon Fiber was studied at filler loading of 0 – 60 wt% filler in Vectra A950RX LCP; the thermal conductivity of the resulting composites was measured in both the through-plane and in-plane directions. Full results of this study are discussed in Chapter 6; in summary, the through-plane and in-plane thermal conductivities were 0.22 W/mK at 0 wt% filler loading and ranged to 1.030 W/mK in the through-plane direction and 2.459 W/mK in the in-plane direction at 60 wt% filler loading. These effects are not as significant as the ones shown by the synthetic graphite as discussed in Chapter 5; however, the geometry of the carbon fiber may be of aid in improving the mechanical properties of a multiple-composite filler.

Section 8.4: Summary of Model Results

Of the three basic thermal conductivity models analyzed, the Rule of Mixtures model was the best fit for the carbon black composites while the Inverse Rule of Mixtures model was the best fit for the synthetic graphite and carbon fiber composites.

Several things were noted in the analysis of the Nielsen's Model cases. The one of most immediate importance was the fact that the Nielsen's Model, before and after optimization of the 'A' parameter, yielded a negative thermal conductivity result on the last data point of both the synthetic graphite and carbon fiber composites. The Modified Nielsen's Model did not have this problem. The next thing of note is that the Modified

Nielsen's Model outperformed the Nielsen's Model, even when the negative thermal

conductivity result data was dropped from the analysis. As expected, the Optimized

Modified Nielsen's Model outperformed the Modified Nielsen's Model; however, the

optimized 'A' parameters are radically different from the literature values of these

parameters in the cases of the carbon black and carbon fiber composites.

Section 8.5: Contributions

The first contribution to the field was made when analyzing the thermal

conductivity of the synthetic graphite composite. The three highest loading samples had

in-plane thermal conductivities greater than 20 W/mK. This is significant in the context

of the announced DOE target values for thermal conductivity in bipolar plates. These

highly-filled synthetic graphite composites are logical starting places for adjusting the

through-plane thermal conductivity of future composites.

The second contribution to the field was made while analyzing the data sets of the

synthetic graphite and carbon fiber composites. A relationship was found between the in-

plane thermal conductivity, the through-plane thermal conductivity, and the volume

fraction of filler in a composite sample. Further rearrangement yielded a model that

isolated the in-plane thermal conductivity in terms of those other two variables. This is

significant because most of the research and model-fitting in the field has been devoted to

through-plane thermal conductivity. An in-plane thermal conductivity model,

particularly one relating to the through-plane thermal conductivity, has not been as well

explored.

Section 8.6: Recommendations for Future Work

Based on the work done in the course of generating this dissertation, the following studies are recommended to follow up on questions raised in this work:

1. A 2^3 factorial design (two levels, three variables) should be conducted using the selected fillers to check for the presence or absence of synergistic or antagonistic effects on thermal conductivity. The three variables would be the three fillers; the two levels would be present at a designated level or totally absent.

2. More work should be done with the Modified Nielsen's Model to see if optimization is an accurate reflection on the physical reality of the system; in addition, work should be done to expand this model to account for multiple-filler systems. The work of Weber et al [1-2] is a good starting place for this.

3. A study should be performed to determine the effect that the method of manufacture has on the properties of the composite, if any. All samples studied in this work were prepared by injection molding, which has the effect of inducing at least some degree of orientation of the filler in the sample. Compression molding of composite pellets would be of a more random orientation, which could change the properties of the sample significantly – or possibly not at all.

Section 8.7: References

1.   E. H. Weber, M. L. Clingerman, and J. A. King, "Thermally Conductive Nylon 6,6 and Polycarbonate Based Resin. Part 1: Synergistic Effects of Carbon Fillers", <u>Journal of Applied Polymer Science</u>, Vol. 88, pp. 112-122, 2003.

2. E. H. Weber, M. L. Clingerman, and J. A. King, "Thermally Conductive Nylon 6,6 and Polycarbonate Based Resin. Part 2: Modelling", <u>Journal of Applied Polymer Science,</u> Vol. 88, pp. 123-130, 2003.

Chapter 9:   Appendices

Section 9.1: Extrusion Screw Designs
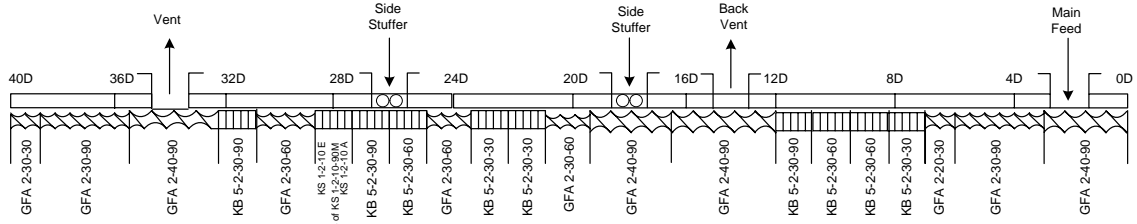
Figure 9.1-1: 5-12-2004 Screw Design (Used for extrusion in this work prior to May 2005)

For Screw Type Elements
GFA-d-ee-ff
G = co-rotating   F = conveying
A = free-meshing   d = number of threads
ee = pitch (length in millimeters for one complete rotation)

ff = length of screw elements in millimeters

Kneading disks
KBj-d-kk-ll   KB = kneading block
j = number of kneading segments   d = number of threads
k = length of kneading block in millimeters
l = twisting angle of the individual kneading segments

Kneading disks
KS1-d-hh-I   KS1 = Kneading disc
d = number of threads   h = length of kneading disc in millimeters
i = A for initial disc and E for end disc

Zones
0D to 4D is Zone 1 (water cooled, not heated)
4D to 8D is Zone 2 and Heating Zone 1
8D to 12D is Zone 3 and Heating Zone 2
12D to 16D is Zone 4 and Heating Zone 3
16D to 20D is Zone 5 and Heating Zone 4
20D to 24D is Zone 6 and Heating Zone 5
24D to 28D is Zone 7 and Heating Zone 6
28D to 32D is Zone 8 and Heating Zone 7
32D to 36D is Zone 9 and Heating Zone 8
36D to 40D is Zone 10 and Heating Zone 9
Nozzle is Heating Zone 10
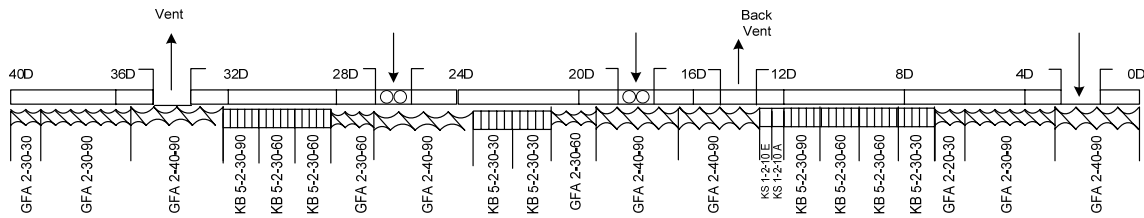
For Screw Type Elements
GFA-d-ee-ff
G = co-rotating
F = conveying
A = Free-Meshing
d = number of threads
ee = pitch (length in millimeters for one complete rotation
ff = length of screw elements in millimeters

Kneading Blocks
KBj-d-kk-ll
KB = kneading block
j = number of kneading segments
d = number of threads
k = length of kneading blocks in millimeters
l = twisting angle (°) of the individual kneading segments

Kneading Disks
KS1-d-hh-i
KS1 = Kneading disk
d = number of threads
h = length of kneading disk in millimeters
i = A for initial disk and E for end disk

Zones
0D to 4D is Zone 1
4D to 8D is Zone 2 and Heating Zone 1
8D to 12D is Zone 3 and Heating Zone 2
12D to 16D is Zone 4 and Heating Zone 3
16D to 20D is Zone 5 and Heating Zone 4
20D to 24D is Zone 6 and Heating Zone 5
24D to 28D is Zone 7 and Heating Zone 6
28D to 32 D is Zone 8 and Heating Zone 7
32D to 36D is Zone 9 and Heating Zone 8
36D to 40D is Zone 10 and Heating Zone 9
Nozzle is Heating Zone

Figure 9.1-2: 5-12-2004 Screw Design (Used for extrusion in this work prior to May 2005)

Section 9.2: Extrusion Conditions

Notes:

Naming Convention – EXVN where:

X denotes the filler (A, B, C, D, E, H).

        A denotes Ketjenblack EC 600-JD.

        B denotes Thermocarb TC-300 Synthetic Graphite.

        C denotes Asbury Synthetic Graphite 4012.

        D denotes Asbury Natural Flake Graphite 3160.

        E denotes Asbury Calcined Needle Coke F108A.

        H denotes Fortafil 243 Carbon Fiber.

V denotes the matrix material Vectra A950RX LCP.

N denotes the weight percent of the filler in Vectra.

An R at the end of the name denotes the first replicate run of the material.

All extrusion dates before 5/14/2005 use the Extrusion Date as shown in Section 9.1, Figure 9.1-1.

All extrusion dates after 5/14/2005 use the Extrusion Date as shown in Section 9.1, Figure 9.1-2.

Feeder Material Codes

EC600 denotes Ketjenblack EC 600-JD.

TC300 denotes Thermocarb TC-300 Synthetic Graphite.

4012 denotes Asbury Synthetic Graphite 4012.

3160 denotes Asbury Natural Flake Graphite 3160.

F108A denotes Asbury Calcined Needle Coke F108A.

F243 denotes Fortafil 243 Carbon Fiber.

Table 9.2-1: Extrusion Conditions, EAV Composites

Material Number	EAV2.5	EAV4R	EAV5R	EAV6
Extrusion Date	7/6/2004	7/7/2004	7/7/2004	7/7/2004
Extruder RPM	250	350	275	300
Motor Amperage, %	63	62		63-66
Melt Temperature, °C	328	320	335	332
Melt Pressure, psig	360-380	450	390-400	490-540
#3 Feeder Setting, lb/hr	40	40	38	31.33
Material in Feeder #3	Vectra	Vectra	Vectra	Vectra
#4 Feeder Setting, lb/hr	1.03	1.67	2	2
Material in Feeder #4	EC600	EC600	EC600	EC600
Vacuum Port	1 atm	1 atm	1 atm	1 atm
Zone 5 Side Stuffer Setting, rpm	300	300	300	300
Feeder at Zone 5	EC600	EC600	EC600	EC600
Feed Section Temperature				
Zone 1 Temperature, °C	230	230	230	230
Zone 2 Temperature, °C	250	250	250	250
Zone 3 Temperature, °C	265	257	263	260
Zone 4 Temperature, °C	267	257	263	260
Zone 5 Temperature, °C	268	257	263	260
Zone 6 Temperature, °C	270	258	269	260
Zone 7 Temperature, °C	270	265	270	264
Zone 8 Temperature, °C	270	273	270	270
Zone 9 Temperature, °C	270	280	270	270
Zone 10 Temperature, °C	270	270	270	270
Die Type and Gap	3x3mm	3x3mm	3x3mm	3x3mm
H_2O Bath/Conveyor	H_2O cooled	H_2O cooled	H_2O cooled	H_2O cooled
Output Rate, lbs/hr	41.03	40	40	33.33

Table 9.2-2: Extrusion Conditions, EAV Composites

Material Number	EAV7.5	EAV10	EAV15
Extrusion Date	7/7/2004	7/7/2004	7/7/2004
Extruder RPM	320	350	400
Motor Amperage, %	65-67	72-74	84
Melt Temperature, °C	323	320-325	325
Melt Pressure, psig	600-650	1150-1190	1660-1760
#3 Feeder Setting, lb/hr	24.67	18	11.33
Material in Feeder #3	Vectra	Vectra	Vectra
#4 Feeder Setting, lb/hr	2	2	2
Material in Feeder #4	EC600	EC600	EC600
Vacuum Port	1 atm	1 atm	1 atm
Zone 5 Side Stuffer Setting, rpm	300	300	300
Feeder at Zone 5	EC600	EC600	EC600
Feed Section Temperature			
Zone 1 Temperature, °C	230	230	230
Zone 2 Temperature, °C	250	250	250
Zone 3 Temperature, °C	258	257	257
Zone 4 Temperature, °C	258	257	257
Zone 5 Temperature, °C	258	257	257
Zone 6 Temperature, °C	259	258	258
Zone 7 Temperature, °C	259	258	258
Zone 8 Temperature, °C	265	263	263
Zone 9 Temperature, °C	270	270	270
Zone 10 Temperature, °C	270	270	270
Die Type and Gap	3x3mm	3x3mm	3x3mm
H_2O Bath/Conveyor	H_2O cooled	H_2O cooled	H_2O cooled
Output Rate, lbs/hr	26.67	20	13.33

Table 9.2-3: Extrusion Conditions, EBV Composites

Material Number	EBV10	EBV15	EBV20	EBV25
Extrusion Date	11/17/2004	11/17/2004	11/17/2004	6/7/2005
Extruder RPM	250	250	250	300
Motor Amperage, %	62	49	46	53
Melt Temperature, °C	315	323	325	333
Melt Pressure, psig	360	350	360	340
#3 Feeder Setting, lb/hr	4.3	4.3	5	10
Material in Feeder #3	TC300	TC300	TC300	TC300
#4 Feeder Setting, lb/hr	38.7	24.4	20	30
Material in Feeder #4	Vectra	Vectra	Vectra	Vectra
Vacuum Port	1 atm	1 atm	1 atm	1 atm
Zone 5 Side Stuffer Setting, rpm	300	300	300	300
Feeder at Zone 5	TC300	TC300	TC300	TC300
Feed Section Temperature				
Zone 1 Temperature, °C	230	230	230	230
Zone 2 Temperature, °C	250	250	250	250
Zone 3 Temperature, °C	258	258	258	258
Zone 4 Temperature, °C	258	258	258	258
Zone 5 Temperature, °C	258	258	258	258
Zone 6 Temperature, °C	259	259	259	259
Zone 7 Temperature, °C	259	259	259	259
Zone 8 Temperature, °C	265	265	265	265
Zone 9 Temperature, °C	270	270	270	270
Zone 10 Temperature, °C	270	270	270	270
Die Type and Gap	3x3mm	3x3mm	3x3mm	3x3mm
H_2O Bath/Conveyor	H_2O cooled	H_2O cooled	H_2O cooled	H_2O cooled
Output Rate, lbs/hr	43	28.7	25	40

Table 9.2-4: Extrusion Conditions, EBV Composites

Material Number	EBV30	EBV35	EBV40	EBV45
Extrusion Date	11/17/2004	6/7/2005	5/12/2004	6/7/2005
Extruder RPM	300	300	300	300
Motor Amperage, %	49	48	37	50
Melt Temperature, °C	324	330	336	323
Melt Pressure, psig	390	330	390	400
#3 Feeder Setting, lb/hr	10	12	12	15
Material in Feeder #3	TC300	TC300	TC300	TC300
#4 Feeder Setting, lb/hr	23.3	22.3	18	18.3
Material in Feeder #4	Vectra	Vectra	Vectra	Vectra
Vacuum Port	1 atm	1 atm	1 atm	1 atm
Zone 5 Side Stuffer Setting, rpm	300	300	300	300
Feeder at Zone 5	TC300	TC300	TC300	TC300
Feed Section Temperature				
Zone 1 Temperature, °C	230	230	230	230
Zone 2 Temperature, °C	250	250	250	250
Zone 3 Temperature, °C	258	258	280	258
Zone 4 Temperature, °C	258	258	285	258
Zone 5 Temperature, °C	258	258	285	258
Zone 6 Temperature, °C	259	259	285	259
Zone 7 Temperature, °C	259	259	285	259
Zone 8 Temperature, °C	265	265	285	265
Zone 9 Temperature, °C	270	270	285	270
Zone 10 Temperature, °C	270	270	285	270
Die Type and Gap	3x3mm	3x3mm	3x3mm	3x3mm
H_2O Bath/Conveyor	H_2O cooled	H_2O Cooled	H_2O Cooled	H_2O Cooled
Output Rate, lbs/hr	33.3	34.3	30	33.3

Table 9.2-5: Extrusion Conditions, EBV Composites

Material Number	EBV50	EBV50R	EBV55	EBV60
Extrusion Date	12/1/2004	6/7/2005	12/1/2004	5/12/2004
Extruder RPM	320	300	350	346
Motor Amperage, %	51	48	51	40
Melt Temperature, °C	324	337	324	337
Melt Pressure, psig	520	490	590	650
#3 Feeder Setting, lb/hr	15	16	16	18
Material in Feeder #3	TC300	TC300	TC300	TC300
#4 Feeder Setting, lb/hr	15	13.1	13.1	12
Material in Feeder #4	Vectra	Vectra	Vectra	Vectra
Vacuum Port	1 atm	1 atm	1 atm	1 atm
Zone 5 Side Stuffer Setting, rpm	300	300	300	300
Feeder at Zone 5	TC300	TC300	TC300	TC300
Feed Section Temperature				
Zone 1 Temperature, °C	230	230	230	230
Zone 2 Temperature, °C	250	250	250	250
Zone 3 Temperature, °C	258	258	258	280
Zone 4 Temperature, °C	258	258	258	285
Zone 5 Temperature, °C	258	258	258	285
Zone 6 Temperature, °C	259	259	259	285
Zone 7 Temperature, °C	259	259	259	285
Zone 8 Temperature, °C	265	265	265	285
Zone 9 Temperature, °C	270	270	270	285
Zone 10 Temperature, °C	270	270	270	290
Die Type and Gap	3x3mm	3x3mm	3x3mm	3x3mm
H_2O Bath/Conveyor	H_2O Cooled	H_2O Cooled	H_2O Cooled	H_2O Cooled
Output Rate, lbs/hr	30	29.1	29.1	30

Table 9.2-6: Extrusion Conditions, EBV Composites

Material Number	EBV60R	EBV65	EBV70	EBV70R
Extrusion Date	6/7/2005	12/1/2004	12/1/2004	6/7/2005
Extruder RPM	350	400	400	400
Motor Amperage, %	50-54	49	46	43
Melt Temperature, °C	337	311	324	358
Melt Pressure, psig	580	730	700-1000	730
#3 Feeder Setting, lb/hr	18	16	12	11
Material in Feeder #3	TC300	TC300	TC300	TC300
#4 Feeder Setting, lb/hr	12	8.6	5.1	4.7
Material in Feeder #4	Vectra	Vectra	Vectra	Vectra
Vacuum Port	1 atm	1 atm	1 atm	1 atm
Zone 5 Side Stuffer Setting, rpm	300	300	300	300
Feeder at Zone 5	TC300	TC300	TC300	TC300
Feed Section Temperature				
Zone 1 Temperature, °C	230	230	230	230
Zone 2 Temperature, °C	250	250	250	250
Zone 3 Temperature, °C	258	258	258	258
Zone 4 Temperature, °C	258	258	258	258
Zone 5 Temperature, °C	258	258	258	258
Zone 6 Temperature, °C	259	259	259	259
Zone 7 Temperature, °C	259	259	259	259
Zone 8 Temperature, °C	265	265	265	265
Zone 9 Temperature, °C	270	270	270	265
Zone 10 Temperature, °C	260	270	270	265
Die Type and Gap	3x3mm	3x3mm	3x3mm	3x3mm
H_2O Bath/Conveyor	H_2O Cooled	H_2O Cooled	H_2O Cooled	H_2O Cooled
Output Rate, lbs/hr	30	24.6	17.1	15.7

Table 9.2-7: Extrusion Conditions, EBV Composites

Material Number	EBV75	EBV75R	EBV80	EBV80R
Extrusion Date	12/1/2004	6/7/2005	5/12/2004	6/7/2005
Extruder RPM	400-450	420	450	450
Motor Amperage, %	45-48	46	34	44
Melt Temperature, °C	330	352	360	351
Melt Pressure, psig	1000-1300	1100	1140	1230
#3 Feeder Setting, lb/hr	14	14	16	16
Material in Feeder #3	TC300	TC300	TC300	TC300
#4 Feeder Setting, lb/hr	4.7	4.7	4	4
Material in Feeder #4	Vectra	Vectra	Vectra	Vectra
Vacuum Port	1 atm	1 atm	1 atm	1 atm
Zone 5 Side Stuffer Setting, rpm	300	300	300	300
Feeder at Zone 5	TC300	TC300	TC300	TC300
Feed Section Temperature				
Zone 1 Temperature, °C	230	230	230	230
Zone 2 Temperature, °C	250	250	250	250
Zone 3 Temperature, °C	258	258	280	258
Zone 4 Temperature, °C	258	258	285	258
Zone 5 Temperature, °C	258	258	285	258
Zone 6 Temperature, °C	259	259	285	259
Zone 7 Temperature, °C	259	259	285	255
Zone 8 Temperature, °C	265	260	285	257
Zone 9 Temperature, °C	270	260	285	257
Zone 10 Temperature, °C	270	250	320	250
Die Type and Gap	3x3mm	3x3mm	3x3mm	3x3mm
H_2O Bath/Conveyor	H_2O Cooled	H_2O Cooled	H_2O Cooled	H_2O Cooled
Output Rate, lbs/hr	18.7	18.7	20	20

Table 9.2-8: Extrusion Conditions, ECV Composites

Material Number	ECV40	ECV60	ECV70	ECV80
Extrusion Date	5/12/2004	5/12/2004	5/12/2004	5/12/2004
Extruder RPM	300	350	375	450
Motor Amperage, %	33	30	33	31
Melt Temperature, °C	305	300	312	360
Melt Pressure, psig	300	460	870	900-1100
#3 Feeder Setting, lb/hr	11	11	11	11
Material in Feeder #3	4012	4012	4012	4012
#4 Feeder Setting, lb/hr	16.5	7.3	4.7	2.75
Material in Feeder #4	Vectra	Vectra	Vectra	Vectra
Vacuum Port	1 atm	1 atm	1 atm	1 atm
Zone 5 Side Stuffer Setting, rpm	300	300	300	300
Feeder at Zone 5	4012	4012	4012	4012
Feed Section Temperature				
Zone 1 Temperature, °C	230	230	230	230
Zone 2 Temperature, °C	250	250	250	250
Zone 3 Temperature, °C	280	280	280	280
Zone 4 Temperature, °C	280	280	280	280
Zone 5 Temperature, °C	285	285	285	285
Zone 6 Temperature, °C	285	285	285	285
Zone 7 Temperature, °C	285	285	285	285
Zone 8 Temperature, °C	285	285	285	285
Zone 9 Temperature, °C	285	285	285	285
Zone 10 Temperature, °C	260	260	270	310
Die Type and Gap	3x3mm	3x3mm	3x3mm	3x3mm
H_2O Bath/Conveyor	H_2O Cooled	H_2O Cooled	H_2O Cooled	H_2O Cooled
Output Rate, lbs/hr	27.5	18.3	15.7	13.75

Table 9.2-9: Extrusion Conditions, EDV Composites

Material Number	EDV40	EDV60	EDV70
Extrusion Date	7/6/2004	7/6/2004	7/6/2004
Extruder RPM	300	350	375
Motor Amperage, %	40	40	35
Melt Temperature, °C	318	316	316
Melt Pressure, psig	360-380	540-570	700-760
#3 Feeder Setting, lb/hr	12	12	12
Material in Feeder #3	3160	3160	3160
#4 Feeder Setting, lb/hr	18	12	11
Material in Feeder #4	Vectra	Vectra	Vectra
Vacuum Port	1 atm	1 atm	1 atm
Zone 5 Side Stuffer Setting, rpm	300	300	300
Feeder at Zone 5	3160	3160	3160
Feed Section Temperature			
Zone 1 Temperature, °C	230	230	230
Zone 2 Temperature, °C	250	250	250
Zone 3 Temperature, °C	270	270	270
Zone 4 Temperature, °C	280	280	280
Zone 5 Temperature, °C	280	280	280
Zone 6 Temperature, °C	282	280	277
Zone 7 Temperature, °C	282	280	271
Zone 8 Temperature, °C	280	275	271
Zone 9 Temperature, °C	277	273	270
Zone 10 Temperature, °C	270	270	270
Die Type and Gap	3x3mm	3x3mm	3x3mm
H_2O Bath/Conveyor	H_2O Cooled	H_2O Cooled	H_2O Cooled
Output Rate, lbs/hr	30	30	15.7

Table 9.2-10: Extrusion Conditions, EEV Composites

Material Number	EEV40	EEV60	EEV70
Extrusion Date	7/6/2004	7/6/2004	7/6/2004
Extruder RPM	300	350	375
Motor Amperage, %	39	40	34
Melt Temperature, °C	315	314	316
Melt Pressure, psig	340	440	510-530
#3 Feeder Setting, lb/hr	12	18	11
Material in Feeder #3	F108A	F108A	F108A
#4 Feeder Setting, lb/hr	18	12	4.7
Material in Feeder #4	Vectra	Vectra	Vectra
Vacuum Port	1 atm	1 atm	1 atm
Zone 5 Side Stuffer Setting, rpm	300	300	300
Feeder at Zone 5	F108A	F108A	F108A
Feed Section Temperature			
Zone 1 Temperature, °C	230	230	230
Zone 2 Temperature, °C	250	250	250
Zone 3 Temperature, °C	270	270	270
Zone 4 Temperature, °C	280	280	280
Zone 5 Temperature, °C	280	280	280
Zone 6 Temperature, °C	277	275	280
Zone 7 Temperature, °C	271	271	270
Zone 8 Temperature, °C	271	271	270
Zone 9 Temperature, °C	270	270	270
Zone 10 Temperature, °C	270	270	270
Die Type and Gap	3x3mm	3x3mm	3x3mm
H_2O Bath/Conveyor	H_2O Cooled	H_2O Cooled	H_2O Cooled
Output Rate, lbs/hr	30	30	15.7

Table 9.2-11: Extrusion Conditions, EHV Composites

Material Number	EHV5	EHV7.5	EHV10	EHV15
Extrusion Date	12/5/2005	12/5/2005	12/5/2005	12/5/2005
Extruder RPM	250	250	250	300
Motor Amperage, %	58	52	52-57	50
Melt Temperature, °C	325	315	321-323	325-328
Melt Pressure, psig	280	250	240-260	250-310
#3 Feeder Setting, lb/hr	2	2.5	3	5
Material in Feeder #3	F243	F243	F243	F243
#4 Feeder Setting, lb/hr	38	30.83	27	28.33
Material in Feeder #4	Vectra	Vectra	Vectra	Vectra
Vacuum Port	1 atm	1 atm	1 atm	1 atm
Zone 5 Side Stuffer Setting, rpm	300	300	300	300
Feeder at Zone 5	F243	F243	F243	F243
Feed Section Temperature				
Zone 1 Temperature, °C	230	230	230	230
Zone 2 Temperature, °C	250	250	250	250
Zone 3 Temperature, °C	255	255	255	255
Zone 4 Temperature, °C	255	255	255	255
Zone 5 Temperature, °C	255	255	255	255
Zone 6 Temperature, °C	255	255	255	255
Zone 7 Temperature, °C	255	255	255	255
Zone 8 Temperature, °C	255	255	255	255
Zone 9 Temperature, °C	255	255	255	255
Zone 10 Temperature, °C	250	250	250	250
Die Type and Gap	3x3mm	3x3mm	3x3mm	3x3mm
H_2O Bath/Conveyor	H_2O Cooled	H_2O Cooled	H_2O Cooled	H_2O Cooled
Output Rate, lbs/hr	40	32.83	30	33.33

Table 9.2-12: Extrusion Conditions, EHV Composites

Material Number	EHV20	EHV25	EHV30	EHV35
Extrusion Date	12/5/2005	12/5/2005	12/6/2005	12/6/2005
Extruder RPM	300	300	325	325
Motor Amperage, %	44-52	41-43	48-50	46-47
Melt Temperature, °C	326	322	334	334
Melt Pressure, psig	240	270-300	290-370	360-380
#3 Feeder Setting, lb/hr	6	6	9	10.5
Material in Feeder #3	F243	F243	F243	F243
#4 Feeder Setting, lb/hr	24	18	21	19.5
Material in Feeder #4	Vectra	Vectra	Vectra	Vectra
Vacuum Port	1 atm	1 atm	1 atm	1 atm
Zone 5 Side Stuffer Setting, rpm	300	300	300	300
Feeder at Zone 5	F243	F243	F243	F243
Feed Section Temperature				
Zone 1 Temperature, °C	230	230	230	230
Zone 2 Temperature, °C	250	250	250	250
Zone 3 Temperature, °C	255	255	255	255
Zone 4 Temperature, °C	255	255	255	255
Zone 5 Temperature, °C	255	255	255	255
Zone 6 Temperature, °C	255	255	255	255
Zone 7 Temperature, °C	255	255	255	255
Zone 8 Temperature, °C	255	255	250	250
Zone 9 Temperature, °C	255	255	250	250
Zone 10 Temperature, °C	250	250	210	210
Die Type and Gap	3x3mm	3x3mm	3x3mm	3x3mm
H_2O Bath/Conveyor	H_2O Cooled	H_2O Cooled	H_2O Cooled	H_2O Cooled
Output Rate, lbs/hr	30	24	30	30

Table 9.2-13: Extrusion Conditions, EHV Composites

Material Number	EHV40	EHV50	EHV50R	EHV55
Extrusion Date	12/6/2005	8/2/2005	2/22/2006	2/22/2006
Extruder RPM	350	250	350	350
Motor Amperage, %	46-48	50	49	49
Melt Temperature, °C	335	340	328	337
Melt Pressure, psig	380-400	490	420-500	500-600
#3 Feeder Setting, lb/hr	12	12.5	15	16.5
Material in Feeder #3	F243	F243	F243	F243
#4 Feeder Setting, lb/hr	18	12.5	15	13.5
Material in Feeder #4	Vectra	Vectra	Vectra	Vectra
Vacuum Port	1 atm	1 atm	1 atm	1 atm
Zone 5 Side Stuffer Setting, rpm	300	300	300	300
Feeder at Zone 5	F243	F243	F243	F243
Feed Section Temperature				
Zone 1 Temperature, °C	230	230	230	230
Zone 2 Temperature, °C	250	250	250	250
Zone 3 Temperature, °C	255	255	255	255
Zone 4 Temperature, °C	255	255	255	255
Zone 5 Temperature, °C	255	255	255	255
Zone 6 Temperature, °C	255	255	255	255
Zone 7 Temperature, °C	255	255	255	255
Zone 8 Temperature, °C	250	257	250	250
Zone 9 Temperature, °C	250	257	250	250
Zone 10 Temperature, °C	210	250	210	210
Die Type and Gap	3x3mm	3x3mm	3x3mm	3x3mm
H_2O Bath/Conveyor	H_2O Cooled	H_2O Cooled	Conveyor	Conveyor
Output Rate, lbs/hr	30	25	30	30

Table 9.2-14: Extrusion Conditions, EHV Composites

Material Number	EHV60	EHV60R
Extrusion Date	8/2/2005	2/22/2006
Extruder RPM	250	350
Motor Amperage, %	57	53
Melt Temperature, °C	340	347
Melt Pressure, psig	940-1000	700-1000
#3 Feeder Setting, lb/hr	15	18
Material in Feeder #3	F243	F243
#4 Feeder Setting, lb/hr	10	12
Material in Feeder #4	Vectra	Vectra
Vacuum Port	1 atm	1 atm
Zone 5 Side Stuffer Setting, rpm	300	300
Feeder at Zone 5	F243	F243
Feed Section Temperature		
Zone 1 Temperature, °C	230	230
Zone 2 Temperature, °C	250	250
Zone 3 Temperature, °C	255	255
Zone 4 Temperature, °C	255	255
Zone 5 Temperature, °C	255	255
Zone 6 Temperature, °C	255	255
Zone 7 Temperature, °C	255	255
Zone 8 Temperature, °C	257	257
Zone 9 Temperature, °C	257	257
Zone 10 Temperature, °C	250	250
Die Type and Gap	3x3mm	3x3mm
H_2O Bath/Conveyor	H_2O Cooled	Conveyor
Output Rate, lbs/hr	25	30

Section 9.3:   Injection Molding Conditions

Notes:

Naming Convention – EXVN where:

X denotes the filler (A, B, C, D, E, H).

   A denotes Ketjenblack EC 600-JD.

   B denotes Thermocarb TC-300 Synthetic Graphite.

   C denotes Asbury Synthetic Graphite 4012.

   D denotes Asbury Natural Flake Graphite 3160.

   E denotes Asbury Calcined Needle Coke F108A.

   H denotes Fortafil 243 Carbon Fiber.

V denotes the matrix material Vectra A950RX LCP.

N denotes the weight percent of the filler in Vectra A950RX LCP.

An R at the end of the name denotes the first replicate run of the material.

An RR at the end of the name denotes the second replicate run of the material.

Table 9.3-1: Injection Molding Conditions for EVRR and EAV Composites

Notation	Injection Molding Conditions	EVRR	EAV2.5	EAV4R	EAV5R	EAV6
T_{mold}	Mold Temperature (F)	190	190	190	190	190
E1	Zone 1 Temperature (F) (nozzle)	580	600	600	600	600
E2	Zone 2 Temperature (F)	545	545	545	545	545
E3	Zone 3 Temperature (F)	545	545	545	545	545
E4	Zone 4 Temperature (F) (feed zone)	530	530	530	530	530
P1	Injection pressure (psi)	9044	9044	11305	11305	11305
P2	Hold Pressure (psi)	9044	9044	11305	11305	11305
P7	Back Pressure (psi)	45.22	45.22	45.22	45.22	45.22
S1	Shot size (mm)	37	47	44	44	45
S2	Shot before (mm)	0	1	1	1	1
S3	Shot after (mm)	0	1	1	1	1
S6	Width of mold (mm)	196	196	196	196	196
S8	Screw Position to switch (mm)	15	15	15	15	15
T1	Injection Time (s)	2	2	2	2	2
T2	Cool Time (s)	6	20	20	20	20
T3	Interval Time (s)	2	2	2	2	2
T6	Retraction Time (s)	0	1	1	1	1
T7	Nozzle Retraction Delay Time (s)	0	0	0	0	0
T8	Injection Delay Time (s)	0	0	0	0	0
T9	Charge Delay Time (s)	0	1	1	1	1
V1	Injection Velocity (mm^3/s)	100909	96832	96832	96832	96832
V6	Screw Rotation (rpm)	288	96	96	96	96
V9	Retraction Velocity (rpm)	288	160	160	160	160
V10	Advance Velocity (rpm)	288	160	160	160	160
V11	Retraction Velocity (rpm)	288	160	160	160	160
CF	Clamp Force (US tons)	80	80	80	80	80

Table 9.3-2: Injection Molding Conditions for EVRR and EAV Composites

Notation	Injection Molding Conditions	EAV7.5	EAV10	EAV15
T_{mold}	Mold Temperature (F)	190	190	200
E1	Zone 1 Temperature (F) (nozzle)	600	640	675
E2	Zone 2 Temperature (F)	585	600	650
E3	Zone 3 Temperature (F)	585	585	590
E4	Zone 4 Temperature (F) (feed zone)	530	550	550
P1	Injection pressure (psi)	11305	16957.5	22383.9
P2	Hold Pressure (psi)	11305	16957.5	22383.9
P7	Back Pressure (psi)	45.22	45.22	45.22
S1	Shot size (mm)	48	56	35
S2	Shot before (mm)	1	1	0
S3	Shot after (mm)	1	1	0
S6	Width of mold (mm)	196	196	196
S8	Screw Position to switch (mm)	15	15	15
T1	Injection Time (s)	2	2	2
T2	Cool Time (s)	20	20	12
T3	Interval Time (s)	2	2	2
T6	Retraction Time (s)	1	1	0
T7	Nozzle Retraction Delay Time (s)	0	0	0
T8	Injection Delay Time (s)	0	0	0
T9	Charge Delay Time (s)	1	1	1
V1	Injection Velocity (mm^3/s)	96832	96832	100909
V6	Screw Rotation (rpm)	96	96	288
V9	Retraction Velocity (rpm)	160	160	288
V10	Advance Velocity (rpm)	160	160	288
V11	Retraction Velocity (rpm)	160	160	288
CF	Clamp Force (US tons)	80	80	80

Table 9.3-3: Injection Molding Conditions for EBV Composites

Notation	Injection Molding Conditions	EBV10	EBV15	EBV20	EBV25	EBV30
T_{mold}	Mold Temperature (F)	190	190	190	190	190
E1	Zone 1 Temperature (F) (nozzle)	580	580	580	580	580
E2	Zone 2 Temperature (F)	545	545	545	545	545
E3	Zone 3 Temperature (F)	545	545	545	545	545
E4	Zone 4 Temperature (F) (feed zone)	530	530	530	530	530
P1	Injection pressure (psi)	9044	9044	10174.5	10174.5	10174.5
P2	Hold Pressure (psi)	9044	9044	10174.5	10174.5	10174.5
P7	Back Pressure (psi)	45.22	45.22	45.22	45.22	45.22
S1	Shot size (mm)	38	38	38	38	38
S2	Shot before (mm)	0	0	0	0	0
S3	Shot after (mm)	0	0	0	0	0
S6	Width of mold (mm)	196	196	196	196	196
S8	Screw Position to switch (mm)	15	15	15	15	15
T1	Injection Time (s)	2	2	2	2	2
T2	Cool Time (s)	6	6	6	6	6
T3	Interval Time (s)	2	2	2	2	2
T6	Retraction Time (s)	0	0	0	0	0
T7	Nozzle Retraction Delay Time (s)	0	0	0	0	0
T8	Injection Delay Time (s)	0	0	0	0	0
T9	Charge Delay Time (s)	0	0	0	0	0
V1	Injection Velocity (mm^3/s)	100909	100909	100909	100909	100909
V6	Screw Rotation (rpm)	288	288	288	288	288
V9	Retraction Velocity (rpm)	288	288	288	288	288
V10	Advance Velocity (rpm)	288	288	288	288	288
V11	Retraction Velocity (rpm)	288	288	288	288	288
CF	Clamp Force (US tons)	80	80	80	80	80

Table 9.3-4: Injection Molding Conditions for EBV Composites

Notation	Injection Molding Conditions	EBV35	EBV40	EBV45	EBV55	EBV60
T_{mold}	Mold Temperature (F)	190	190	190	190	190
E1	Zone 1 Temperature (F) (nozzle)	580	560	625	650	610
E2	Zone 2 Temperature (F)	545	545	600	625	585
E3	Zone 3 Temperature (F)	545	545	550	600	585
E4	Zone 4 Temperature (F) (feed zone)	530	530	530	550	550
P1	Injection pressure (psi)	10174.5	9044	10174.5	9044	18088
P2	Hold Pressure (psi)	10174.5	9044	10174.5	9044	18088
P7	Back Pressure (psi)	45.22	45.22	45.22	45.22	45.22
S1	Shot size (mm)	38	65	38	39	70
S2	Shot before (mm)	0	1	0	0	1
S3	Shot after (mm)	0	2	0	0	2
S6	Width of mold (mm)	196	N/A	196	196	196
S8	Screw Position to switch (mm)	15	15	15	15	15
T1	Injection Time (s)	2	2	2	2	2
T2	Cool Time (s)	6	30	6	6	30
T3	Interval Time (s)	2	2	2	2	2
T6	Retraction Time (s)	0	1	0	0	1
T7	Nozzle Retraction Delay Time (s)	0	0	0	0	0
T8	Injection Delay Time (s)	0	0.5	0	0	0.5
T9	Charge Delay Time (s)	0	1	0	0	1
V1	Injection Velocity (mm^3/s)	100909	96832	100909	100909	96832
V6	Screw Rotation (rpm)	288	96	288	288	96
V9	Retraction Velocity (rpm)	288	160	288	288	160
V10	Advance Velocity (rpm)	288	160	288	288	160
V11	Retraction Velocity (rpm)	288	160	288	288	160
CF	Clamp Force (US tons)	80	80	80	80	80

Table 9.3-5: Injection Molding Conditions for EBV Composites

Notation	Injection Molding Conditions	EBV65	EBV70	EBV75
T_{mold}	Mold Temperature (F)	190	190	190
E1	Zone 1 Temperature (F) (nozzle)	675	700	691
E2	Zone 2 Temperature (F)	650	675	675
E3	Zone 3 Temperature (F)	625	640	640
E4	Zone 4 Temperature (F) (feed zone)	550	550	530-550
P1	Injection pressure (psi)	14696.5	21479.5	22383.9
P2	Hold Pressure (psi)	14696.5	21479.5	22383.9
P7	Back Pressure (psi)	45.22	45.22	45.22
S1	Shot size (mm)	37.5	36	40
S2	Shot before (mm)	0	0	0
S3	Shot after (mm)	0	0	0
S6	Width of mold (mm)	196	196	196
S8	Screw Position to switch (mm)	15	15	15
T1	Injection Time (s)	2	2	2
T2	Cool Time (s)	6	6	6
T3	Interval Time (s)	2	2	2
T6	Retraction Time (s)	0	0	0
T7	Nozzle Retraction Delay Time (s)	0	0	0
T8	Injection Delay Time (s)	0	0	0
T9	Charge Delay Time (s)	0	0	0
V1	Injection Velocity (mm^3/s)	100909	100909	100909
V6	Screw Rotation (rpm)	288	288	288
V9	Retraction Velocity (rpm)	288	288	288
V10	Advance Velocity (rpm)	288	288	288
V11	Retraction Velocity (rpm)	288	288	288
CF	Clamp Force (US tons)	80	80	80

Table 9.3-6: Injection Molding Conditions for ECV Composites

Notation	Injection Molding Conditions	ECV40	ECV60	ECV70
T_{mold}	Mold Temperature (F)	190	190	190
E1	Zone 1 Temperature (F) (nozzle)	560	610	640
E2	Zone 2 Temperature (F)	545	585	630
E3	Zone 3 Temperature (F)	545	585	620
E4	Zone 4 Temperature (F) (feed zone)	530	550	560
P1	Injection pressure (psi)	9044	16957.5	22383.9
P2	Hold Pressure (psi)	9044	16957.5	22383.9
P7	Back Pressure (psi)	45.22	45.22	45.22
S1	Shot size (mm)	70	70	80
S2	Shot before (mm)	1	1	1
S3	Shot after (mm)	2	2	2
S6	Width of mold (mm)	196	196	196
S8	Screw Position to switch (mm)	15	15	15
T1	Injection Time (s)	2	2	2
T2	Cool Time (s)	30	30	30
T3	Interval Time (s)	2	2	2
T6	Retraction Time (s)	1	1	1
T7	Nozzle Retraction Delay Time (s)	0	0	0
T8	Injection Delay Time (s)	0.5	0.5	0.5
T9	Charge Delay Time (s)	1	1	1
V1	Injection Velocity (mm^3/s)	96832	96832	96832
V6	Screw Rotation (rpm)	96	96	96
V9	Retraction Velocity (rpm)	160	160	160
V10	Advance Velocity (rpm)	160	160	160
V11	Retraction Velocity (rpm)	160	160	160
CF	Clamp Force (US tons)	80	80	80

Table 9.3-7: Injection Molding Conditions for EDV Composites

Notation	Injection Molding Conditions	EDV40	EDV60	EDV70
T_{mold}	Mold Temperature (F)	190	190	190
E1	Zone 1 Temperature (F) (nozzle)	600	650	675
E2	Zone 2 Temperature (F)	585	625	650
E3	Zone 3 Temperature (F)	585	600	625
E4	Zone 4 Temperature (F) (feed zone)	540	550	550
P1	Injection pressure (psi)	9044	11305	14696.5
P2	Hold Pressure (psi)	9044	11305	14696.5
P7	Back Pressure (psi)	45.22	45.22	45.22
S1	Shot size (mm)	37	41	41
S2	Shot before (mm)	0	0	0
S3	Shot after (mm)	0	0	0
S6	Width of mold (mm)	196	196	196
S8	Screw Position to switch (mm)	15	15	15
T1	Injection Time (s)	2	2	2
T2	Cool Time (s)	6	6	6
T3	Interval Time (s)	2	2	2
T6	Retraction Time (s)	0	0	0
T7	Nozzle Retraction Delay Time (s)	0	0	0
T8	Injection Delay Time (s)	0	0	0
T9	Charge Delay Time (s)	0	0	0
V1	Injection Velocity (mm^3/s)	100909	100909	100909
V6	Screw Rotation (rpm)	288	288	288
V9	Retraction Velocity (rpm)	288	288	288
V10	Advance Velocity (rpm)	288	288	288
V11	Retraction Velocity (rpm)	288	288	288
CF	Clamp Force (US tons)	80	80	80

Table 9.3-8: Injection Molding Conditions for EEV Composites

Notation	Injection Molding Conditions	EEV40	EEV60	EEV70
T_{mold}	Mold Temperature (F)	190	190	190
E1	Zone 1 Temperature (F) (nozzle)	600	650	675
E2	Zone 2 Temperature (F)	585	625	650
E3	Zone 3 Temperature (F)	600	600	625
E4	Zone 4 Temperature (F) (feed zone)	550	550	550
P1	Injection pressure (psi)	9044	11305	14696.5
P2	Hold Pressure (psi)	9044	11305	14696.5
P7	Back Pressure (psi)	45.22	45.22	45.22
S1	Shot size (mm)	37	42	38
S2	Shot before (mm)	0	0	0
S3	Shot after (mm)	0	0	0
S6	Width of mold (mm)	196	196	196
S8	Screw Position to switch (mm)	15	15	15
T1	Injection Time (s)	2	2	2
T2	Cool Time (s)	6	6	6
T3	Interval Time (s)	2	2	2
T6	Retraction Time (s)	0	0	0
T7	Nozzle Retraction Delay Time (s)	0	0	0
T8	Injection Delay Time (s)	0	0	0
T9	Charge Delay Time (s)	0	0	0
V1	Injection Velocity (mm^3/s)	100909	100909	100909
V6	Screw Rotation (rpm)	288	288	288
V9	Retraction Velocity (rpm)	288	288	288
V10	Advance Velocity (rpm)	288	288	288
V11	Retraction Velocity (rpm)	288	288	288
CF	Clamp Force (US tons)	80	80	80

Table 9.3-9: Injection Molding Conditions for EHV Composites

Notation	Injection Molding Conditions	EHV5	EHV7.5	EHV10	EHV15	EHV20
T_{mold}	Mold Temperature (F)	190	190	190	190	190
E1	Zone 1 Temperature (F) (nozzle)	580	580	580	600	600
E2	Zone 2 Temperature (F)	545	545	545	550	550
E3	Zone 3 Temperature (F)	545	545	545	550	550
E4	Zone 4 Temperature (F) (feed zone)	530	530	530	530	530
P1	Injection pressure (psi)	9044	9044	9044	10174.5	10174.5
P2	Hold Pressure (psi)	9044	9044	9044	10174.5	10174.5
P7	Back Pressure (psi)	45.22	45.22	45.22	45.22	45.22
S1	Shot size (mm)	37	37	37	37	37
S2	Shot before (mm)	0	0	0	0	0
S3	Shot after (mm)	0	0	0	0	0
S6	Width of mold (mm)	196	196	196	196	196
S8	Screw Position to switch (mm)	15	15	15	15	15
T1	Injection Time (s)	2	2	2	2	2
T2	Cool Time (s)	6	6	6	6	6
T3	Interval Time (s)	2	2	2	2	2
T6	Retraction Time (s)	0	0	0	0	0
T7	Nozzle Retraction Delay Time (s)	0	0	0	0	0
T8	Injection Delay Time (s)	0	0	0	0	0
T9	Charge Delay Time (s)	0	0	0	0	0
V1	Injection Velocity (mm^3/s)	100909	100909	100909	100909	100909
V6	Screw Rotation (rpm)	288	288	288	288	288
V9	Retraction Velocity (rpm)	288	288	288	288	288
V10	Advance Velocity (rpm)	288	288	288	288	288
V11	Retraction Velocity (rpm)	288	288	288	288	288
CF	Clamp Force (US tons)	80	80	80	80	80

Table 9.3-10: Injection Molding Conditions for EHV Composites

Notation	Injection Molding Conditions	EHV25	EHV30	EHV35	EHV40	EHV45
T_{mold}	Mold Temperature (F)	190	190	190	190	190
E1	Zone 1 Temperature (F) (nozzle)	600	600	600	600	600
E2	Zone 2 Temperature (F)	550	550	550	550	550
E3	Zone 3 Temperature (F)	550	550	550	550	550
E4	Zone 4 Temperature (F) (feed zone)	530	530	530	530	530
P1	Injection pressure (psi)	10174.5	10174.5	10174.5	10174.5	11305
P2	Hold Pressure (psi)	10174.5	10174.5	10174.5	10174.5	11305
P7	Back Pressure (psi)	45.22	45.22	45.22	45.22	45.22
S1	Shot size (mm)	37	37	37	37	37
S2	Shot before (mm)	0	0	0	0	0
S3	Shot after (mm)	0	0	0	0	0
S6	Width of mold (mm)	196	196	196	196	196
S8	Screw Position to switch (mm)	15	15	15	15	15
T1	Injection Time (s)	2	2	2	2	2
T2	Cool Time (s)	6	6	6	6	6
T3	Interval Time (s)	2	2	2	2	2
T6	Retraction Time (s)	0	0	0	0	0
T7	Nozzle Retraction Delay Time (s)	0	0	0	0	0
T8	Injection Delay Time (s)	0	0	0	0	0
T9	Charge Delay Time (s)	0	0	0	0	0
V1	Injection Velocity (mm^3/s)	100909	100909	100909	100909	100909
V6	Screw Rotation (rpm)	288	288	288	288	288
V9	Retraction Velocity (rpm)	288	288	288	288	288
V10	Advance Velocity (rpm)	288	288	288	288	288
V11	Retraction Velocity (rpm)	288	288	288	288	288
CF	Clamp Force (US tons)	80	80	80	80	80

Table 9.3-11: Injection Molding Conditions for EHV Composites

Notation	Injection Molding Conditions	EHV50	EHV50R	EHV55	EHV60	EHV60R
T_{mold}	Mold Temperature (F)	190	220	220	190	220
E1	Zone 1 Temperature (F) (nozzle)	600	630	630	630	630
E2	Zone 2 Temperature (F)	550	615	615	615	615
E3	Zone 3 Temperature (F)	550	580	580	580	580
E4	Zone 4 Temperature (F) (feed zone)	530	530	530	530	530
P1	Injection pressure (psi)	10174.5	11305	11305	14696.5	14696.5
P2	Hold Pressure (psi)	10174.5	11305	11305	14696.5	14696.5
P7	Back Pressure (psi)	45.22	45.22	45.22	45.22	45.22
S1	Shot size (mm)	38	38	38	38	38
S2	Shot before (mm)	0	0	0	0	0
S3	Shot after (mm)	0	0	0	0	0
S6	Width of mold (mm)	196	196	196	196	196
S8	Screw Position to switch (mm)	15	15	15	15	15
T1	Injection Time (s)	2	2	2	2	2
T2	Cool Time (s)	6	6	6	6	6
T3	Interval Time (s)	2	2	2	2	2
T6	Retraction Time (s)	0	0	0	0	0
T7	Nozzle Retraction Delay Time (s)	0	0	0	0	0
T8	Injection Delay Time (s)	0	0	0	0	0
T9	Charge Delay Time (s)	0	0	0	0	0
V1	Injection Velocity (mm^3/s)	100909	100909	100909	100909	100909
V6	Screw Rotation (rpm)	288	288	288	288	288
V9	Retraction Velocity (rpm)	288	288	288	288	288
V10	Advance Velocity (rpm)	288	288	288	288	288
V11	Retraction Velocity (rpm)	288	288	288	288	288
CF	Clamp Force (US tons)	80	80	80	80	80

Section 9.4: TCA Through-Plane Thermal Conductivity

Table 9.4-1: Vectra A950RX LCP

Test Date	Sample Number	Through-Plane Thermal Conductivity (W/mK)	Temperature (^{o}C)
10/11/2004	EVR-TC-18	0.226	55
10/11/2004	EVR-TC-20	0.214	55
10/11/2004	EVR-TC-23	0.210	55
10/18/2004	EVR-TC-15	0.218	55
Average		0.217	
Standard Deviation		0.007	
Number of Samples		4	

Table 9.4-2: 2.5 wt% Ketjenblack EC600 JD / Vectra A950RX LCP

Test Date	Sample Number	Through-Plane Thermal Conductivity (W/mK)	Temperature (^{o}C)
10/11/2004	EAV2.5-TC-16	0.245	55
10/11/2004	EAV2.5-TC-19	0.242	55
10/11/2004	EAV2.5-TC-27	0.242	55
10/18/2004	EAV2.5-TC-24	0.239	55
Average		0.242	
Standard Deviation		0.002	
Number of Samples		4	

Table 9.4-3: 4 wt% Ketjenblack EC600 JD / Vectra A950RX LCP

Test Date	Sample Number	Through-Plane Thermal Conductivity (W/mK)	Temperature (^{o}C)
10/12/2004	EAV4R-TC-16	0.260	55
10/12/2004	EAV4R-TC-14	0.265	55
10/12/2004	EAV4R-TC-27	0.255	55
10/18/2004	EAV4R-TC-20	0.252	55
Average		0.258	
Standard Deviation		0.006	
Number of Samples		4	

Table 9.4-4: 5 wt% Ketjenblack EC600 JD / Vectra A950RX LCP

Test Date	Sample Number	Through-Plane Thermal Conductivity (W/mK)	Temperature (^{o}C)
10/12/2004	EAV5R-TC-17	0.277	55
10/12/2004	EAV5R-TC-22	0.272	55
10/12/2004	EAV5R-TC-27	0.270	55
10/18/2004	EAV5R-TC-14	0.256	55
Average		0.269	
Standard Deviation		0.009	
Number of Samples		4	

Table 9.4-5: 6 wt% Ketjenblack EC600 JD / Vectra A950RX LCP

Test Date	Sample Number	Through-Plane Thermal Conductivity (W/mK)	Temperature (^{o}C)
10/12/2004	EAV6-TC-13	0.296	55
10/12/2004	EAV6-TC-19	0.301	55
10/12/2004	EAV6-TC-36	0.292	55
10/18/2004	EAV6-TC-23	0.285	55
Average		0.293	
Standard Deviation		0.007	
Number of Samples		4	

Table 9.4-6: 7.5 wt% Ketjenblack EC600 JD / Vectra A950RX LCP

Test Date	Sample Number	Through-Plane Thermal Conductivity (W/mK)	Temperature (^{o}C)
10/12/2004	EAV7.5-TC-16	0.321	55
10/12/2004	EAV7.5-TC-20	0.330	55
10/12/2004	EAV7.5-TC-23	0.321	55
10/18/2004	EAV7.5-TC-26	0.315	55
Average		0.322	
Standard Deviation		0.006	
Number of Samples		4	

Table 9.4-7: 10 wt% Ketjenblack EC600 JD / Vectra A950RX LCP

Test Date	Sample Number	Through-Plane Thermal Conductivity (W/mK)	Temperature (^{o}C)
10/12/2004	EAV10-TC-23	0.365	55
10/12/2004	EAV10-TC-24	0.369	55
10/12/2004	EAV10-TC-32	0.375	55
10/19/2004	EAV10-TC-20	0.346	55
Average		0.364	
Standard Deviation		0.012	
Number of Samples		4	

Table 9.4-8: 15 wt% Ketjenblack EC600 JD / Vectra A950RX LCP

Test Date	Sample Number	Through-Plane Thermal Conductivity (W/mK)	Temperature (^{o}C)
10/13/2004	EAV15-TC-24	0.402	55
10/13/2004	EAV15-TC-26	0.407	55
10/19/2004	EAV15-TC-13	0.428	55
10/19/2004	EAV15-TC-18	0.427	55
Average		0.416	
Standard Deviation		0.013	
Number of Samples		4	

Table 9.4-9: 10 wt% Thermocarb TC300 / Vectra A950RX LCP

Test Date	Sample Number	Through-Plane Thermal Conductivity (W/mK)	Temperature (^{o}C)
3/24/2005	EBV10-TC-19	0.279	55
3/24/2005	EBV10-TC-16	0.303	55
3/24/2005	EBV10-TC-18	0.296	55
3/24/2005	EBV10-TC-28	0.296	55
Average		0.293	
Standard Deviation		0.010	
Number of Samples		4	

Table 9.4-10: 15 wt% Thermocarb TC300 / Vectra A950RX LCP

Test Date	Sample Number	Through-Plane Thermal Conductivity (W/mK)	Temperature (^{o}C)
3/24/2005	EBV15-TC-23	0.354	55
3/24/2005	EBV15-TC-19	0.355	55
3/24/2005	EBV15-TC-21	0.358	55
3/24/2005	EBV15-TC-28	0.330	55
Average		0.349	
Standard Deviation		0.013	
Number of Samples		4	

Table 9.4-11: 20 wt% Thermocarb TC300 / Vectra A950RX LCP

Test Date	Sample Number	Through-Plane Thermal Conductivity (W/mK)	Temperature (^{o}C)
3/24/2005	EBV20-TC-19	0.372	55
3/24/2005	EBV20-TC-22	0.395	55
3/24/2005	EBV20-TC-24	0.376	55
3/24/2005	EBV20-TC-25	0.397	55
3/24/2005	EBV20-TC-28	0.395	55
Average		0.387	
Standard Deviation		0.012	
Number of Samples		5	

Table 9.4-12: 25 wt% Thermocarb TC300 / Vectra A950RX LCP

Test Date	Sample Number	Through-Plane Thermal Conductivity (W/mK)	Temperature (^{o}C)
9/28/2005	EBV25-TC-18	0.483	55
9/28/2005	EBV25-TC-21	0.456	55
9/28/2005	EBV25-TC-15	0.477	55
9/28/2005	EBV25-TC-27	0.473	55
9/28/2005	EBV25-TC-24	0.460	55
Average		0.470	
Standard Deviation		0.012	
Number of Samples		5	

Table 9.4-13: 30 wt% Thermocarb TC300 / Vectra A950RX LCP

Test Date	Sample Number	Through-Plane Thermal Conductivity (W/mK)	Temperature (^{o}C)
3/24/2005	EBV30-TC-17	0.557	55
3/24/2005	EBV30-TC-19	0.518	55
3/24/2005	EBV30-TC-25	0.556	55
3/24/2005	EBV30-TC-29	0.554	55
Average		0.546	
Standard Deviation		0.019	
Number of Samples		4	

Table 9.4-14: 35 wt% Thermocarb TC300 / Vectra A950RX LCP

Test Date	Sample Number	Through-Plane Thermal Conductivity (W/mK)	Temperature (^{o}C)
9/28/2005	EBV35-TC-21	0.620	55
9/28/2005	EBV35-TC-15	0.593	55
9/28/2005	EBV35-TC-27	0.585	55
9/28/2005	EBV35-TC-18	0.623	55
9/28/2005	EBV35-TC-30	0.633	55
Average		0.611	
Standard Deviation		0.021	
Number of Samples		5	

Table 9.4-15: 40 wt% Thermocarb TC300 / Vectra A950RX LCP

Test Date	Sample Number	Through-Plane Thermal Conductivity (W/mK)	Temperature (^{o}C)
3/11/2005	EBV40-TC-20	0.720	55
3/11/2005	EBV40-TC-18	0.703	55
3/11/2005	EBV40-TC-16	0.695	55
3/11/2005	EBV40-TC-17	0.708	55
Average		0.706	
Standard Deviation		0.010	
Number of Samples		4	

Table 9.4-16: 45 wt% Thermocarb TC300 / Vectra A950RX LCP

Test Date	Sample Number	Through-Plane Thermal Conductivity (W/mK)	Temperature (^{o}C)
9/29/2005	EBV45-TC-15	0.859	55
9/29/2005	EBV45-TC-24	0.882	55
9/29/2005	EBV45-TC-18	0.929	55
9/29/2005	EBV45-TC-21	0.821	55
9/29/2005	EBV45-TC-30	0.911	55
Average		0.880	
Standard Deviation		0.043	
Number of Samples		5	

Table 9.4-17: 50 wt% Thermocarb TC300 / Vectra A950RX LCP

Test Date	Sample Number	Through-Plane Thermal Conductivity (W/mK)	Temperature (^{o}C)
3/14/2005	EBV50-TC-21	1.122	55
3/14/2005	EBV50-TC-13	1.141	55
3/14/2005	EBV50-TC-18	1.102	55
3/14/2005	EBV50-TC-16	1.068	55
Average		1.108	
Standard Deviation		0.031	
Number of Samples		4	

Table 9.4-18: 55 wt% Thermocarb TC300 / Vectra A950RX LCP

Test Date	Sample Number	Through-Plane Thermal Conductivity (W/mK)	Temperature (^{o}C)
3/14/2005	EBV55-TC-13	1.287	55
3/14/2005	EBV55-TC-21	1.314	55
3/14/2005	EBV55-TC-19	1.291	55
3/14/2005	EBV55-TC-30	1.249	55
Average		1.285	
Standard Deviation		0.027	
Number of Samples		4	

Table 9.4-19: 60 wt% Thermocarb TC300 / Vectra A950RX LCP

Test Date	Sample Number	Through-Plane Thermal Conductivity (W/mK)	Temperature (^{o}C)
3/14/2005	EBV60-TC-25	1.608	55
3/14/2005	EBV60-TC-28	1.561	55
3/14/2005	EBV60-TC-31	1.625	55
3/15/2005	EBV60-TC-14	1.518	55
3/15/2005	EBV60-TC-22	1.446	55
3/15/2005	EBV60-TC-31	1.498	55
3/15/2005	EBV60-TC-28	1.539	55
3/15/2005	EBV60-TC-25	1.673	55
Average		1.559	
Standard Deviation		0.074	
Number of Samples		8	

Table 9.4-20: 65 wt% Thermocarb TC300 / Vectra A950RX LCP

Test Date	Sample Number	Through-Plane Thermal Conductivity (W/mK)	Temperature (^{o}C)
3/15/2005	EBV65-TC-20	2.106	55
3/15/2005	EBV65-TC-22	2.025	55
3/15/2005	EBV65-TC-16	1.833	55
3/15/2005	EBV65-TC-24	1.809	55
3/15/2005	EBV65-TC-25	1.923	55
3/16/2005	EBV65-TC-31	1.870	55
3/16/2005	EBV65-TC-18	2.033	55
Average		1.943	
Standard Deviation		0.113	
Number of Samples		7	

Table 9.4-21: 70 wt% Thermocarb TC300 / Vectra A950RX LCP

Test Date	Sample Number	Through-Plane Thermal Conductivity (W/mK)	Temperature (^{o}C)
3/16/2005	EBV70-TC-25	2.246	55
3/16/2005	EBV70-TC-24	2.342	55
3/16/2005	EBV70-TC-31	2.464	55
3/17/2005	EBV70-TC-28	2.254	55
3/17/2005	EBV70-TC-20	2.398	55
3/17/2005	EBV70-TC-16	2.312	55
3/17/2005	EBV70-TC-19	2.242	55
Average		2.323	
Standard Deviation		0.085	
Number of Samples		7	

Table 9.4-22: 75 wt% Thermocarb TC300 / Vectra A950RX LCP

Test Date	Sample Number	Through-Plane Thermal Conductivity (W/mK)	Temperature (^{o}C)
3/18/2005	EBV75-TC-13	2.779	55
3/18/2005	EBV75-TC-15	2.629	55
3/18/2005	EBV75-TC-21	2.614	55
3/18/2005	EBV75-TC-14	2.513	55
3/18/2005	EBV75-TC-33	2.591	55
Average		2.625	
Standard Deviation		0.097	
Number of Samples		5	

Table 9.4-23: 40 wt% Asbury Synthetic Graphite 4012 / Vectra A950RX LCP

Test Date	Sample Number	Through-Plane Thermal Conductivity (W/mK)	Temperature (^{o}C)
6/9/2004	ECV40-TC-11	0.610	55
6/9/2004	ECV40-TC-13	0.628	55
6/10/2004	ECV40-TC-23	0.610	55
11/19/2004	ECV40-TC-21	0.610	55
Average		0.615	
Standard Deviation		0.009	
Number of Samples		4	

Table 9.4-24: 60 wt% Asbury Synthetic Graphite 4012 / Vectra A950RX LCP

Test Date	Sample Number	Through-Plane Thermal Conductivity (W/mK)	Temperature (^{o}C)
6/14/2004	ECV60-TC-16	1.517	55
6/14/2004	ECV60-TC-21	1.407	55
11/11/2004	ECV60-TC-20	1.503	55
11/29/2004	ECV60-TC-29	1.434	55
Average		1.465	
Standard Deviation		0.053	
Number of Samples		4	

Table 9.4-25: 70 wt% Asbury Synthetic Graphite 4012 / Vectra A950RX LCP

Test Date	Sample Number	Through-Plane Thermal Conductivity (W/mK)	Temperature (^{o}C)
6/14/2004	ECV70-TC-12	1.954	55
6/14/2004	ECV70-TC-15	2.087	55
6/15/2004	ECV70-TC-17	1.931	55
11/28/2004	ECV70-TC-20	2.203	55
Average		2.044	
Standard Deviation		0.126	
Number of Samples		4	

Table 9.4-26: 40 wt% Asbury 3160 Natural Flake Graphite / Vectra A950RX LCP

Test Date	Sample Number	Through-Plane Thermal Conductivity (W/mK)	Temperature (^{o}C)
10/7/2004	EDV40-TC-18	0.604	55
10/7/2004	EDV40-TC-20	0.571	55
10/7/2004	EDV40-TC-23	0.596	55
11/16/2004	EDV40-TC-29	0.599	55
Average		0.593	
Standard Deviation		0.015	
Number of Samples		4	

Table 9.4-27: 60 wt% Asbury 3160 Natural Flake Graphite / Vectra A950RX LCP

Test Date	Sample Number	Through-Plane Thermal Conductivity (W/mK)	Temperature (^{o}C)
10/5/2004	EDV60-TC-21	1.417	55
10/5/2004	EDV60-TC-23	1.328	55
10/5/2004	EDV60-TC-31	1.327	55
11/29/2004	EDV60-TC-24	1.436	55
Average		1.377	
Standard Deviation		0.058	
Number of Samples		4	

Table 9.4-28: 70 wt% Asbury 3160 Natural Flake Graphite / Vectra A950RX LCP

Test Date	Sample Number	Through-Plane Thermal Conductivity (W/mK)	Temperature (^{o}C)
10/5/2004	EDV70-TC-12	1.947	55
10/5/2004	EDV70-TC-27	2.075	55
10/5/2004	EDV70-TC-16	1.921	55
11/18/2004	EDV70-TC-25	1.844	55
Average		1.946	
Standard Deviation		0.096	
Number of Samples		4	

Table 9.4-29: 40 wt% Asbury F108A CNC / Vectra A950RX LCP

Test Date	Sample Number	Through-Plane Thermal Conductivity (W/mK)	Temperature (^{o}C)
9/30/2004	EEV40-TC-12	0.483	55
9/30/2004	EEV40-TC-16	0.477	55
9/30/2004	EEV40-TC-28	0.444	55
11/16/2004	EEV40-TC-23	0.504	55
Average		0.477	
Standard Deviation		0.025	
Number of Samples		4	

Table 9.4-30: 60 wt% Asbury F108A CNC / Vectra A950RX LCP

Test Date	Sample Number	Through-Plane Thermal Conductivity (W/mK)	Temperature (^{o}C)
9/30/2004	EEV60-TC-18	0.730	55
9/30/2004	EEV60-TC-20	0.712	55
9/30/2004	EEV60-TC-24	0.749	55
11/18/2004	EEV60-TC-6	0.652	55
Average		0.711	
Standard Deviation		0.042	
Number of Samples		4	

Table 9.4-31: 70 wt% Asbury F108A CNC / Vectra A950RX LCP

Test Date	Sample Number	Through-Plane Thermal Conductivity (W/mK)	Temperature (^{o}C)
10/5/2004	EEV70-TC-14	0.979	55
10/5/2004	EEV70-TC-21	0.933	55
10/5/2004	EEV70-TC-23	0.975	55
11/18/2004	EEV70-TC-4	0.976	55
Average		0.966	
Standard Deviation		0.022	
Number of Samples		4	

Table 9.4-32: 5 wt% Fortafil 243 / Vectra A950RX LCP

Test Date	Sample Number	Through-Plane Thermal Conductivity (W/mK)	Temperature (^{o}C)
1/10/2006	EHV5-TC-15	0.242	55
1/10/2006	EHV5-TC-18	0.233	55
1/10/2006	EHV5-TC-21	0.231	55
1/10/2006	EHV5-TC-24	0.234	55
1/10/2006	EHV5-TC-27	0.247	55
1/10/2006	EHV5-TC-30	0.235	55
Average		0.237	
Standard Deviation		0.006	
Number of Samples		6	

Table 9.4-33: 7.5 wt% Fortafil 243 / Vectra A950RX LCP

Test Date	Sample Number	Through-Plane Thermal Conductivity (W/mK)	Temperature (^{o}C)
1/10/2006	EHV7.5-TC-15	0.252	55
1/10/2006	EHV7.5-TC-18	0.253	55
1/10/2006	EHV7.5-TC-21	0.260	55
1/10/2006	EHV7.5-TC-24	0.254	55
1/10/2006	EHV7.5-TC-27	0.260	55
1/10/2006	EHV7.5-TC-30	0.255	55
Average		0.256	
Standard Deviation		0.004	
Number of Samples		6	

Table 9.4-34: 10 wt% Fortafil 243 / Vectra A950RX LCP

Test Date	Sample Number	Through-Plane Thermal Conductivity (W/mK)	Temperature (^{o}C)
1/11/2006	EHV10-TC-12	0.265	55
1/11/2006	EHV10-TC-15	0.266	55
1/11/2006	EHV10-TC-18	0.278	55
1/11/2006	EHV10-TC-21	0.271	55
1/11/2006	EHV10-TC-24	0.271	55
1/11/2006	EHV10-TC-27	0.279	55
Average		0.272	
Standard Deviation		0.006	
Number of Samples		6	

Table 9.4-35: 15 wt% Fortafil 243 / Vectra A950RX LCP

Test Date	Sample Number	Through-Plane Thermal Conductivity (W/mK)	Temperature (^{o}C)
1/11/2006	EHV15-TC-15	0.281	55
1/11/2006	EHV15-TC-18	0.295	55
1/11/2006	EHV15-TC-21	0.286	55
1/11/2006	EHV15-TC-24	0.282	55
1/11/2006	EHV15-TC-27	0.273	55
1/11/2006	EHV15-TC-30	0.275	55
Average		0.282	
Standard Deviation		0.008	
Number of Samples		6	

Table 9.4-36: 20 wt% Fortafil 243 / Vectra A950RX LCP

Test Date	Sample Number	Through-Plane Thermal Conductivity (W/mK)	Temperature (^{o}C)
1/12/2006	EHV20-TC-12	0.304	55
1/12/2006	EHV20-TC-15	0.322	55
1/12/2006	EHV20-TC-18	0.325	55
1/12/2006	EHV20-TC-21	0.317	55
1/12/2006	EHV20-TC-24	0.314	55
1/12/2006	EHV20-TC-27	0.313	55
Average		0.316	
Standard Deviation		0.007	
Number of Samples		6	

Table 9.4-37: 25 wt% Fortafil 243 / Vectra A950RX LCP

Test Date	Sample Number	Through-Plane Thermal Conductivity (W/mK)	Temperature (^{o}C)
1/12/2006	EHV25-TC-15	0.354	55
1/12/2006	EHV25-TC-18	0.340	55
1/12/2006	EHV25-TC-21	0.358	55
1/12/2006	EHV25-TC-24	0.354	55
1/12/2006	EHV25-TC-27	0.355	55
1/12/2006	EHV25-TC-30	0.354	55
Average		0.352	
Standard Deviation		0.006	
Number of Samples		6	

Table 9.4-38: 30 wt% Fortafil 243 / Vectra A950RX LCP

Test Date	Sample Number	Through-Plane Thermal Conductivity (W/mK)	Temperature (^{o}C)
1/16/2006	EHV30-TC-15	0.370	55
1/16/2006	EHV30-TC-21	0.376	55
1/16/2006	EHV30-TC-24	0.370	55
1/16/2006	EHV30-TC-27	0.355	55
1/16/2006	EHV30-TC-30	0.359	55
Average		0.366	
Standard Deviation		0.009	
Number of Samples		5	

Table 9.4-39: 35 wt% Fortafil 243 / Vectra A950RX LCP

Test Date	Sample Number	Through-Plane Thermal Conductivity (W/mK)	Temperature (^{o}C)
1/16/2006	EHV35-TC-15	0.391	55
1/16/2006	EHV35-TC-18	0.419	55
1/16/2006	EHV35-TC-21	0.456	55
1/16/2006	EHV35-TC-24	0.439	55
1/16/2006	EHV35-TC-27	0.421	55
1/16/2006	EHV35-TC-30	0.456	55
Average		0.430	
Standard Deviation		0.025	
Number of Samples		6	

Table 9.4-40: 40 wt% Fortafil 243 / Vectra A950RX LCP

Test Date	Sample Number	Through-Plane Thermal Conductivity (W/mK)	Temperature (^{o}C)
1/17/2006	EHV40-TC-15	0.530	55
1/17/2006	EHV40-TC-18	0.532	55
1/17/2006	EHV40-TC-21	0.502	55
1/17/2006	EHV40-TC-24	0.544	55
1/17/2006	EHV40-TC-27	0.528	55
1/17/2006	EHV40-TC-30	0.525	55
Average		0.527	
Standard Deviation		0.014	
Number of Samples		6	

Table 9.4-41: 45 wt% Fortafil 243 / Vectra A950RX LCP

Test Date	Sample Number	Through-Plane Thermal Conductivity (W/mK)	Temperature (^{o}C)
1/18/2006	EHV45-TC-15	0.613	55
1/18/2006	EHV45-TC-18	0.633	55
1/18/2006	EHV45-TC-21	0.563	55
1/18/2006	EHV45-TC-24	0.627	55
1/18/2006	EHV45-TC-27	0.554	55
1/18/2006	EHV45-TC-30	0.601	55
Average		0.599	
Standard Deviation		0.033	
Number of Samples		6	

Table 9.4-42: 50 wt% Fortafil 243 / Vectra A950RX LCP

Test Date	Sample Number	Through-Plane Thermal Conductivity (W/mK)	Temperature (^{o}C)
1/18/2006	EHV50R-TC-15	0.728	55
1/18/2006	EHV50R-TC-18	0.702	55
1/18/2006	EHV50R-TC-24	0.650	55
1/18/2006	EHV50R-TC-27	0.671	55
Average		0.687	
Standard Deviation		0.034	
Number of Samples		4	

Table 9.4-43: 55 wt% Fortafil 243 / Vectra A950RX LCP

Test Date	Sample Number	Through-Plane Thermal Conductivity (W/mK)	Temperature (^{o}C)
1/18/2006	EHV55-TC-15	0.889	55
1/18/2006	EHV55-TC-18	0.782	55
1/18/2006	EHV55-TC-21	0.882	55
1/18/2006	EHV55-TC-27	0.835	55
1/18/2006	EHV55-TC-30	0.793	55
Average		0.836	
Standard Deviation		0.050	
Number of Samples		5	

Table 9.4-44: 60 wt% Fortafil 243 / Vectra A950RX LCP

Test Date	Sample Number	Through-Plane Thermal Conductivity (W/mK)	Temperature (^{o}C)
1/18/2006	EHV60R-TC-18	1.039	55
1/18/2006	EHV60R-TC-21	1.042	55
1/18/2006	EHV60R-TC-24	1.012	55
1/18/2006	EHV60R-TC-27	1.038	55
1/18/2006	EHV60R-TC-30	1.062	55
Average		1.039	
Standard Deviation		0.018	
Number of Samples		5	

Section 9.5: Specific Heat Data

Table 9.5-1: Vectra A950RX LCP

Test Date	Sample Number	Specific Heat (J/kgK)
6/27/2005	EVR-TC-17	1002.9
6/27/2005	EVR-TC-17	1049.3
6/27/2005	EVR-TC-17	1067.8
6/27/2005	EVR-TC-17	1075.3
6/27/2005	EVR-TC-17	1077.5
	Average	1054.6
	Standard Deviation	30.9
	Number of Samples	5

Table 9.5-2: 10 wt% Thermocarb TC300 / Vectra A950RX LCP

Test Date	Sample Number	Specific Heat (J/kgK)
6/28/2005	EBV10-TC-15	1020.0
7/13/2005	EBV10-TC-15	1030.3
6/28/2005	EBV10-TC-15	1034.8
6/29/2005	EBV10-TC-15	1062.8
	Average	1037.0
	Standard Deviation	18.3
	Number of Samples	4

Table 9.5-3: 15 wt% Thermocarb TC300 / Vectra A950RX LCP

Test Date	Sample Number	Specific Heat (J/kgK)
6/28/2005	EBV15-TC-13	1005.6
7/21/2005	EBV15-TC-13	1012.7
6/29/2005	EBV15-TC-13	1037.4
6/29/2008	EBV15-TC-22	1064.2
7/13/2005	EBV15-TC-22	1054.1
	Average	1034.8
	Standard Deviation	25.4
	Number of Samples	5

Table 9.5-4: 20 wt% Thermocarb TC300 / Vectra A950RX LCP

Test Date	Sample Number	Specific Heat (J/kgK)
6/30/2005	EBV20-TC-11	990.3
6/29/2005	EBV20-TC-11	1000.3
6/29/2005	EBV20-TC-17	996.7
7/12/2005	EBV20-TC-17	1011.8
6/29/2005	EBV20-TC-21	985.1
7/13/2005	EBV20-TC-21	992.9
	Average	996.2
	Standard Deviation	9.3
	Number of Samples	6

Table 9.5-5: 30 wt% Thermocarb TC300 / Vectra A950RX LCP

Test Date	Sample Number	Specific Heat (J/kgK)
6/30/2005	EBV30-TC-16	979.8
6/30/2005	EBV30-TC-16	1007.1
6/30/2005	EBV30-TC-18	973.4
6/30/2005	EBV30-TC-18	977.4
6/30/2005	EBV30-TC-22	974.1
7/13/2005	EBV30-TC-22	1014.5
	Average	987.7
	Standard Deviation	18.2
	Number of Samples	6

Table 9.5-6: 30 wt% Thermocarb TC300 / Vectra A950RX LCP

Test Date	Sample Number	Specific Heat (J/kgK)
6/27/2005	EBV40-TC-10	972.2
6/14/2005	EBV40-TC-12	929.5
6/14/2005	EBV40-TC-12	949.4
6/9/2005	EBV40-TC-12	974.5
6/9/2005	EBV40-TC-12	976.8
6/10/2005	EBV40-TC-12	981.6
6/13/2005	EBV40-TC-12	985.7
6/10/2005	EBV40-TC-14	960.0
6/9/2005	EBV40-TC-14	970.2
6/13/2005	EBV40-TC-14	976.1
	Average	967.6
	Standard Deviation	17.0
	Number of Samples	10

Table 9.5-7: 50 wt% Thermocarb TC300 / Vectra A950RX LCP

Test Date	Sample Number	Specific Heat (J/kgK)
7/5/2005	EBV50-TC-11	894.6
7/5/2005	EBV50-TC-11	895.5
7/5/2005	EBV50-TC-17	898.8
7/12/2005	EBV50-TC-17	974.7
7/5/2005	EBV50-TC-22	897.2
7/12/2005	EBV50-TC-22	958.1
	Average	919.8
	Standard Deviation	36.5
	Number of Samples	6

Table 9.5-8: 55 wt% Thermocarb TC300 / Vectra A950RX LCP

Test Date	Sample Number	Specific Heat (J/kgK)
7/5/2005	EBV55-TC-11	902.9
7/7/2005	EBV55-TC-11	921.8
7/5/2005	EBV55-TC-16	874.4
7/6/2005	EBV55-TC-16	902.8
7/6/2005	EBV55-TC-28	909.1
	Average	902.2
	Standard Deviation	17.4
	Number of Samples	5

Table 9.5-9: 60 wt% Thermocarb TC300 / Vectra A950RX LCP

Test Date	Sample Number	Specific Heat (J/kgK)
6/15/2005	EBV60-TC-11	853.4
6/14/2005	EBV60-TC-11	865.5
6/16/2005	EBV60-TC-11	878.2
6/14/2005	EBV60-TC-13	821.9
6/15/2005	EBV60-TC-13	888.3
6/15/2005	EBV60-TC-13	898.4
	Average	867.6
	Standard Deviation	27.5
	Number of Samples	6

Table 9.5-10: 65 wt% Thermocarb TC300 / Vectra A950RX LCP

Test Date	Sample Number	Specific Heat (J/kgK)
7/6/2005	EBV65-TC-17	852.7
7/7/2005	EBV65-TC-17	859.6
7/6/2005	EBV65-TC-21	875.2
7/6/2005	EBV65-TC-26	849.3
7/21/2005	EBV65-TC-26	867.1
	Average	860.8
	Standard Deviation	10.6
	Number of Samples	5

Table 9.5-11: 70 wt% Thermocarb TC300 / Vectra A950RX LCP

Test Date	Sample Number	Specific Heat (J/kgK)
7/7/2005	EBV70-TC-11	846.2
7/11/2005	EBV70-TC-18	875.3
7/11/2005	EBV70-TC-27	858.8
	Average	860.1
	Standard Deviation	14.6
	Number of Samples	3

Table 9.5-12: 75 wt% Thermocarb TC300 / Vectra A950RX LCP

Test Date	Sample Number	Specific Heat (J/kgK)
7/21/2005	EBV75-TC-9	852.2
7/11/2005	EBV75-TC-9	855.8
7/12/2005	EBV75-TC-9	879.7
7/21/2005	EBV75-TC-10	797.6
7/12/2005	EBV75-TC-10	843.5
7/13/2005	EBV75-TC-10	857.7
7/12/2005	EBV75-TC-10	863.7
	Average	850.0
	Standard Deviation	25.7
	Number of Samples	7

Table 9.5-13: 40 wt% Asbury Synthetic Graphite 4012 / Vectra A950RX LCP

Test Date	Sample Number	Specific Heat (J/kgK)
6/17/2005	ECV40-TC-11	905.9
6/17/2005	ECV40-TC-11	921.7
6/16/2005	ECV40-TC-11	933.2
6/16/2005	ECV40-TC-11	955.1
6/16/2005	ECV40-TC-16	897.4
6/16/2005	ECV40-TC-16	903.6
6/16/2005	ECV40-TC-16	904.1
	Average	917.3
	Standard Deviation	20.8
	Number of Samples	7

Table 9.5-14: 60 wt% Asbury Synthetic Graphite 4012 / Vectra A950RX LCP

Test Date	Sample Number	Specific Heat (J/kgK)
6/20/2005	ECV60-TC-14	852.1
6/17/2005	ECV60-TC-14	879.4
6/17/2005	ECV60-TC-14	888.7
6/20/2005	ECV60-TC-19	853.3
6/17/2005	ECV60-TC-19	855.9
6/20/2005	ECV60-TC-19	867.2
	Average	866.1
	Standard Deviation	15.2
	Number of Samples	6

Table 9.5-15: 70 wt% Asbury Synthetic Graphite 4012 / Vectra A950RX LCP

Test Date	Sample Number	Specific Heat (J/kgK)
6/20/2005	ECV70-TC-11	789.6
6/20/2005	ECV70-TC-11	793.2
6/21/2005	ECV70-TC-11	834.0
6/23/2005	ECV70-TC-11	838.8
6/21/2005	ECV70-TC-13	853.7
6/21/2005	ECV70-TC-13	856.8
	Average	827.7
	Standard Deviation	29.4
	Number of Samples	6

Table 9.5-16: 40 wt% Asbury 3160 Natural Flake Graphite / Vectra A950RX LCP

Test Date	Sample Number	Specific Heat (J/kgK)
8/29/2005	EDV40-TC-13	972.6
8/29/2005	EDV40-TC-17	1016.9
8/29/2005	EDV40-TC-25	988.7
9/1/2005	EDV40-TC-25	1010.0
	Average	997.0
	Standard Deviation	20.2
	Number of Samples	4

Table 9.5-17: 60 wt% Asbury 3160 Natural Flake Graphite / Vectra A950RX LCP

Test Date	Sample Number	Specific Heat (J/kgK)
8/30/2005	EDV60-TC-11	878.8
8/30/2005	EDV60-TC-11	888.3
8/30/2005	EDV60-TC-14	888.2
9/1/2005	EDV60-TC-14	932.1
8/30/2005	EDV60-TC-20	861.5
8/30/2005	EDV60-TC-20	870.9
	Average	886.6
	Standard Deviation	24.5
	Number of Samples	6

Table 9.5-18: 70 wt% Asbury 3160 Natural Flake Graphite / Vectra A950RX LCP

Test Date	Sample Number	Specific Heat (J/kgK)
8/31/2005	EDV70-TC-14	856.6
8/31/2005	EDV70-TC-17	855.6
8/31/2005	EDV70-TC-17	869.6
8/31/2005	EDV70-TC-22	870.1
8/31/2005	EDV70-TC-22	956.1
9/1/2005	EDV70-TC-28	882.8
9/1/2005	EDV70-TC-28	900.9
	Average	884.5
	Standard Deviation	35.2
	Number of Samples	7

Table 9.5-19: 40 wt% Asbury F108A CNC / Vectra A950RX LCP

Test Date	Sample Number	Specific Heat (J/kgK)
9/2/2005	EEV40-TC-17	784.3
9/2/2005	EEV40-TC-21	779.3
9/2/2005	EEV40-TC-21	771.2
	Average	778.3
	Standard Deviation	6.6
	Number of Samples	3

Table 9.5-20: 60 wt% Asbury F108A CNC / Vectra A950RX LCP

Test Date	Sample Number	Specific Heat (J/kgK)
9/3/2005	EEV60-TC-17	763.2
9/3/2005	EEV60-TC-21	751.2
9/3/2005	EEV60-TC-21	784.7
	Average	766.4
	Standard Deviation	17.0
	Number of Samples	3

Table 9.5-21: 70 wt% Asbury F108A CNC / Vectra A950RX LCP

Test Date	Sample Number	Specific Heat (J/kgK)
9/4/2005	EEV70-TC-18	746.6
9/4/2005	EEV70-TC-34	778.4
9/4/2005	EEV70-TC-34	754.9
	Average	760.0
	Standard Deviation	16.5
	Number of Samples	3

Table 9.5-22: 5 wt% Fortafil 243 / Vectra A950RX LCP

Test Date	Sample Number	Specific Heat (J/kgK)
3/27/2006	EHV5-TC-14	1050.3
3/27/2006	EHV5-TC-29	1042.2
	Average	1046.3
	Standard Deviation	5.8
	Number of Samples	2
	Theory Value	1048.3

Table 9.5-23: 7.5 wt% Fortafil 243 / Vectra A950RX LCP

Test Date	Sample Number	Specific Heat (J/kgK)
3/28/2006	EHV7.5-TC-14	1041.7
3/28/2006	EHV7.5-TC-19	1036.2
	Average	1039.0
	Standard Deviation	3.9
	Number of Samples	2
	Theory Value	1045.0

Table 9.5-24: 10 wt% Fortafil 243 / Vectra A950RX LCP

Test Date	Sample Number	Specific Heat (J/kgK)
3/29/2006	EHV10-TC-19	1006.4
3/29/2006	EHV10-TC-29	1037.1
	Average	1021.7
	Standard Deviation	21.6
	Number of Samples	2
	Theory Value	1041.6

Table 9.5-25: 15 wt% Fortafil 243 / Vectra A950RX LCP

Test Date	Sample Number	Specific Heat (J/kgK)
3/29/2006	EHV15-TC-14	1016.4
3/29/2006	EHV15-TC-19	1019.2
3/29/2006	EHV15-TC-29	1021.2
	Average	1018.9
	Standard Deviation	2.4
	Number of Samples	3
	Theory Value	1034.9

Table 9.5-26: 20 wt% Fortafil 243 / Vectra A950RX LCP

Test Date	Sample Number	Specific Heat (J/kgK)
4/1/2006	EHV20-TC-14	1024.8
4/1/2006	EHV20-TC-19	1014.5
4/1/2006	EHV20-TC-29	1023.5
	Average	1020.9
	Standard Deviation	5.6
	Number of Samples	3
	Theory Value	1028.2

Table 9.5-27: 30 wt% Fortafil 243 / Vectra A950RX LCP

Test Date	Sample Number	Specific Heat (J/kgK)
4/2/2006	EHV30-TC-19	1011.8
4/2/2006	EHV30-TC-29	1007.9
	Average	1009.9
	Standard Deviation	2.8
	Number of Samples	2
	Theory Value	1014.8

Table 9.5-28: 35 wt% Fortafil 243 / Vectra A950RX LCP

Test Date	Sample Number	Specific Heat (J/kgK)
4/3/2006	EHV35-TC-14	988.9
4/3/2006	EHV35-TC-29	1003.7
	Average	996.3
	Standard Deviation	10.5
	Number of Samples	2
	Theory Value	1008.1

Table 9.5-29: Theoretical Values for Fortafil 243 / Vectra Composites

Sample Number	Specific Heat (J/kgK)
EHV5	1048.3
EHV7.5	1045.0
EHV10	1041.6
EHV15	1034.9
EHV20	1028.2
EHV25	1021.5
EHV30	1014.8
EHV35	1008.1
EHV40	1001.4
EHV45	994.7
EHV50R	988.0
EHV55	981.3
EHV60R	974.6

The results in Table E.29 were derived from the following formula:

$$\sum_{i=1}^{2} M_i * Cp_i \tag{1}$$

In this equation, M is the mass fraction of the material, Cp is the specific heat of the material, $i=1$ denotes the Vectra and $i=2$ denotes the Fortafil 243 carbon fiber. Values used for Cp were 1055 J/(kgK) for the Vectra and 921 J/(kgK) for the Fortafil 243 carbon fiber. As shown above in Tables 9.5-22 – 9.5-28, the formula results showed good agreement with experimental data.

Section 9.6: Hot Disk Thermal Conductivity Data

Table 9.6-1: 10 wt% Thermocarb TC300 / Vectra A950RX LCP

Test Date	Disk Numbers	Axial Thermal Conductivity (W/mK)	Radial Thermal Conductivity (W/mK)	Power (W)	Time (s)
1/20/2006	14,13,12,11	0.2835	1.4224	0.030	40
1/20/2006	29,27,22,20	0.2858	1.3828	0.030	40
1/20/2006	22,11,20,12	0.2836	1.4717	0.040	40
Average		0.2843	1.4256		
Standard Deviation		0.0013	0.0445		
Number of Samples		3	3		

Table 9.6-2: 15 wt% Thermocarb TC300 / Vectra A950RX LCP

Test Date	Disk Numbers	Axial Thermal Conductivity (W/mK)	Radial Thermal Conductivity (W/mK)	Power (W)	Time (s)
1/19/2006	11,20,27,15	0.3238	1.8154	0.035	40
1/19/2006	12,24,26,27	0.3223	1.8339	0.050	40
1/19/2006	24,18,17,26	0.3239	1.9101	0.040	40
Average		0.3233	1.8531		
Standard Deviation		0.0009	0.0502		
Number of Samples		3	3		

Table 9.6-3: 20 wt% Thermocarb TC300 / Vectra A950RX LCP

Test Date	Disk Numbers	Axial Thermal Conductivity (W/mK)	Radial Thermal Conductivity (W/mK)	Power (W)	Time (s)
12/19/2005	09,13,16,26	0.3905	1.9969	0.180	40
12/19/2005	10,14,18,27	0.3899	2.0915	0.180	40
12/19/2005	08,12,15,23	0.3736	1.9971	0.180	40
Average		0.3847	2.0285		
Standard Deviation		0.0096	0.0546		
Number of Samples		3	3		

Table 9.6-4: 25 wt% Thermocarb TC300 / Vectra A950RX LCP

Test Date	Disk Numbers	Axial Thermal Conductivity (W/mK)	Radial Thermal Conductivity (W/mK)	Power (W)	Time (s)
12/15/2005	25,28,16,29	0.4837	2.2703	0.210	40
12/15/2005	14,23,17,12	0.4409	2.5213	0.220	40
12/15/2005	19,32,22,11	0.4519	2.5092	0.220	40
Average		0.4588	2.4336		
Standard Deviation		0.0222	0.1416		
Number of Samples		3	3		

Table 9.6-5: 30 wt% Thermocarb TC300 / Vectra A950RX LCP

Test Date	Disk Numbers	Axial Thermal Conductivity (W/mK)	Radial Thermal Conductivity (W/mK)	Power (W)	Time (s)
12/15/2005	13,21,12,23	0.5621	2.9000	0.200	40
12/15/2005	27,26,20,11	0.5345	2.9032	0.200	40
12/15/2005	21,15,13,14	0.5379	3.0119	0.210	40
Average		0.5448	2.9384		
Standard Deviation		0.0151	0.0637		
Number of Samples		3	3		

Table 9.6-6: 35 wt% Thermocarb TC300 / Vectra A950RX LCP

Test Date	Disk Numbers	Axial Thermal Conductivity (W/mK)	Radial Thermal Conductivity (W/mK)	Power (W)	Time (s)
12/15/2005	14,17,16,25	0.6244	4.3845	0.190	20
12/15/2005	14,28,12,33	0.6596	4.3850	0.195	20
12/15/2005	26,17,25,16	0.6220	4.4439	0.200	20
Average		0.6353	4.4045		
Standard Deviation		0.0210	0.0342		
Number of Samples		3	3		

Table 9.6-7: 40 wt% Fortafil 243 Carbon Fiber / Vectra A950RX LCP

Test Date	Disk Numbers	Axial Thermal Conductivity (W/mK)	Radial Thermal Conductivity (W/mK)	Power (W)	Time (s)
9/1/2005	13,15	0.7750	5.0466	0.050	5
9/1/2005	21,24	0.6425	6.4717	0.050	5
9/1/2005	25,13	0.5981	6.6101	0.050	5
9/1/2005	15,21	0.7703	5.6035	0.050	5
9/1/2005	24,25	0.7232	5.6712	0.050	5
Average		0.7018	5.8806		
Standard Deviation		0.0787	0.6515		
Number of Samples		5	5		

Table 9.6-8: 45 wt% Thermocarb TC300 / Vectra A950RX LCP

Test Date	Disk Numbers	Axial Thermal Conductivity (W/mK)	Radial Thermal Conductivity (W/mK)	Power (W)	Time (s)
12/15/2005	16,26,19,11	0.8668	6.2507	0.700	10
12/15/2005	31,22,23,12	0.8795	6.7666	0.700	10
12/15/2005	33,14,17,25	0.8728	6.3041	0.700	10
Average		0.8730	6.4405		
Standard Deviation		0.0064	0.2837		
Number of Samples		3	3		

Table 9.6-9: 50 wt% Thermocarb TC300 / Vectra A950RX LCP

Test Date	Disk Numbers	Axial Thermal Conductivity (W/mK)	Radial Thermal Conductivity (W/mK)	Power (W)	Time (s)
12/12/2005	14,25,26,12	1.1010	9.0403	0.270	10
12/12/2005	15,19,28,24	1.1110	8.9916	0.260	10
12/12/2005	25,14,12,26	1.0898	9.0273	0.250	10
Average		1.1006	9.0198		
Standard Deviation		0.0106	0.0252		
Number of Samples		3	3		

Table 9.6-10: 55 wt% Thermocarb TC300 / Vectra A950RX LCP

Test Date	Disk Numbers	Axial Thermal Conductivity (W/mK)	Radial Thermal Conductivity (W/mK)	Power (W)	Time (s)
12/12/2005	20,15,17,24	1.2751	12.3004	0.290	10
12/12/2005	20,15,32,12	1.2546	13.4946	0.290	10
12/12/2005	31,29,32,12	1.2659	12.5972	0.300	10
Average		1.2652	12.7974		
Standard Deviation		0.0103	0.6217		
Number of Samples		3	3		

Table 9.6-11: 60 wt% Thermocarb TC300 / Vectra A950RX LCP

Test Date	Disk Numbers	Axial Thermal Conductivity (W/mK)	Radial Thermal Conductivity (W/mK)	Power (W)	Time (s)
12/15/2005	29,12,18,30	1.5639	15.7023	0.310	10
12/15/2005	16,24,19,26	1.4953	16.2898	0.310	10
12/15/2005	19,30,16,24	1.5771	16.1134	0.300	10
Average		1.5454	16.0351		
Standard Deviation		0.0439	0.3015		
Number of Samples		3	3		

Table 9.6-12: 65 wt% Thermocarb TC300 / Vectra A950RX LCP

Test Date	Disk Numbers	Axial Thermal Conductivity (W/mK)	Radial Thermal Conductivity (W/mK)	Power (W)	Time (s)
12/15/2005	10,27,12,15	1.9250	21.0332	0.405	2.5
12/15/2005	27,10,15,12	2.0259	22.2389	0.410	2.5
12/15/2005	10,9,11,15	1.9950	21.5280	0.425	2.5
Average		1.9820	21.6000		
Standard Deviation		0.0517	0.6061		
Number of Samples		3	3		

Table 9.6-13: 70 wt% Thermocarb TC300 / Vectra A950RX LCP

Test Date	Disk Numbers	Axial Thermal Conductivity (W/mK)	Radial Thermal Conductivity (W/mK)	Power (W)	Time (s)
1/17/2006	12,15,29,23	2.3369	32.0626	0.500	2.5
1/18/2006	12,29,30,23	2.2631	31.6455	1.240	2.5
1/18/2006	29,12,23,30	2.3556	33.9381	1.210	2.5
Average		2.3186	32.5488		
Standard Deviation		0.0489	1.2212		
Number of Samples		3	3		

Table 9.6-14: 75 wt% Thermocarb TC300 / Vectra A950RX LCP

Test Date	Disk Numbers	Axial Thermal Conductivity (W/mK)	Radial Thermal Conductivity (W/mK)	Power (W)	Time (s)
1/18/2006	5,12,11,6	2.6282	50.1980	1.250	2.5
1/18/2006	5,10,8,12	2.6983	47.1954	1.250	2.5
1/18/2006	11,12,5,6	2.5460	46.8229	1.250	2.5
Average		2.6242	48.0721		
Standard Deviation		0.0762	1.8505		
Number of Samples		3	3		

Table 9.6-15: 40 wt% Asbury Synthetic Graphite 4012 / Vectra A950RX LCP

Test Date	Disk Numbers	Axial Thermal Conductivity (W/mK)	Radial Thermal Conductivity (W/mK)	Power (W)	Time (s)
10/11/2005	15-25	0.5860	3.4907	0.050	5
10/11/2005	17-19	0.5746	3.9981	0.050	5
10/11/2005	18-23	0.6590	3.3976	0.050	5
10/11/2005	13-22	0.6358	3.5570	0.050	5
10/11/2005	14-27	0.6756	3.3010	0.050	5
Average		0.6262	3.5489		
Standard Deviation		0.0444	0.2691		
Number of Samples		5	5		

Table 9.6-16: 60 wt% Asbury Synthetic Graphite 4012 / Vectra A950RX LCP

Test Date	Disk Numbers	Axial Thermal Conductivity (W/mK)	Radial Thermal Conductivity (W/mK)	Power (W)	Time (s)
9/27/2005	13-16	1.4956	11.8618	1.500	2.5
9/27/2005	14-27	1.5120	12.7100	0.100	10
9/27/2005	25-28	1.4648	13.1632	1.500	2.5
9/27/2005	30-31	1.3850	12.7209	1.500	2.5
9/27/2005	32-33	1.4457	14.5137	1.500	2.5
Average		1.4606	12.9939		
Standard Deviation		0.0496	0.9715		
Number of Samples		5	5		

Table 9.6-17: 70 wt% Asbury Synthetic Graphite 4012 / Vectra A950RX LCP

Test Date	Disk Numbers	Axial Thermal Conductivity (W/mK)	Radial Thermal Conductivity (W/mK)	Power (W)	Time (s)
9/30/2005	10-14	2.0567	28.2574	2.000	2.5
9/30/2005	6-7	2.0525	28.4006	2.000	2.5
9/30/2005	10-14	2.0980	26.6300	2.000	2.5
9/30/2005	6-10	2.0874	27.5018	2.000	2.5
9/30/2005	7-14	2.0478	28.7163	2.000	2.5
Average		2.0685	27.9012		
Standard Deviation		0.0226	0.8391		
Number of Samples		5	5		

Table 9.6-18: 40 wt% Asbury 3160 Natural Flake Graphite / Vectra A950RX LCP

Test Date	Disk Numbers	Axial Thermal Conductivity (W/mK)	Radial Thermal Conductivity (W/mK)	Power (W)	Time (s)
9/26/2005	11-13	0.5696	6.5730	0.050	5
9/26/2005	16-19	0.6060	6.4663	0.050	5
9/26/2005	28-32	0.6000	6.9260	0.050	5
9/26/2005	26-27	0.5956	7.6353	0.050	5
9/26/2005	28-32	0.6036	6.9499	0.050	5
Average		0.5950	6.9101		
Standard Deviation		0.0147	0.4578		
Number of Samples		5	5		

Table 9.6-19: 60 wt% Asbury 3160 Natural Flake Graphite / Vectra A950RX LCP

Test Date	Disk Numbers	Axial Thermal Conductivity (W/mK)	Radial Thermal Conductivity (W/mK)	Power (W)	Time (s)
10/3/2005	12-13	1.3561	1.3561	0.120	10
10/3/2005	13-32	1.3300	1.3300	0.100	10
10/3/2005	16-18	1.4283	1.4283	0.070	10
10/3/2005	27-29	1.3723	1.3723	0.200	10
10/3/2005	16-27	1.3170	1.3170	0.055	10
Average		1.3607	1.3607		
Standard Deviation		0.0435	0.0435		
Number of Samples		5	5		

Table 9.6-20: 70 wt% Asbury 3160 Natural Flake Graphite / Vectra A950RX LCP

Test Date	Disk Numbers	Axial Thermal Conductivity (W/mK)	Radial Thermal Conductivity (W/mK)	Power (W)	Time (s)
9/29/2005	11-13	1.8961	35.5461	0.500	5
10/13/2005	20-24	1.7630	34.8700	0.300	5
9/29/2005	20-24	2.0762	33.7310	0.250	5
10/13/2005	20-24	1.8708	34.2274	0.300	10
9/29/2005	13-15	1.8714	35.1012	0.500	5
Average		1.8955	34.6951		
Standard Deviation		0.1134	0.7190		
Number of Samples		5	5		

Table 9.6-21: 5wt% Fortafil 243 Carbon Fiber / Vectra A950RX LCP

Test Date	Disk Numbers	Axial Thermal Conductivity (W/mK)	Radial Thermal Conductivity (W/mK)	Power (W)	Time (s)
03/22/06	23,28,17,16	0.2366	1.1510	0.25	40
03/22/06	26,8,10,31	0.2364	1.1810	0.25	40
03/29/06	31,26,16,23	0.2365	1.1010	0.25	40
03/29/06	28,11,22,17	0.2411	1.1450	0.4	40
03/29/06	10,23,16,12	0.2405	1.1640	0.4	40
Average		0.2382	1.1484		
Standard Deviation		0.0024	0.0299		
Number of Samples		5	5		

Table 9.6-22: 7.5wt% Fortafil 243 Carbon Fiber / Vectra A950RX LCP

Test Date	Disk Numbers	Axial Thermal Conductivity (W/mK)	Radial Thermal Conductivity (W/mK)	Power (W)	Time (s)
03/22/06	25,31,23,26	0.2522	1.2440	0.4	20
03/22/06	11,22,16,13	0.2553	1.2330	0.4	20
03/30/06	17,28,25,22	0.2562	1.1950	0.4	20
03/29/06	13,28,17,12	0.2586	1.2090	0.4	20
03/29/06	23,26,22,11	0.2546	1.1580	0.4	20
Average		0.2554	1.2078		
Standard Deviation		0.0023	0.0339		
Number of Samples		5	5		

Table 9.6-23: 10wt% Fortafil 243 Carbon Fiber / Vectra A950RX LCP

Test Date	Disk Numbers	Axial Thermal Conductivity (W/mK)	Radial Thermal Conductivity (W/mK)	Power (W)	Time (s)
03/22/06	2,25,13,1	0.2662	1.1650	0.4	20
03/29/06	16,10,13,25	0.2761	1.2110	0.4	20
03/29/06	16,11,17,22	0.2673	1.2430	0.4	20
03/29/06	25,13,28,20	0.2755	1.3060	0.4	20
03/29/06	8,26,10,9	0.2690	1.2430	0.4	20
Average		0.2708	1.2336		
Standard Deviation		0.0047	0.0516		
Number of Samples		5	5		

Table 9.6-24: 15wt% Fortafil 243 Carbon Fiber / Vectra A950RX LCP

Test Date	Disk Numbers	Axial Thermal Conductivity (W/mK)	Radial Thermal Conductivity (W/mK)	Power (W)	Time (s)
03/22/06	12,28,26,17	0.2831	1.3970	0.4	20
03/22/06	11,32,31,22	0.2832	1.3950	0.4	20
03/29/06	17,28,10,26	0.2775	1.4080	0.4	20
03/29/06	13,23,20,16	0.2873	1.4260	0.4	20
03/29/06	28,22,20,32	0.2812	1.4090	0.4	20
Average		0.2825	1.4070		
Standard Deviation		0.0036	0.0123		
Number of Samples		5	5		

Table 9.6-25: 20wt% Fortafil 243 Carbon Fiber / Vectra A950RX LCP

Test Date	Disk Numbers	Axial Thermal Conductivity (W/mK)	Radial Thermal Conductivity (W/mK)	Power (W)	Time (s)
03/22/06	32,28,10,13	0.3162	1.5540	0.4	20
03/22/06	16,20,22,35	0.3151	1.5650	0.4	20
03/29/06	26,31,11,25	0.3220	1.5380	0.4	20
03/29/06	17,28,32,16	0.3235	1.5080	0.4	20
03/29/06	28,13,32,22	0.3210	1.5730	0.4	20
Average		0.3196	1.5476		
Standard Deviation		0.0037	0.0257		
Number of Samples		5	5		

Table 9.6-26: 25wt% Fortafil 243 Carbon Fiber / Vectra A950RX LCP

Test Date	Disk Numbers	Axial Thermal Conductivity (W/mK)	Radial Thermal Conductivity (W/mK)	Power (W)	Time (s)
03/24/06	26,22,12,32	0.3541	1.6430	0.45	10
03/24/06	31,13,16,23	0.3526	1.6820	0.45	10
03/24/06	32,28,20,12	0.3523	1.6720	0.45	10
03/24/06	20,32,31,25	0.3516	1.7160	0.45	10
03/24/06	28,33,17,22	0.3522	1.6880	0.45	10
Average		0.3526	1.6802		
Standard Deviation		0.0009	0.0264		
Number of Samples		5	5		

Table 9.6-27: 30wt% Fortafil 243 Carbon Fiber / Vectra A950RX LCP

Test Date	Disk Numbers	Axial Thermal Conductivity (W/mK)	Radial Thermal Conductivity (W/mK)	Power (W)	Time (s)
03/30/06	8,10,17,22	0.3650	1.8870	0.43	10
03/30/06	2,7,20,31	0.3708	1.8680	0.43	10
03/30/06	26,22,13,25	0.3641	1.8560	0.3	10
03/30/06	31,22,20,25	0.3619	1.8610	0.3	10
03/30/06	13,20,12,22	0.3652	1.8120	0.4	10
Average		0.3654	1.8568		
Standard Deviation		0.0033	0.0277		
Number of Samples		5	5		

Table 9.6-28: 35wt% Fortafil 243 Carbon Fiber / Vectra A950RX LCP

Test Date	Disk Numbers	Axial Thermal Conductivity (W/mK)	Radial Thermal Conductivity (W/mK)	Power (W)	Time (s)
03/27/06	31,32,23,25	0.4285	1.9920	0.4	10
03/27/06	32,31,13,20	0.4303	2.0030	0.4	10
03/27/06	26,17,20,16	0.4304	1.9950	0.4	10
03/27/06	23,28,32,10	0.4314	1.9970	0.4	10
03/27/06	26,17,16,20	0.4386	1.9910	0.4	10
Average		0.4318	1.9956		
Standard Deviation		0.0039	0.0048		
Number of Samples		5	5		

Table 9.6-29: 40wt% Fortafil 243 Carbon Fiber / Vectra A950RX LCP

Test Date	Disk Numbers	Axial Thermal Conductivity (W/mK)	Radial Thermal Conductivity (W/mK)	Power (W)	Time (s)
03/22/06	20,28,31,22	0.5315	2.1060	0.5	10
03/22/06	32,25,11,26	0.5234	2.0250	0.5	10
03/24/06	13,20,22,31	0.5266	2.0350	0.5	10
03/29/06	17,16,28,12	0.5263	2.0650	0.5	10
03/24/06	28,26,32,13	0.5249	2.0200	0.5	10
Average		0.5265	2.0502		
Standard Deviation		0.0031	0.0357		
Number of Samples		5	5		

Table 9.6-30: 45wt% Fortafil 243 Carbon Fiber / Vectra A950RX LCP

Test Date	Disk Numbers	Axial Thermal Conductivity (W/mK)	Radial Thermal Conductivity (W/mK)	Power (W)	Time (s)
03/24/06	12,22,23,32	0.5957	2.128	0.6	10
03/24/06	26,13,20,28	0.5965	2.095	0.6	10
03/24/06	25,17,16,31	0.6074	2.106	0.55	10
03/29/06	9,17,26,11	0.6037	2.122	0.6	10
03/29/06	26,22,11,20	0.6065	2.096	0.6	10
Average		0.6020	2.1094		
Standard Deviation		0.0055	0.0150		
Number of Samples		5	5		

Table 9.6-31: 50wt% Fortafil 243 Carbon Fiber / Vectra A950RX LCP

Test Date	Disk Numbers	Axial Thermal Conductivity (W/mK)	Radial Thermal Conductivity (W/mK)	Power (W)	Time (s)
04/18/06	25,23,28,36	0.6900	2.275	0.65	10
04/18/06	28,11,37,26	0.6882	2.268	0.65	10
04/18/06	7,10,31,25	0.6920	2.192	0.62	10
04/18/06	7,26,10,31	0.6808	2.208	0.62	10
04/18/06	11,12,36,9	0.6886	2.251	0.62	10
Average		0.6879	2.239		
Standard Deviation		0.0042	0.037		
Number of Samples		5	5		

Table 9.6-32: 55wt% Fortafil 243 Carbon Fiber / Vectra A950RX LCP

Test Date	Disk Numbers	Axial Thermal Conductivity (W/mK)	Radial Thermal Conductivity (W/mK)	Power (W)	Time (s)
04/19/06	17,12,16,26	0.8361	2.247	0.65	10
04/19/06	32,13,25,28	0.8361	2.406	0.65	10
04/19/06	10,26,22,8	0.8430	2.418	0.70	5
04/19/06	17,28,11,32	0.8290	2.222	0.70	5
04/19/06	28,13,22,33	0.8411	2.375	0.70	5
04/19/06	25,20,28,31	0.8349	2.345	0.70	5
04/19/06	26,31,33,13	0.8537	2.301	0.70	5
04/19/06	32,17,23,12	0.8359	2.296	0.65	10
04/19/06	28,25,13,32	0.8362	2.254	0.65	5
04/19/06	7,8,23,17	0.8485	2.262	0.70	5
04/19/06	4,20,16,32	0.8427	2.355	0.70	5
04/19/06	5,10,26,6	0.8474	2.242	0.70	5
04/19/06	23,17,20,4	0.8312	2.420	0.70	5
04/19/06	16,32,13,3	0.8415	2.383	0.70	5
04/19/06	7,12,28,8	0.8436	2.222	0.70	5
04/19/06	6,11,9,17	0.8337	2.384	0.70	5
04/19/06	32,13,20,4	0.8201	2.420	0.70	5
04/19/06	25,22,33,5	0.8233	2.284	0.70	5
04/19/06	31,10,12,7	0.8513	2.296	0.70	5
04/19/06	28,8,11,6	0.8264	2.340	0.70	5
Average		0.8378	2.324		
Standard Deviation		0.0091	0.069		
Number of Samples		20	20		

Table 9.6-33: 60wt% Fortafil 243 Carbon Fiber / Vectra A950RX LCP

Test Date	Disk Numbers	Axial Thermal Conductivity (W/mK)	Radial Thermal Conductivity (W/mK)	Power (W)	Time (s)
04/20/06	8,28,23,3	1.016	2.376	0.80	10
04/20/06	28,13,26,32	1.038	2.403	0.75	10
04/20/06	8,28,23,3	1.036	2.410	0.80	10
04/20/06	13,20,32,6	1.028	2.437	0.80	10
04/20/06	11,32,13,20	1.054	2.451	0.80	5
04/20/06	28,10,17,25	1.017	2.464	0.80	5
04/20/06	31,22,11,32	0.980	2.476	0.80	5
04/20/06	6,13,32,17	1.056	2.478	0.80	10
04/20/06	8,13,17,16	1.051	2.541	0.80	5
04/20/06	20,13,32,6	1.021	2.554	0.80	10
Average		1.0297	2.4590		
Standard Deviation		0.0230	0.0572		
Number of Samples		10	10		

Section 9.7: Density Data

Table 9.7-1: Vectra A950RX LCP

Test Date	Sample Number	Theoretical Density (g/mL)	Measured Density (g/mL)
7/27/2004	EVR-TC-15	1.400	1.395
7/27/2004	EVR-TC-17	1.400	1.396
7/27/2004	EVR-TC-19	1.400	1.395
7/27/2004	EVR-TC-26	1.400	1.400
7/27/2004	EVR-TC-16	1.400	1.396
		Average	1.396
		Standard Deviation	0.002
		Number of Samples	5

Table 9.7-2: 2.5 wt% Ketjenblack EC600 JD / Vectra A950RX LCP

Test Date	Sample Number	Theoretical Density (g/mL)	Measured Density (g/mL)
7/27/2004	EAV2.5-TC-15	1.408	1.400
7/27/2004	EAV2.5-TC-21	1.408	1.401
7/27/2004	EAV2.5-TC-23	1.408	1.399
7/27/2004	EAV2.5-TC-25	1.408	1.396
7/27/2004	EAV2.5-TC-28	1.408	1.403
		Average	1.400
		Standard Deviation	0.003
		Number of Samples	5

Table 9.7-3: 4 wt% Ketjenblack EC600 JD / Vectra A950RX LCP

Test Date	Sample Number	Theoretical Density (g/mL)	Measured Density (g/mL)
7/27/2004	EAV4R-TC-20	1.413	1.409
7/27/2004	EAV4R-TC-23	1.413	1.411
7/27/2004	EAV4R-TC-26	1.413	1.413
7/27/2004	EAV4R-TC-29	1.413	1.412
7/27/2004	EAV4R-TC-32	1.413	1.413
		Average	1.412
		Standard Deviation	0.002
		Number of Samples	5

Table 9.7-4: 5 wt% Ketjenblack EC600 JD / Vectra A950RX LCP

Test Date	Sample Number	Theoretical Density (g/mL)	Measured Density (g/mL)
7/27/2004	EAV5R-TC-16	1.416	1.415
7/27/2004	EAV5R-TC-23	1.416	1.416
7/27/2004	EAV5R-TC-24	1.416	1.416
7/27/2004	EAV5R-TC-25	1.416	1.414
7/27/2004	EAV5R-TC-29	1.416	1.415
		Average	1.415
		Standard Deviation	0.001
		Number of Samples	5

Table 9.7-5: 6 wt% Ketjenblack EC600 JD / Vectra A950RX LCP

Test Date	Sample Number	Theoretical Density (g/mL)	Measured Density (g/mL)
7/27/2004	EAV6-TC-17	1.419	1.420
7/27/2004	EAV6-TC-20	1.419	1.422
7/27/2004	EAV6-TC-24	1.419	1.418
7/27/2004	EAV6-TC-25	1.419	1.417
7/27/2004	EAV6-TC-18	1.419	1.424
		Average	1.420
		Standard Deviation	0.003
		Number of Samples	5

Table 9.7-6: 7.5 wt% Ketjenblack EC600 JD / Vectra A950RX LCP

Test Date	Sample Number	Theoretical Density (g/mL)	Measured Density (g/mL)
7/27/2004	EAV7.5-TC-17	1.424	1.428
7/27/2004	EAV7.5-TC-19	1.424	1.428
7/27/2004	EAV7.5-TC-21	1.424	1.428
7/27/2004	EAV7.5-TC-24	1.424	1.428
7/27/2004	EAV7.5-TC-28	1.424	1.428
		Average	1.428
		Standard Deviation	0.000
		Number of Samples	5

Table 9.7-7: 10 wt% Ketjenblack EC600 JD / Vectra A950RX LCP

Test Date	Sample Number	Theoretical Density (g/mL)	Measured Density (g/mL)
7/27/2004	EAV10-TC-13	1.432	1.437
7/27/2004	EAV10-TC-14	1.432	1.438
7/27/2004	EAV10-TC-26	1.432	1.437
7/27/2004	EAV10-TC-31	1.432	1.437
7/27/2004	EAV10-TC-33	1.432	1.438
		Average	1.437
		Standard Deviation	0.000
		Number of Samples	5

Table 9.7-8: 15 wt% Ketjenblack EC600 JD / Vectra A950RX LCP

Test Date	Sample Number	Theoretical Density (g/mL)	Measured Density (g/mL)
7/27/2004	EAV15-TC-13	1.448	1.457
7/27/2004	EAV15-TC-18	1.448	1.457
7/27/2004	EAV15-TC-20	1.448	1.456
7/27/2004	EAV15-TC-21	1.448	1.457
7/27/2004	EAV15-TC-24	1.448	1.456
		Average	1.457
		Standard Deviation	0.000
		Number of Samples	5

Table 9.7-9: 10 wt% Thermocarb TC300 / Vectra A950RX LCP

Test Date	Sample Number	Theoretical Density (g/mL)	Measured Density (g/mL)
3/9/2005	EBV10-TC-26	1.455	1.442
3/9/2005	EBV10-TC-27	1.455	1.450
3/9/2005	EBV10-TC-16	1.455	1.445
		Average	1.446
		Standard Deviation	0.004
		Number of Samples	3

Table 9.7-10: 15 wt% Thermocarb TC300 / Vectra A950RX LCP

Test Date	Sample Number	Theoretical Density (g/mL)	Measured Density (g/mL)
3/9/2005	EBV15-TC-26	1.483	1.476
3/9/2005	EBV15-TC-32	1.483	1.474
3/9/2005	EBV15-TC-14	1.483	1.474
		Average	1.475
		Standard Deviation	0.001
		Number of Samples	3

Table 9.7-11: 20 wt% Thermocarb TC300 / Vectra A950RX LCP

Test Date	Sample Number	Theoretical Density (g/mL)	Measured Density (g/mL)
3/9/2005	EBV20-TC-23	1.514	1.490
3/9/2005	EBV20-TC-27	1.514	1.507
3/9/2005	EBV20-TC-16	1.514	1.507
		Average	1.501
		Standard Deviation	0.010
		Number of Samples	3

Table 9.7-12: 25 wt% Thermocarb TC300 / Vectra A950RX LCP

Test Date	Sample Number	Theoretical Density (g/mL)	Measured Density (g/mL)
	EBV25-TC-12	1.548	1.546
	EBV25-TC-17	1.548	1.542
	EBV25-TC-22	1.548	1.540
		Average	1.543
		Standard Deviation	0.003
		Number of Samples	3

Table 9.7-13: 30 wt% Thermocarb TC300 / Vectra A950RX LCP

Test Date	Sample Number	Theoretical Density (g/mL)	Measured Density (g/mL)
3/9/2005	EBV30-TC-21	1.578	1.567
3/9/2005	EBV30-TC-26	1.578	1.567
3/9/2005	EBV30-TC-14	1.578	1.568
3/9/2005	EBV30-TC-16	1.578	1.567
3/9/2005	EBV30-TC-21	1.578	1.567
3/9/2005	EBV30-TC-26	1.578	1.568
3/9/2005	EBV30-TC-15	1.578	1.571
3/9/2005	EBV30-TC-22	1.578	1.568
3/9/2005	EBV30-TC-27	1.578	1.570
		Average	1.568
		Standard Deviation	0.002
		Number of Samples	9

Table 9.7-14: 35 wt% Thermocarb TC300 / Vectra A950RX LCP

Test Date	Sample Number	Theoretical Density (g/mL)	Measured Density (g/mL)
9/22/2005	EBV35-TC-12	1.6115	1.602
9/22/2005	EBV35-TC-17	1.6115	1.599
9/22/2005	EBV35-TC-22	1.6115	1.602
		Average	1.601
		Standard Deviation	0.002
		Number of Samples	3

Table 9.7-15: 40 wt% Thermocarb TC300 / Vectra A950RX LCP

Test Date	Sample Number	Theoretical Density (g/mL)	Measured Density (g/mL)
5/27/2004	EBV40-TC-17	1.647	1.640
5/27/2004	EBV40-TC-19	1.647	1.641
5/27/2004	EBV40-TC-21	1.647	1.640
5/27/2004	EBV40-TC-23	1.647	1.640
5/27/2004	EBV40-TC-24	1.647	1.641
		Average	1.640
		Standard Deviation	0.000
		Number of Samples	5

Table 9.7-16: 45 wt% Thermocarb TC300 / Vectra A950RX LCP

Test Date	Sample Number	Theoretical Density (g/mL)	Measured Density (g/mL)
9/22/2005	EBV45-TC-12	1.6842	1.674
9/22/2005	EBV45-TC-17	1.6842	1.674
9/22/2055	EBV45-TC-22	1.6842	1.668
		Average	1.672
		Standard Deviation	0.003
		Number of Samples	3

Table 9.7-17: 50 wt% Thermocarb TC300 / Vectra A950RX LCP

Test Date	Sample Number	Theoretical Density (g/mL)	Measured Density (g/mL)
3/9/2005	EBV50-TC-19	1.723	1.714
3/9/2005	EBV50-TC-23	1.723	1.720
3/9/2005	EBV50-TC-15	1.723	1.714
		Average	1.716
		Standard Deviation	0.003
		Number of Samples	3

Table 9.7-18: 55 wt% Thermocarb TC300 / Vectra A950RX LCP

Test Date	Sample Number	Theoretical Density (g/mL)	Measured Density (g/mL)
3/9/2005	EBV55-TC-27	1.764	1.738
3/9/2005	EBV55-TC-33	1.764	1.756
3/9/2005	EBV55-TC-11	1.764	1.792
3/9/2005	EBV55-TC-15	1.764	1.738
3/9/2005	EBV55-TC-27	1.764	1.756
3/9/2005	EBV55-TC-33	1.764	1.792
3/9/2005	EBV55-TC-17	1.764	1.756
3/9/2005	EBV55-TC-26	1.764	1.753
3/9/2005	EBV55-TC-32	1.764	1.756
		Average	1.760
		Standard Deviation	0.020
		Number of Samples	9

Table 9.7-19: 60 wt% Thermocarb TC300 / Vectra A950RX LCP

Test Date	Sample Number	Theoretical Density (g/mL)	Measured Density (g/mL)
5/27/2004	EBV60-TC-18	1.807	1.807
5/27/2004	EBV60-TC-21	1.807	1.807
5/27/2004	EBV60-TC-24	1.807	1.807
5/27/2004	EBV60-TC-31	1.807	1.807
		Average	1.807
		Standard Deviation	0.000
		Number of Samples	4

Table 9.7-20: 65 wt% Thermocarb TC300 / Vectra A950RX LCP

Test Date	Sample Number	Theoretical Density (g/mL)	Measured Density (g/mL)
3/9/2005	EBV65-TC-19	1.851	1.823
3/9/2005	EBV65-TC-26	1.851	1.862
3/9/2005	EBV65-TC-15	1.851	1.845
3/9/2005	EBV65-TC-11	1.851	1.823
3/9/2005	EBV65-TC-19	1.851	1.862
3/9/2005	EBV65-TC-26	1.851	1.845
3/9/2005	EBV65-TC-12	1.851	1.841
3/9/2005	EBV65-TC-17	1.851	1.845
3/9/2005	EBV65-TC-21	1.851	1.843
		Average	1.843
		Standard Deviation	0.014
		Number of Samples	9

Table 9.7-21: 70 wt% Thermocarb TC300 / Vectra A950RX LCP

Test Date	Sample Number	Theoretical Density (g/mL)	Measured Density (g/mL)
3/9/2005	EBV70-TC-27	1.898	1.906
3/9/2005	EBV70-TC-30	1.898	1.901
3/9/2005	EBV70-TC-10	1.898	1.903
		Average	1.903
		Standard Deviation	0.003
		Number of Samples	3

Table 9.7-22: 75 wt% Thermocarb TC300 / Vectra A950RX LCP

Test Date	Sample Number	Theoretical Density (g/mL)	Measured Density (g/mL)
3/9/2005	EBV75-TC-11	1.948	1.950
3/9/2005	EBV75-TC-12	1.948	1.954
3/9/2005	EBV75-TC-11	1.948	1.946
		Average	1.950
		Standard Deviation	0.004
		Number of Samples	3

Table 9.7-23: 40 wt% Asbury Synthetic Graphite 4012 / Vectra A950RX LCP

Test Date	Sample Number	Theoretical Density (g/mL)	Measured Density (g/mL)
5/27/2004	ECV40-TC-14	1.647	1.642
5/27/2004	ECV40-TC-21	1.647	1.641
5/27/2004	ECV40-TC-24	1.647	1.639
5/27/2004	ECV40-TC-26	1.647	1.639
5/27/2004	ECV40-TC-27	1.647	1.640
		Average	1.640
		Standard Deviation	0.001
		Number of Samples	5

Table 9.7-24: 60 wt% Asbury Synthetic Graphite 4012 / Vectra A950RX LCP

Test Date	Sample Number	Theoretical Density (g/mL)	Measured Density (g/mL)
5/27/2004	ECV60-TC-15	1.807	1.804
5/27/2004	ECV60-TC-17	1.807	1.804
5/27/2004	ECV60-TC-18	1.807	1.803
5/27/2004	ECV60-TC-22	1.807	1.805
5/27/2004	ECV60-TC-28	1.807	1.804
5/27/2004	ECV60-TC-35	1.807	1.804
		Average	1.804
		Standard Deviation	0.001
		Number of Samples	6

Table 9.7-25: 70 wt% Asbury Synthetic Graphite 4012 / Vectra A950RX LCP

Test Date	Sample Number	Theoretical Density (g/mL)	Measured Density (g/mL)
5/27/2004	ECV70-TC-14	1.898	1.896
5/27/2004	ECV70-TC-16	1.898	1.897
5/27/2004	ECV70-TC-18	1.898	1.896
5/27/2004	ECV70-TC-19	1.898	1.897
5/27/2004	ECV70-TC-20	1.898	1.897
		Average	1.897
		Standard Deviation	0.000
		Number of Samples	5

Table 9.7-26: 40 wt% Asbury 3160 Natural Flake Graphite / Vectra A950RX LCP

Test Date	Sample Number	Theoretical Density (g/mL)	Measured Density (g/mL)
7/27/2004	EDV40-TC-14	1.647	1.643
7/27/2004	EDV40-TC-17	1.647	1.643
7/27/2004	EDV40-TC-21	1.647	1.644
7/27/2004	EDV40-TC-26	1.647	1.643
7/27/2004	EDV40-TC-29	1.647	1.645
		Average	1.644
		Standard Deviation	0.001
		Number of Samples	5

Table 9.7-27: 60 wt% Asbury 3160 Natural Flake Graphite / Vectra A950RX LCP

Test Date	Sample Number	Theoretical Density (g/mL)	Measured Density (g/mL)
7/27/2004	EDV60-TC-11	1.807	1.808
7/27/2004	EDV60-TC-12	1.807	1.809
7/27/2004	EDV60-TC-22	1.807	1.808
7/27/2004	EDV60-TC-28	1.807	1.810
7/27/2004	EDV60-TC-30	1.807	1.807
		Average	1.808
		Standard Deviation	0.001
		Number of Samples	5

Table 9.7-28: 70 wt% Asbury 3160 Natural Flake Graphite / Vectra A950RX LCP

Test Date	Sample Number	Theoretical Density (g/mL)	Measured Density (g/mL)
7/27/2004	EDV70-TC-17	1.898	1.904
7/27/2004	EDV70-TC-20	1.898	1.901
7/27/2004	EDV70-TC-22	1.898	1.901
7/27/2004	EDV70-TC-23	1.898	1.900
7/27/2004	EDV70-TC-26	1.898	1.902
		Average	1.901
		Standard Deviation	0.001
		Number of Samples	5

Table 9.7-29: 40 wt% Asbury F108A CNC / Vectra A950RX LCP

Test Date	Sample Number	Theoretical Density (g/mL)	Measured Density (g/mL)
7/27/2004	EEV40-TC-14	1.615	1.616
7/27/2004	EEV40-TC-15	1.615	1.618
7/27/2004	EEV40-TC-22	1.615	1.620
7/27/2004	EEV40-TC-26	1.615	1.617
7/27/2004	EEV40-TC-27	1.615	1.620
		Average	1.618
		Standard Deviation	0.002
		Number of Samples	5

Table 9.7-30: 60 wt% Asbury F108A CNC / Vectra A950RX LCP

Test Date	Sample Number	Theoretical Density (g/mL)	Measured Density (g/mL)
7/27/2004	EEV60-TC-19	1.750	1.747
7/27/2004	EEV60-TC-25	1.750	1.759
7/27/2004	EEV60-TC-26	1.750	1.760
7/27/2004	EEV60-TC-27	1.750	1.757
7/27/2004	EEV60-TC-31	1.750	1.760
		Average	1.757
		Standard Deviation	0.005
		Number of Samples	5

Table 9.7-31: 70 wt% Asbury F108A CNC / Vectra A950RX LCP

Test Date	Sample Number	Theoretical Density (g/mL)	Measured Density (g/mL)
7/27/2004	EEV70-TC-11	1.826	1.840
7/27/2004	EEV70-TC-26	1.826	1.842
7/27/2004	EEV70-TC-27	1.826	1.840
7/27/2004	EEV70-TC-33	1.826	1.842
7/27/2004	EEV70-TC-35	1.826	1.842
		Average	1.841
		Standard Deviation	0.001
		Number of Samples	5

Table 9.7-32: 5 wt% Fortafil 243 / Vectra A950RX LCP

Test Date	Sample Number	Theoretical Density (g/mL)	Measured Density (g/mL)
1/10/2006	EHV5-TC-2	1.414	1.408
1/10/2006	EHV5-TC-10	1.414	1.407
1/10/2006	EHV5-TC-12	1.414	1.406
1/10/2006	EHV5-TC-22	1.414	1.407
		Average	1.407
		Standard Deviation	0.001
		Number of Samples	4

Table 9.7-33: 7.5 wt% Fortafil 243 / Vectra A950RX LCP

Test Date	Sample Number	Theoretical Density (g/mL)	Measured Density (g/mL)
1/10/2006	EHV7.5-TC-2	1.421	1.414
1/10/2006	EHV7.5-TC-10	1.421	1.422
1/10/2006	EHV7.5-TC-12	1.421	1.419
1/10/2006	EHV7.5-TC-22	1.421	1.417
		Average	1.418
		Standard Deviation	0.003
		Number of Samples	4

Table 9.7-34: 10 wt% Fortafil 243 / Vectra A950RX LCP

Test Date	Sample Number	Theoretical Density (g/mL)	Measured Density (g/mL)
1/10/2006	EHV10-TC-2	1.428	1.422
1/10/2006	EHV10-TC-10	1.428	1.425
1/10/2006	EHV10-TC-12	1.428	1.423
1/10/2006	EHV10-TC-22	1.428	1.424
		Average	1.424
		Standard Deviation	0.001
		Number of Samples	4

Table 9.7-35: 15 wt% Fortafil 243 / Vectra A950RX LCP

Test Date	Sample Number	Theoretical Density (g/mL)	Measured Density (g/mL)
1/10/2006	EHV15-TC-2	1.442	1.437
1/10/2006	EHV15-TC-10	1.442	1.437
1/10/2006	EHV15-TC-12	1.442	1.439
1/10/2006	EHV15-TC-22	1.442	1.437
		Average	1.438
		Standard Deviation	0.001
		Number of Samples	4

Table 9.7-36: 20 wt% Fortafil 243 / Vectra A950RX LCP

Test Date	Sample Number	Theoretical Density (g/mL)	Measured Density (g/mL)
1/10/2006	EHV20-TC-2	1.457	1.451
1/10/2006	EHV20-TC-10	1.457	1.453
1/10/2006	EHV20-TC-13	1.457	1.452
1/10/2006	EHV20-TC-22	1.457	1.459
		Average	1.454
		Standard Deviation	0.004
		Number of Samples	4

Table 9.7-37: 25 wt% Fortafil 243 / Vectra A950RX LCP

Test Date	Sample Number	Theoretical Density (g/mL)	Measured Density (g/mL)
1/10/2006	EHV25-TC-2	1.472	1.470
1/10/2006	EHV25-TC-10	1.472	1.468
1/10/2006	EHV25-TC-12	1.472	1.468
1/10/2006	EHV25-TC-22	1.472	1.474
		Average	1.470
		Standard Deviation	0.003
		Number of Samples	4

Table 9.7-38: 30 wt% Fortafil 243 / Vectra A950RX LCP

Test Date	Sample Number	Theoretical Density (g/mL)	Measured Density (g/mL)
1/10/2006	EHV30-TC-2	1.487	1.484
1/10/2006	EHV30-TC-10	1.487	1.484
1/10/2006	EHV30-TC-12	1.487	1.485
1/10/2006	EHV30-TC-22	1.487	1.484
		Average	1.484
		Standard Deviation	0.000
		Number of Samples	4

Table 9.7-39: 35 wt% Fortafil 243 / Vectra A950RX LCP

Test Date	Sample Number	Theoretical Density (g/mL)	Measured Density (g/mL)
1/10/2006	EHV35-TC-2	1.503	1.499
1/10/2006	EHV35-TC-10	1.503	1.499
1/10/2006	EHV35-TC-12	1.503	1.500
1/10/2006	EHV35-TC-22	1.503	1.500
		Average	1.500
		Standard Deviation	0.001
		Number of Samples	4

Table 9.7-40: 40 wt% Fortafil 243 / Vectra A950RX LCP

Test Date	Sample Number	Theoretical Density (g/mL)	Measured Density (g/mL)
1/10/2006	EHV40-TC-2	1.519	1.515
1/10/2006	EHV40-TC-10	1.519	1.515
1/10/2006	EHV40-TC-12	1.519	1.516
1/10/2006	EHV40-TC-22	1.519	1.517
		Average	1.516
		Standard Deviation	0.001
		Number of Samples	4

Table 9.7-41: 45 wt% Fortafil 243 / Vectra A950RX LCP

Test Date	Sample Number	Theoretical Density (g/mL)	Measured Density (g/mL)
1/10/2006	EHV45-TC-2	1.535	1.532
1/10/2006	EHV45-TC-10	1.535	1.534
1/10/2006	EHV45-TC-12	1.535	1.533
1/10/2006	EHV45-TC-22	1.535	1.532
		Average	1.533
		Standard Deviation	0.001
		Number of Samples	4

Table 9.7-42: 50 wt% Fortafil 243 / Vectra A950RX LCP

Test Date	Sample Number	Theoretical Density (g/mL)	Measured Density (g/mL)
3/1/2006	EHV50R-TC-13	1.552	1.556
3/1/2006	EHV50R-TC-23	1.552	1.552
3/1/2006	EHV50R-TC-28	1.552	1.551
		Average	1.553
		Standard Deviation	0.002
		Number of Samples	3

Table 9.7-43: 55 wt% Fortafil 243 / Vectra A950RX LCP

Test Date	Sample Number	Theoretical Density (g/mL)	Measured Density (g/mL)
3/1/2006	EHV55-TC-13	1.569	1.570
3/1/2006	EHV55-TC-23	1.569	1.570
3/1/2006	EHV55-TC-28	1.569	1.569
		Average	1.570
		Standard Deviation	0.000
		Number of Samples	3

Table 9.7-44: 60 wt% Fortafil 243 / Vectra A950RX LCP

Test Date	Sample Number	Theoretical Density (g/mL)	Measured Density (g/mL)
3/1/2006	EHV60R-TC-13	1.586	1.584
3/1/2006	EHV60R-TC-23	1.586	1.587
3/1/2006	EHV60R-TC-28	1.586	1.584
		Average	1.585
		Standard Deviation	0.002
		Number of Samples	3

Section 9.8: Orientation Data

Table 9.8-1: Thermocarb TC300 / Vectra A950RX LCP (In-Plane)

Sample	Average (degrees)	Standard Deviation (degrees)	Number of Data Points
EBV40	19.90	21.16	1690
EBV60	23.84	22.10	650
EBV70	28.38	25.43	1064

Table 9.8-2: Thermocarb TC300 / Vectra A950RX LCP (Through-Plane)

Sample	Average (degrees)	Standard Deviation (degrees)	Number of Data Points
EBV40	51.92	31.09	571
EBV60	52.71	30.22	1564
EBV70	44.38	29.71	1422

Table 9.8-3: Asbury Synthetic Graphite 4012 / Vectra A950RX LCP (In-Plane)

Sample	Average (degrees)	Standard Deviation (degrees)	Number of Data Points
ECV40	23.56	21.01	621
ECV60	29.16	25.27	1657
ECV70	34.60	26.05	595

Table 9.8-4: Asbury Synthetic Graphite 4012 / Vectra A950RX LCP (Through-Plane)

Sample	Average (degrees)	Standard Deviation (degrees)	Number of Data Points
ECV40	53.25	29.90	1169
ECV60	46.80	29.46	1664
ECV70	40.26	27.46	1458

Table 9.8-5: Asbury 3160 Natural Flake Graphite / Vectra A950RX LCP (In-Plane)

Sample	Average (degrees)	Standard Deviation (degrees)	Number of Data Points
EDV40	13.89	16.00	1577
EDV60	27.68	24.78	408
EDV70	39.26	30.18	373

Table 9.8-6: Asbury 3160 Natural Flake Graphite / Vectra A950RX LCP (Through-Plane)

Sample	Average (degrees)	Standard Deviation (degrees)	Number of Data Points
EDV40	50.15	28.80	2094
EDV60	40.17	28.25	1811
EDV70	38.18	25.00	1851

Table 9.8-7: Asbury F108A CNC / Vectra A950RX LCP (In-Plane)

Sample	Average (degrees)	Standard Deviation (degrees)	Number of Data Points
EEV40	23.43	22.21	585
EEV60	32.02	25.81	1469
EEV70	31.07	27.44	769

Table 9.8-8: Asbury F108A CNC / Vectra A950RX LCP (Through-Plane)

Sample	Average (degrees)	Standard Deviation (degrees)	Number of Data Points
EEV40	51.57	29.51	884
EEV60	48.59	29.21	595
EEV70	44.95	28.26	756

Table 9.8-9: Fortafil 243 Carbon Fiber / Vectra A950RX LCP (In-Plane)

Sample	Average (degrees)	Standard Deviation (degrees)	Number of Data Points
EHV10	33.42	24.09	545
EHV20	36.50	26.53	2620
EHV40	14.36	17.44	2373
EHV60	17.93	19.56	4225

Table 9.8-10: Fortafil 243 Carbon Fiber / Vectra A950RX LCP (Through-Plane)

Sample	Average (degrees)	Standard Deviation (degrees)	Number of Data Points
EHV10	61.49	31.40	2693
EHV20	62.23	28.88	989
EHV40	59.89	27.17	1294
EHV60	62.16	24.01	386

Section 9.9: Through-Plane Micrographs
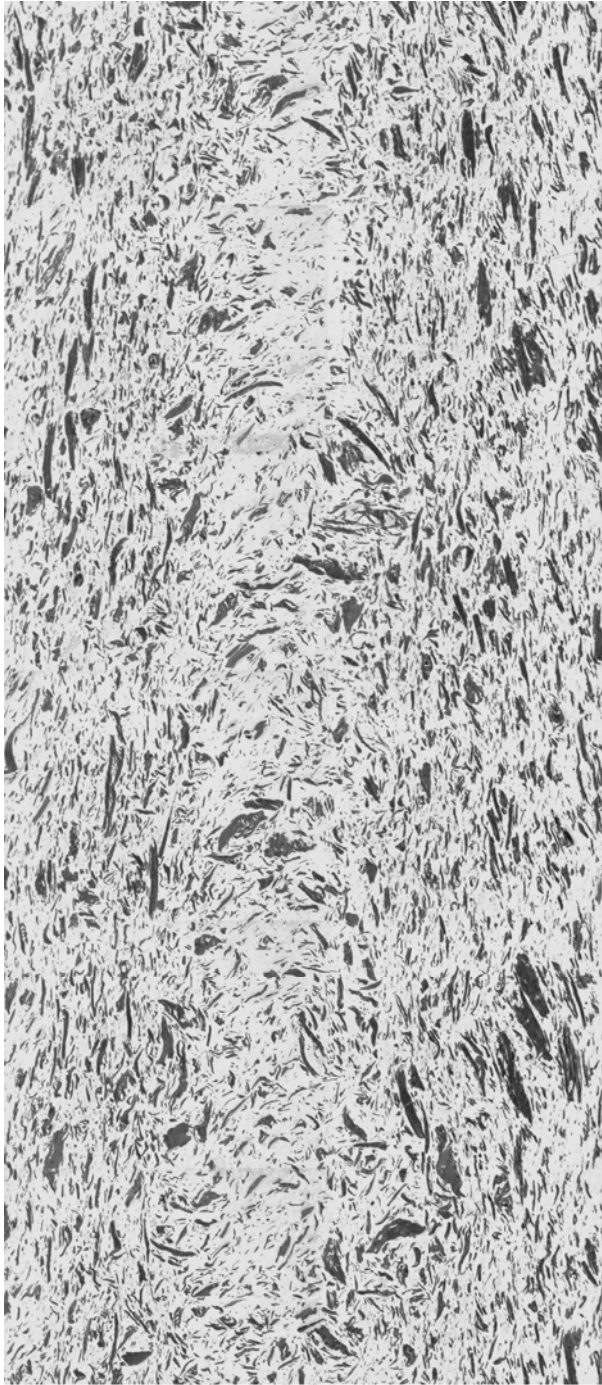
DIRECTION OF CONDUCTION

Figure 9.9-1: Optical Micrograph by reflected light of a through-plane thermal conductivity sample containing 40 wt% Thermocarb TC-300 synthetic graphite in Vectra A950RX LCP at 100x magnification.
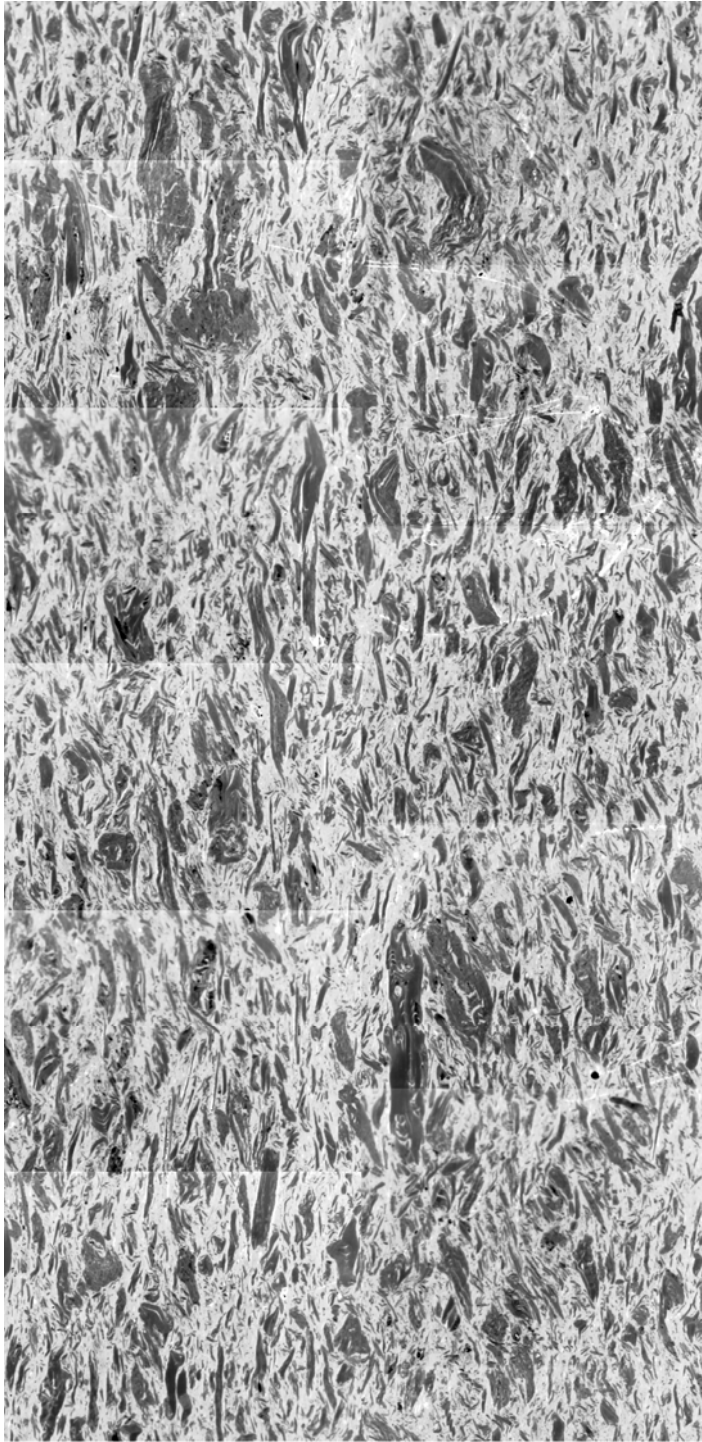
DIRECTION OF CONDUCTION

Figure 9.9-2: Optical Micrograph by reflected light of a through-plane thermal conductivity sample containing 60 wt% Thermocarb TC-300 synthetic graphite in Vectra A950RX LCP at 200x magnification.

DIRECTION OF CONDUCTION

Figure 9.9-3: Optical Micrograph by reflected light of a through-plane thermal conductivity sample containing 70 wt% Thermocarb TC-300 synthetic graphite in Vectra A950RX LCP at 100x magnification.

DIRECTION OF CONDUCTION

Figure 9.9-4: Optical Micrograph by reflected light of a through-plane thermal conductivity sample containing 40 wt% Asbury 4012 synthetic graphite in Vectra A950RX LCP at 100x magnification.

DIRECTION OF CONDUCTION

Figure 9.9-5: Optical Micrograph by reflected light of a through-plane thermal conductivity sample containing 60 wt% Asbury 4012 synthetic graphite in Vectra A950RX LCP at 100x magnification.

DIRECTION OF CONDUCTION

Figure 9.9-6: Optical Micrograph by reflected light of a through-plane thermal conductivity sample containing 70 wt% Asbury 4012 synthetic graphite in Vectra A950RX LCP at 100x magnification.

DIRECTION OF CONDUCTION

Figure 9.9-7: Optical Micrograph by reflected light of a through-plane thermal conductivity sample containing 40 wt% Asbury 3160 natural flake graphite in Vectra A950RX LCP at 200x magnification.

DIRECTION OF CONDUCTION

Figure 9.9-8: Optical Micrograph by reflected light of a through-plane thermal conductivity sample containing 60 wt% Asbury 3160 natural flake graphite in Vectra A950RX LCP at 200x magnification.

DIRECTION OF CONDUCTION

Figure 9.9-9: Optical Micrograph by reflected light of a through-plane thermal conductivity sample containing 70 wt% Asbury 3160 natural flake graphite in Vectra A950RX LCP at 200x magnification.

DIRECTION OF CONDUCTION

Figure 9.9-10: Optical Micrograph by reflected light of a through-plane thermal conductivity sample containing 40 wt% Asbury F108A CNC in Vectra A950RX LCP at 100x magnification.

DIRECTION OF CONDUCTION

Figure 9.9-11: Optical Micrograph by reflected light of a through-plane thermal conductivity sample containing 60 wt% Asbury F108A CNC in Vectra A950RX LCP at 100x magnification.

DIRECTION OF CONDUCTION

Figure 9.9-12: Optical Micrograph by reflected light of a through-plane thermal conductivity sample containing 70 wt% Asbury F108A CNC in Vectra A950RX LCP at 100x magnification.

DIRECTION OF CONDUCTION

Figure 9.9-13: Optical Micrograph by reflected light of a through-plane thermal conductivity sample containing 10 wt% Fortafil 243 carbon fiber in Vectra A950RX LCP at 100x magnification.

DIRECTION OF CONDUCTION

Figure 9.9-14: Optical Micrograph by reflected light of a through-plane thermal conductivity sample containing 20 wt% Fortafil 243 carbon fiber in Vectra A950RX LCP at 100x magnification.

DIRECTION OF CONDUCTION

Figure 9.9-15: Optical Micrograph by reflected light of a through-plane thermal conductivity sample containing 40 wt% Fortafil 243 carbon fiber in Vectra A950RX LCP at 100x magnification.
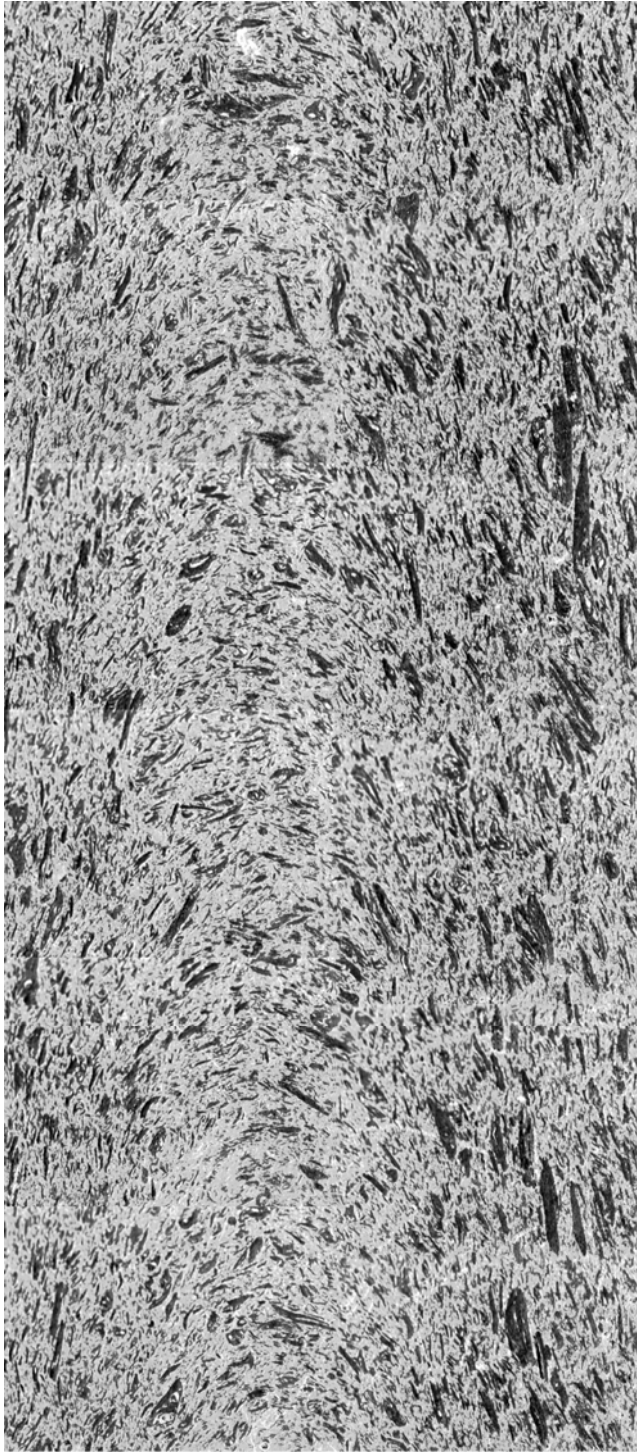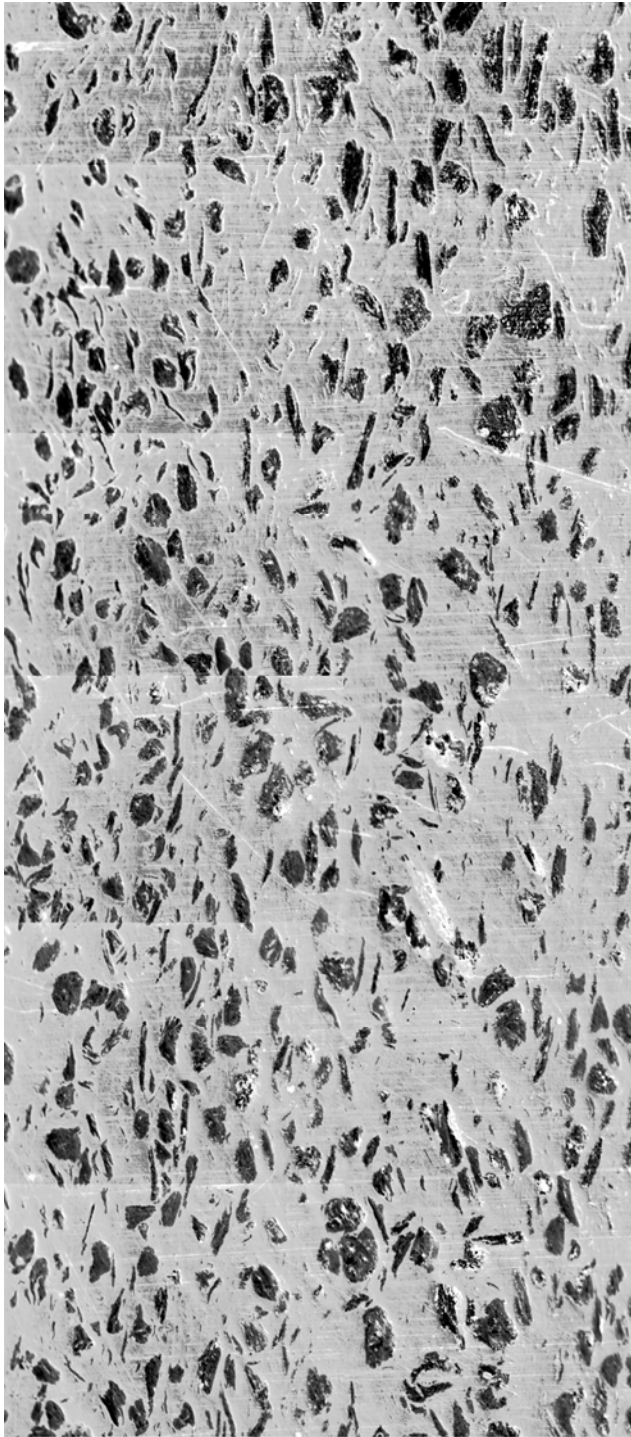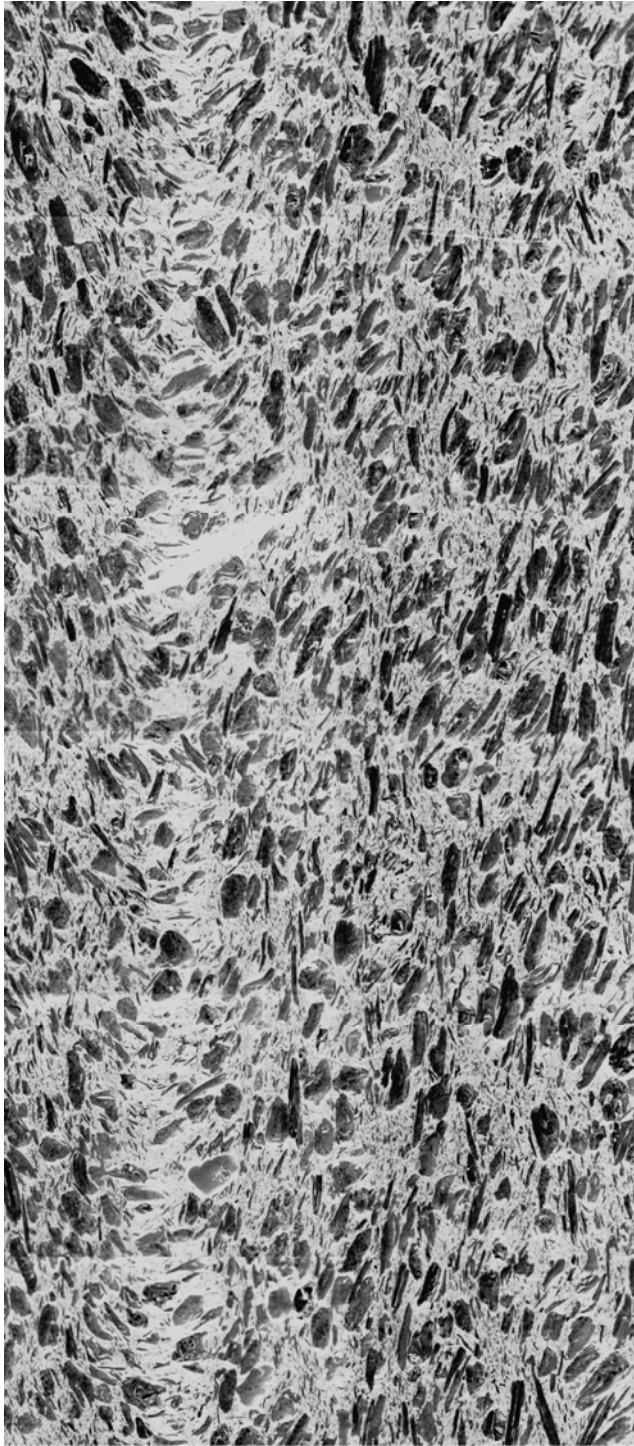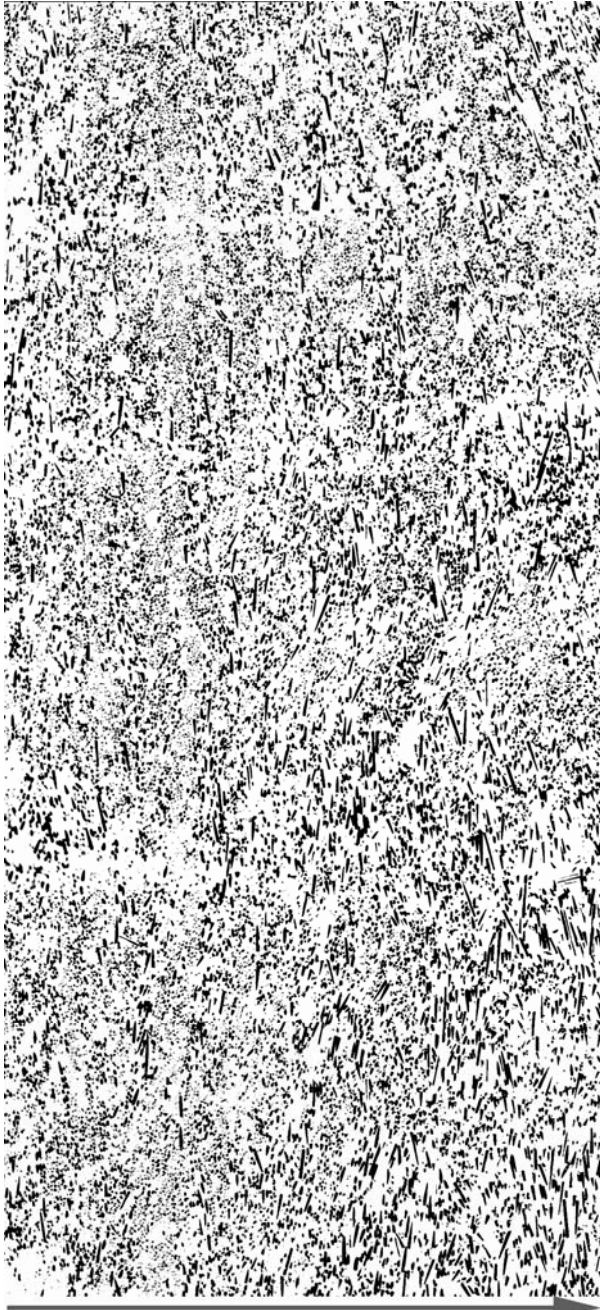
DIRECTION OF CONDUCTION

Figure 9.9-16: Optical Micrograph by reflected light of a through-plane thermal conductivity sample containing 60 wt% Fortafil 243 carbon fiber in Vectra A950RX LCP at 100x magnification.

Section 9.10: In-Plane Micrographs
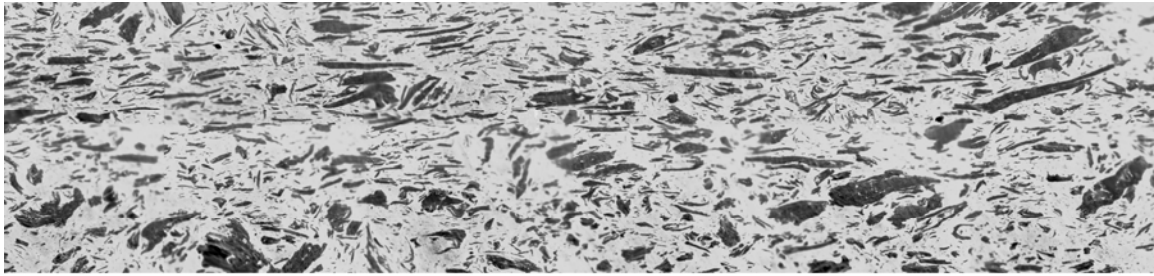
DIRECTION OF CONDUCTION

Figure 9.10-1: Optical Micrograph by reflected light of an in-plane electrical resistivity sample containing 40 wt% Thermocarb TC-300 synthetic graphite in Vectra A950RX LCP at 200x magnification.
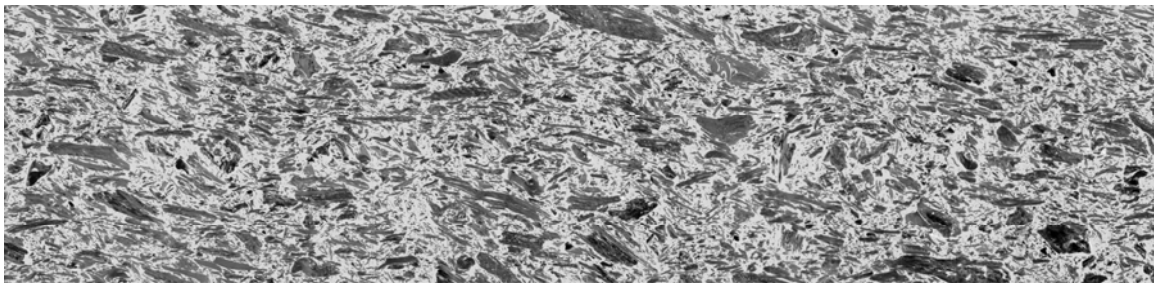
DIRECTION OF CONDUCTION

Figure 9.10-2: Optical Micrograph by reflected light of an in-plane electrical resistivity sample containing 60 wt% Thermocarb TC-300 synthetic graphite in Vectra A950RX LCP at 200x magnification.
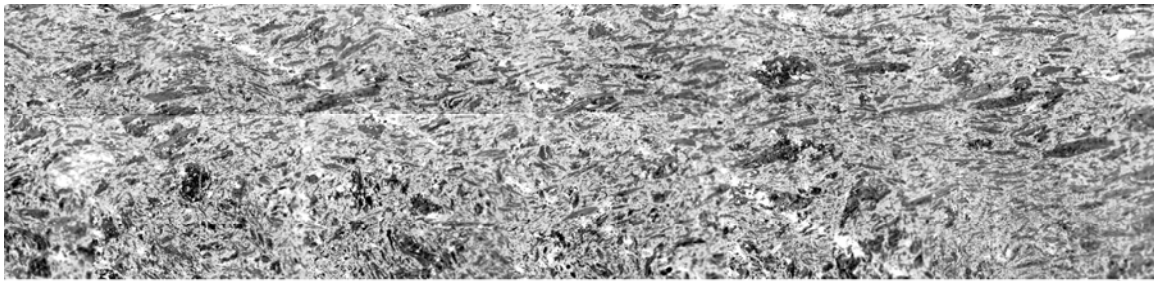
DIRECTION OF CONDUCTION

Figure 9.10-3: Optical Micrograph by reflected light of an in-plane electrical resistivity sample containing 70 wt% Thermocarb TC-300 synthetic graphite in Vectra A950RX LCP at 200x magnification.
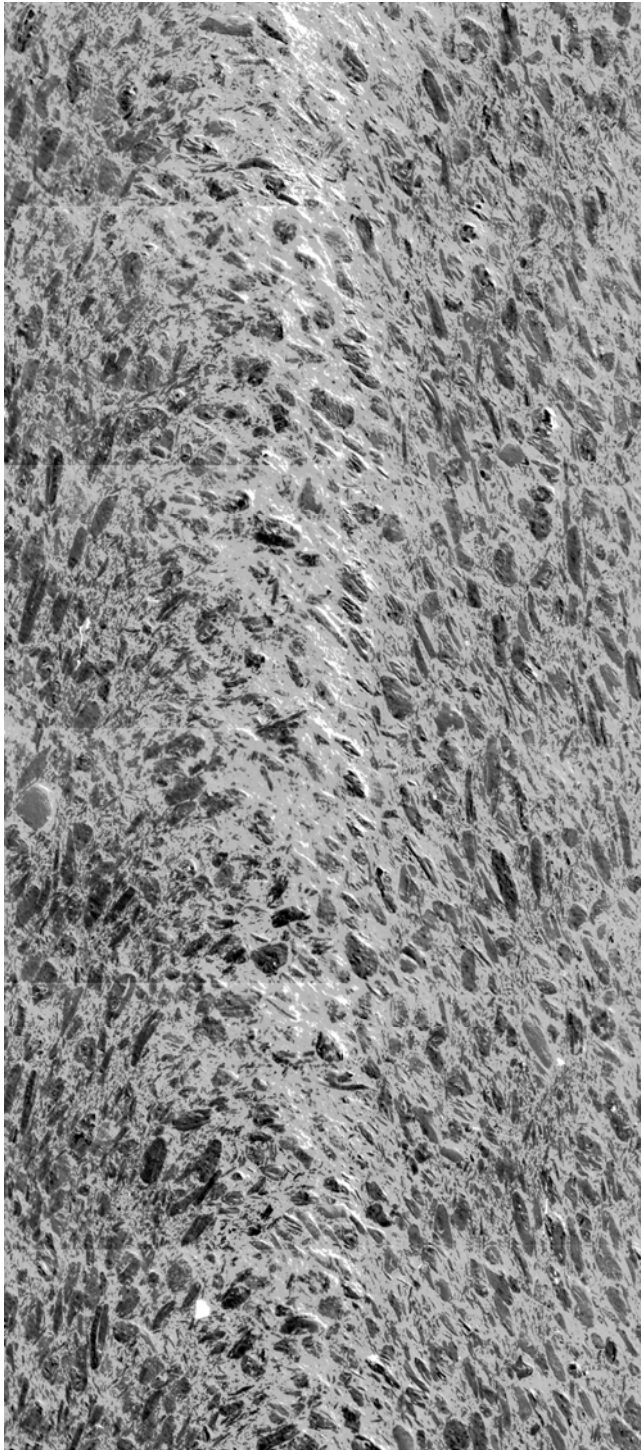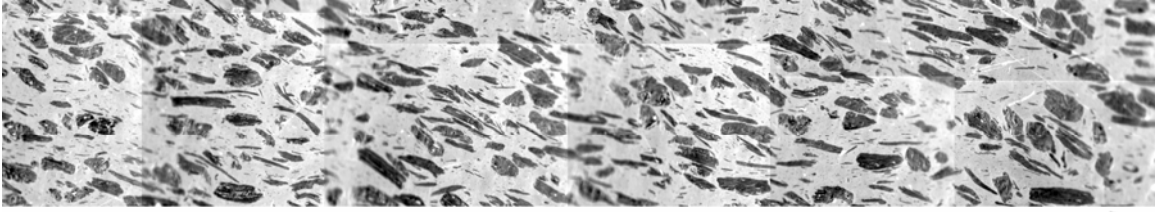
DIRECTION OF CONDUCTION

Figure 9.10-4: Optical Micrograph by reflected light of an in-plane electrical resistivity sample containing 40 wt% Asbury 4012 synthetic graphite in Vectra A950RX LCP at 100x magnification.
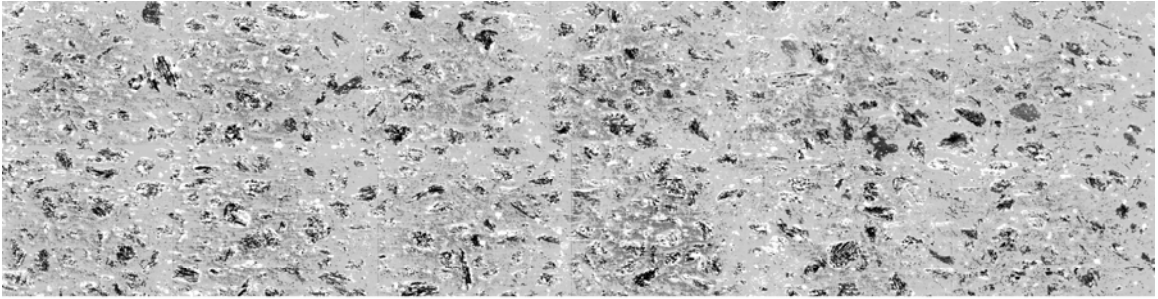
DIRECTION OF CONDUCTION

Figure 9.10-5: Optical Micrograph by reflected light of an in-plane electrical resistivity sample containing 60 wt% Asbury 4012 synthetic graphite in Vectra A950RX LCP at 100x magnification.
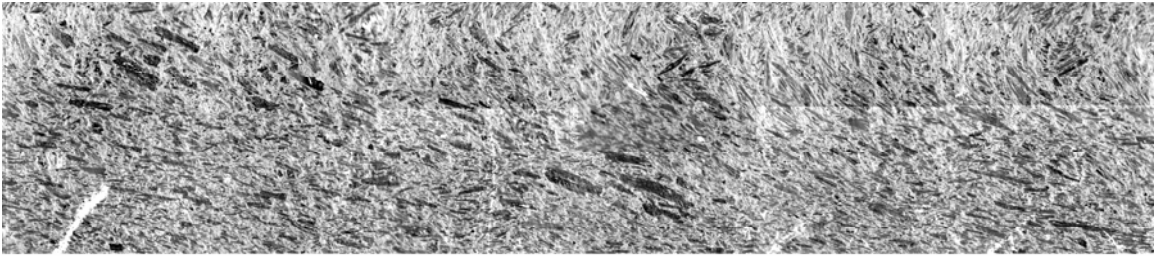
DIRECTION OF CONDUCTION

Figure 9.10-6: Optical Micrograph by reflected light of an in-plane electrical resistivity sample containing 70 wt% Asbury 4012 synthetic graphite in Vectra A950RX LCP at 100x magnification.
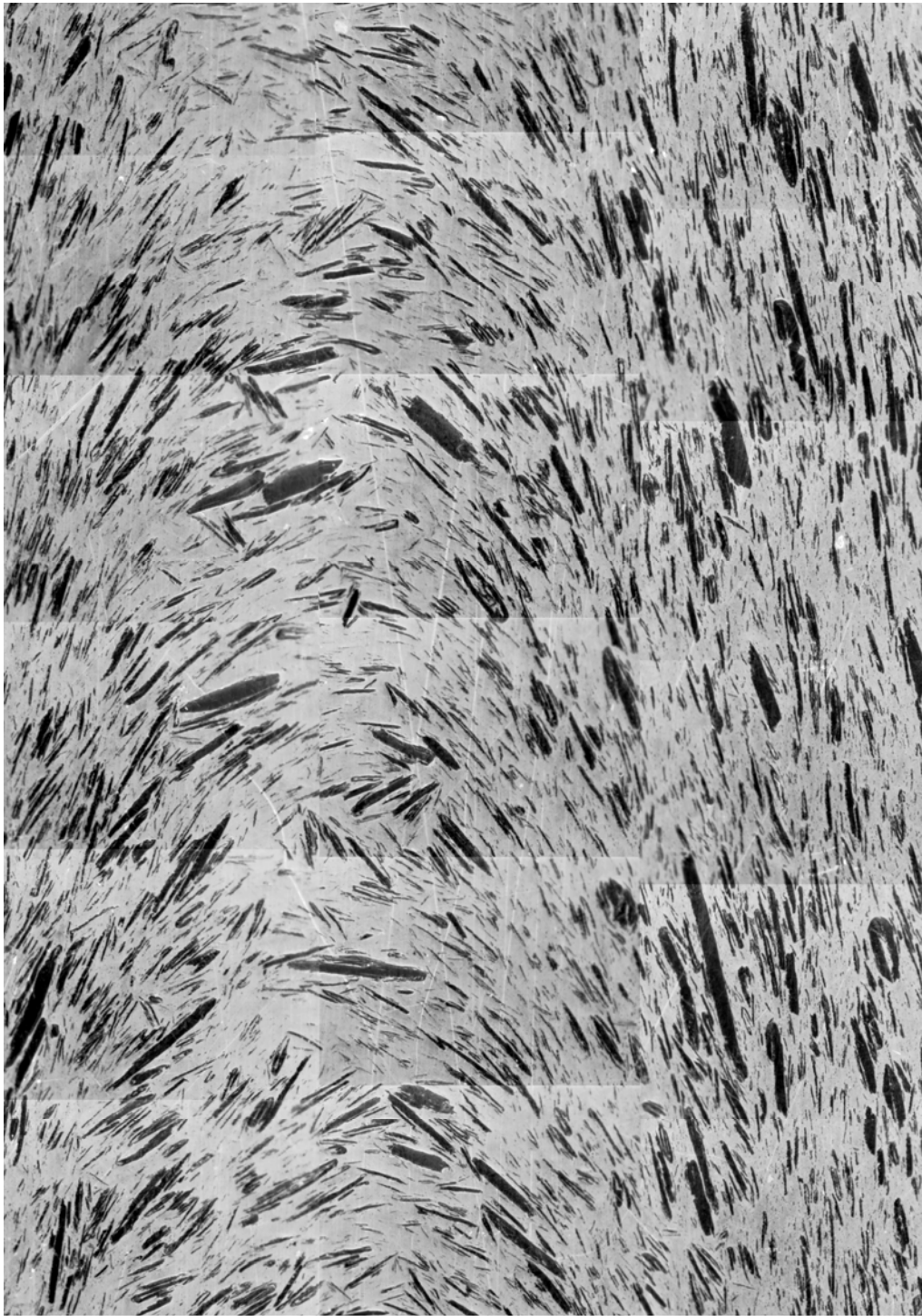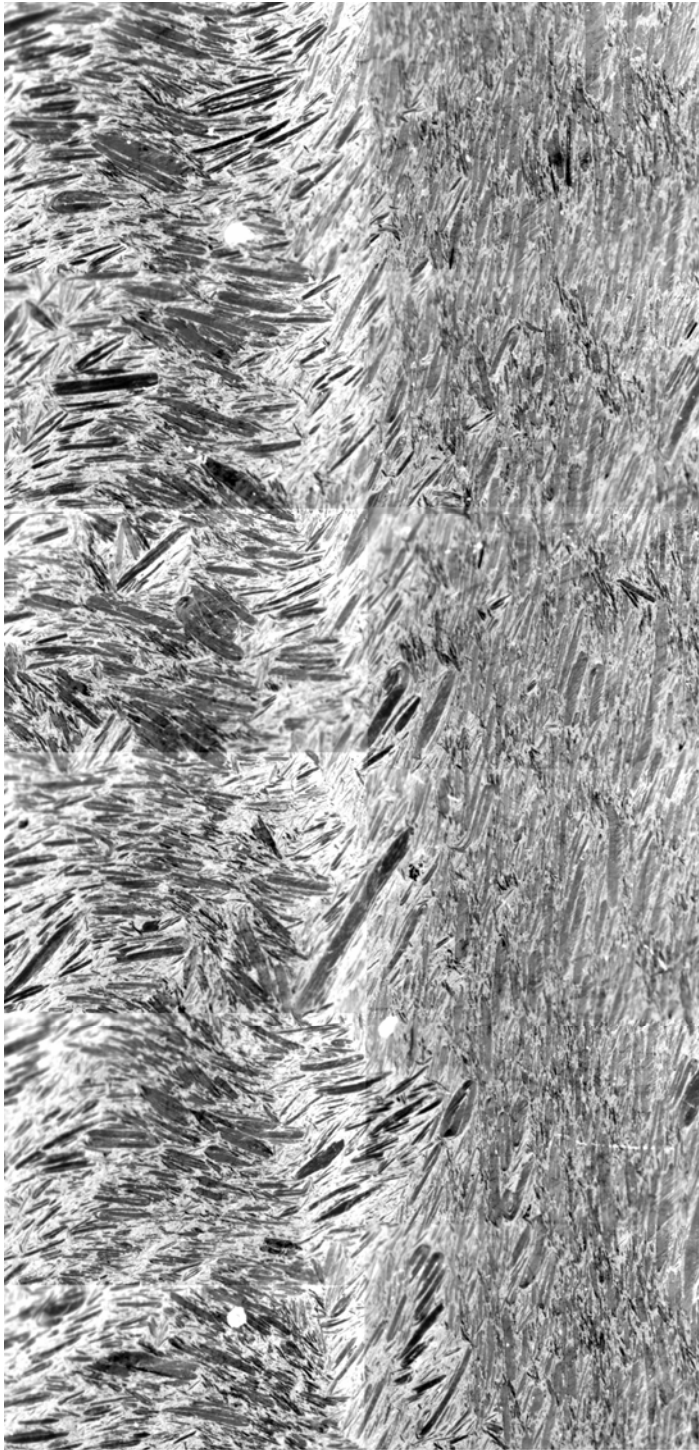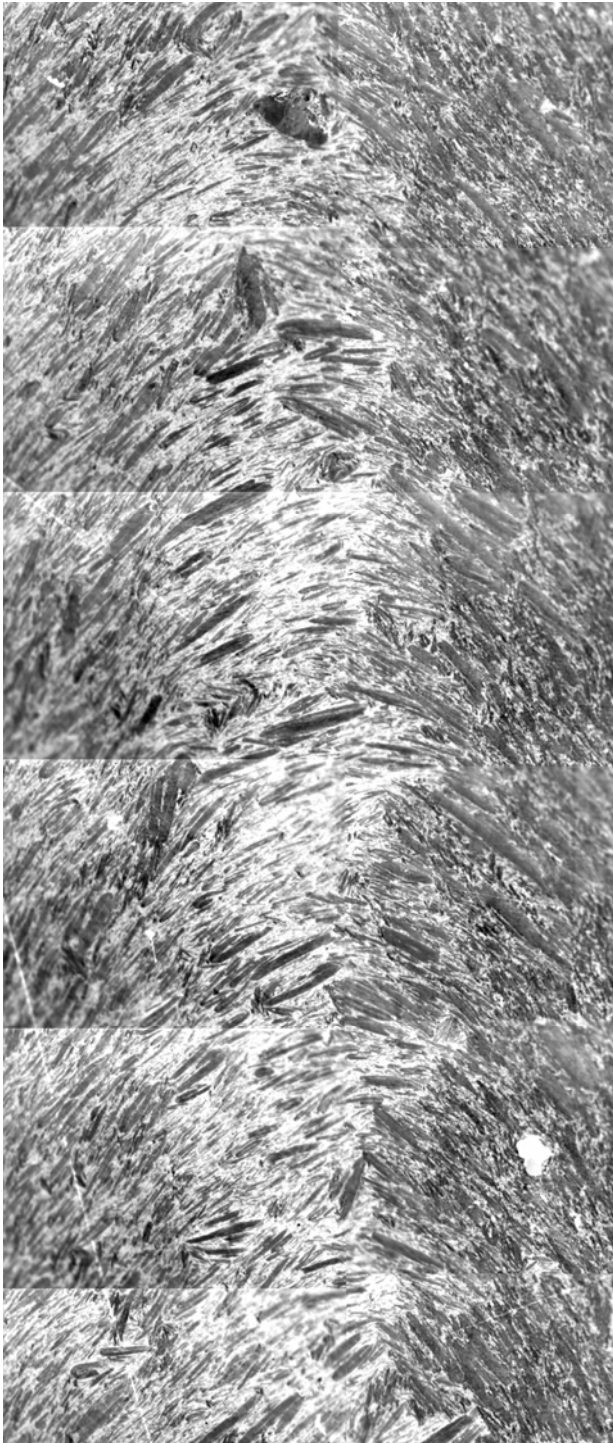
DIRECTION OF CONDUCTION

Figure 9.10-7: Optical Micrograph by reflected light of an in-plane electrical resistivity sample containing 40 wt% Asbury 3160 natural flake graphite in Vectra A950RX LCP at 200x magnification.
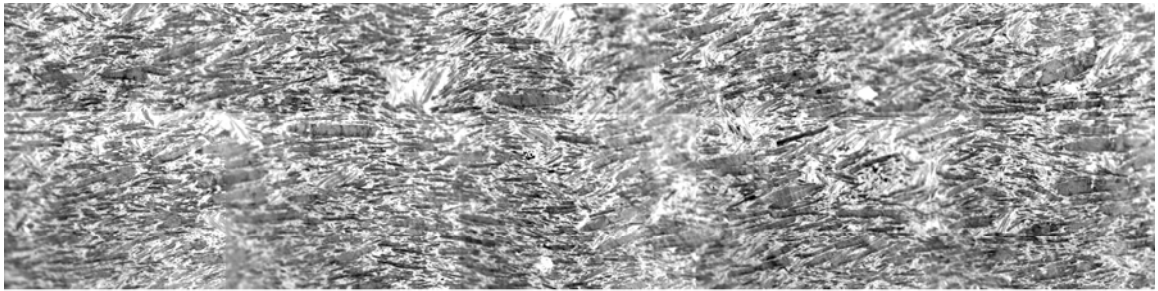
DIRECTION OF CONDUCTION

Figure 9.10-8: Optical Micrograph by reflected light of an in-plane electrical resistivity sample containing 60 wt% Asbury 3160 natural flake graphite in Vectra A950RX LCP at 200x magnification.

DIRECTION OF CONDUCTION

Figure 9.10-9: Optical Micrograph by reflected light of an in-plane electrical resistivity sample containing 70 wt% Asbury 3160 natural flake graphite in Vectra A950RX LCP at 100x magnification.
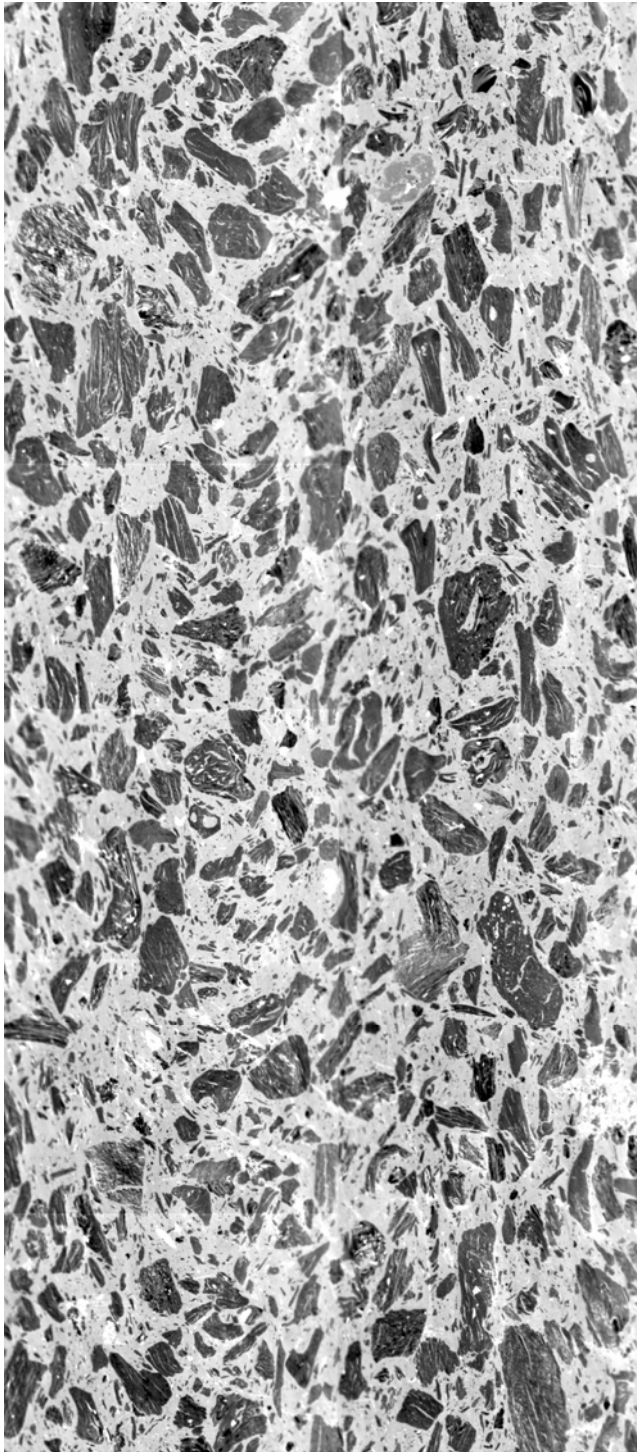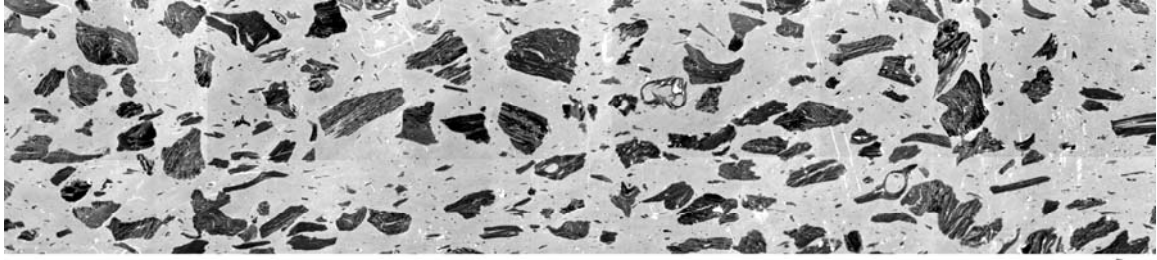
DIRECTION OF CONDUCTION

Figure 9.10-10: Optical Micrograph by reflected light of an in-plane electrical resistivity sample containing 40 wt% Asbury F108A CNC in Vectra A950RX LCP at 100x magnification.
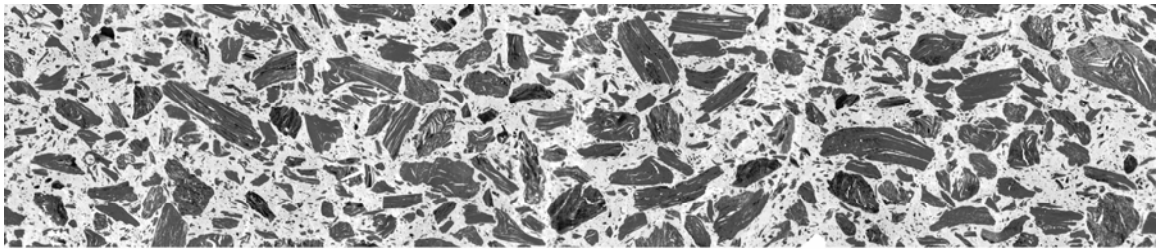
DIRECTION OF CONDUCTION

Figure 9.10-11: Optical Micrograph by reflected light of an in-plane electrical resistivity sample containing 60 wt% Asbury F108A CNC in Vectra A950RX LCP at 100x magnification.
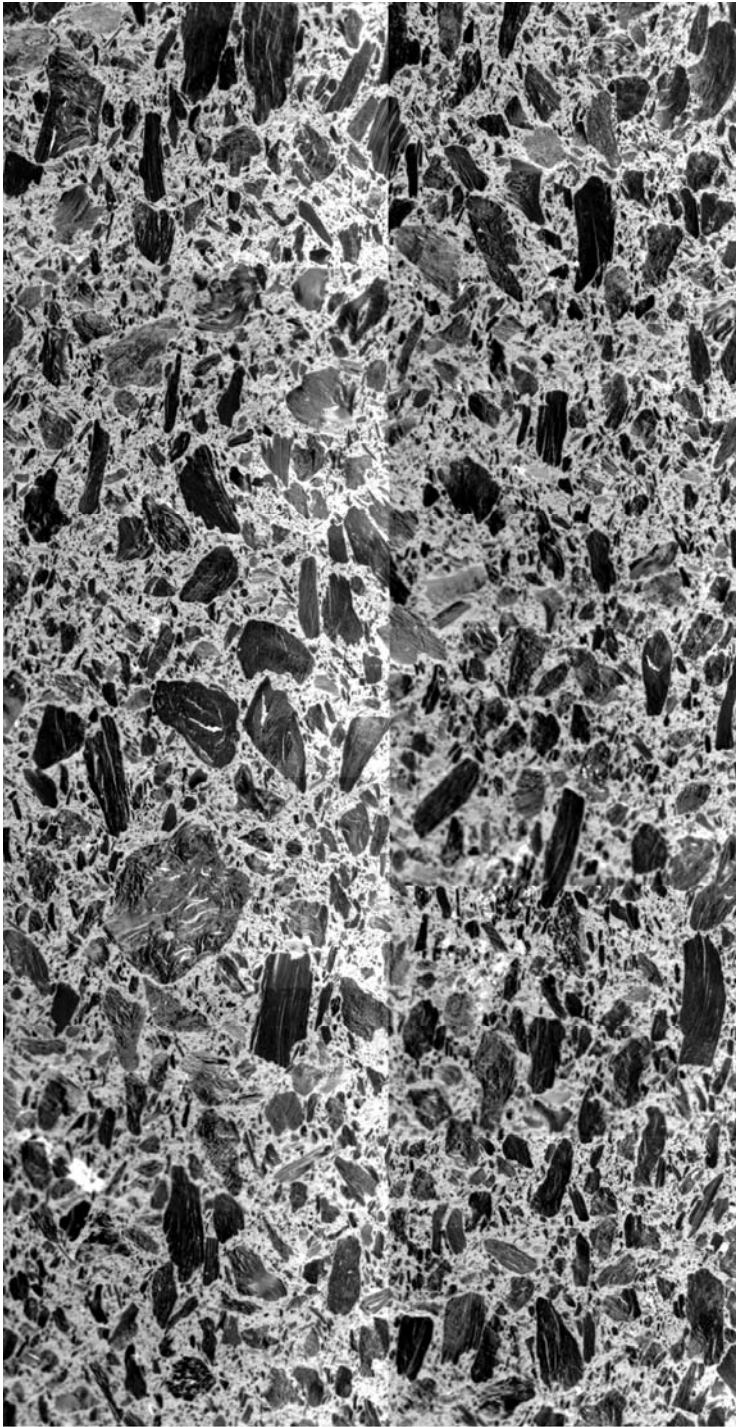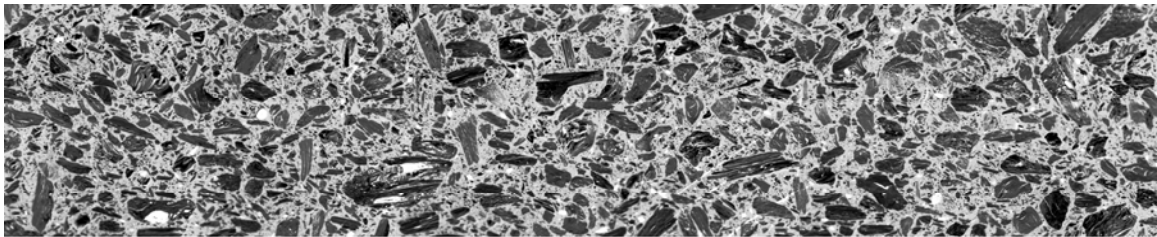

DIRECTION OF CONDUCTION

Figure 9.10-12: Optical Micrograph by reflected light of an in-plane electrical resistivity sample containing 40 wt% Asbury F108A CNC in Vectra A950RX LCP at 100x magnification.

DIRECTION OF CONDUCTION
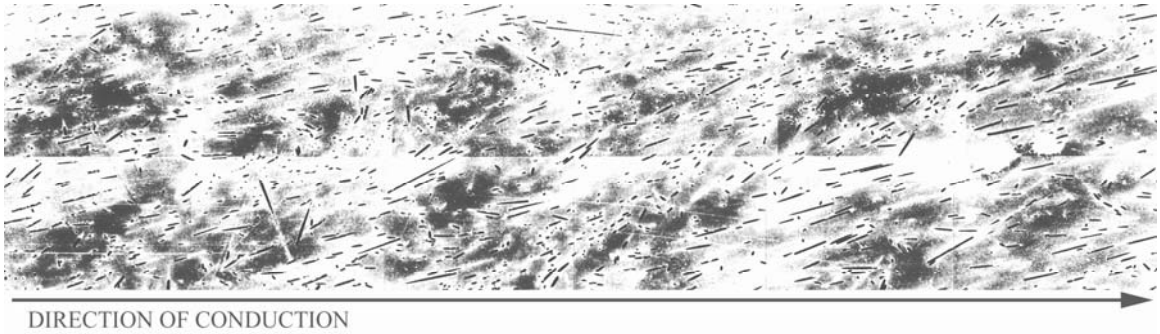
Figure 9.10-13: Optical Micrograph by reflected light of an in-plane electrical resistivity sample containing 10 wt% Fortafil 243 carbon fiber in Vectra A950RX LCP at 100x magnification.

DIRECTION OF CONDUCTION
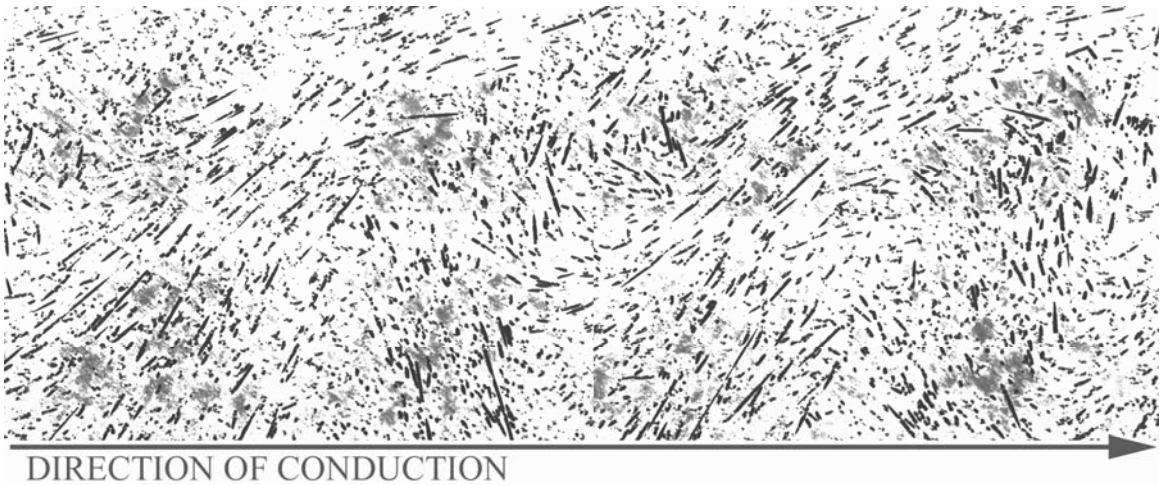
Figure 9.10-14: Optical Micrograph by reflected light of an in-plane electrical resistivity sample containing 20 wt% Fortafil 243 carbon fiber in Vectra A950RX LCP at 100x magnification.

DIRECTION OF CONDUCTION
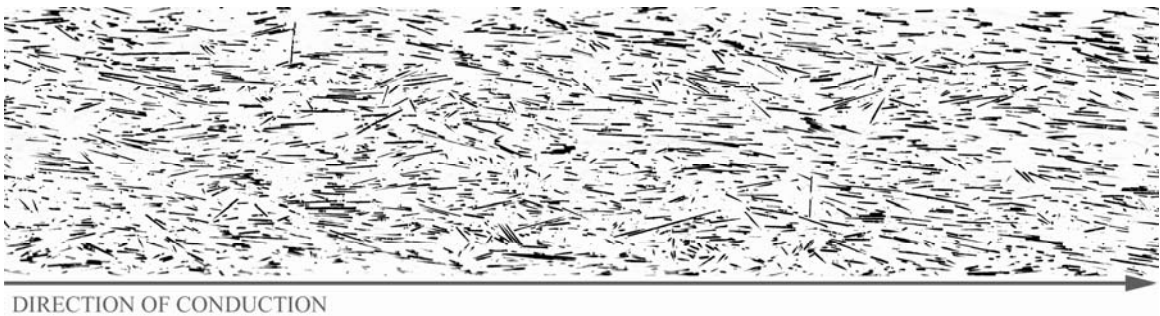
Figure 9.10-15: Optical Micrograph by reflected light of an in-plane electrical resistivity sample containing 40 wt% Fortafil 243 carbon fiber in Vectra A950RX LCP at 100x magnification.
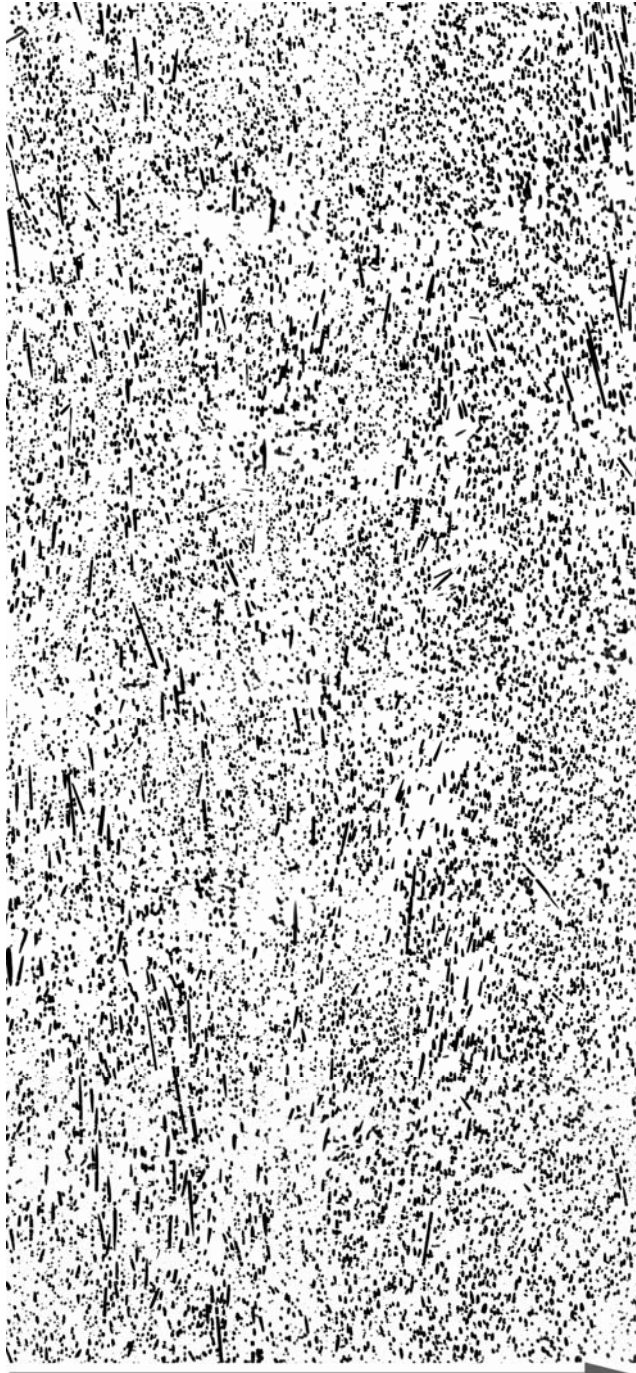
DIRECTION OF CONDUCTION

Figure 9.10-16: Optical Micrograph by reflected light of an in-plane electrical resistivity sample containing 60 wt% Fortafil 243 carbon fiber in Vectra A950RX LCP at 100x magnification.

Section 9.11: Modeling Results

Table 9.11-1: Rule of Mixtures, Carbon Black Composite

	TC (W/mK)			0.003577	0.002643	0.738959
Vectra	0.22			epsilon(y)	sum((y(i)-y(mod))^2)	sum(y(i)^2)
Filler	2.1					
			TC (W/mK)	TC (W/mK)		
Formulation	wt% filler	vol% filler	Experimental	Calculated	(y(i)-y(mod))^2	y(i)^2
EVR	0	0.000	0.217	0.220	0.000010	0.047046
EAV2.5	2.5	0.019	0.242	0.256	0.000218	0.058419
EAV4R	4	0.031	0.258	0.279	0.000438	0.066616
EAV5R	5	0.039	0.269	0.294	0.000634	0.072200
EAV6	6	0.047	0.293	0.308	0.000224	0.086084
EAV7.5	7.5	0.060	0.322	0.332	0.000103	0.103491
EAV10	10	0.080	0.364	0.370	0.000043	0.132132
EAV15	15	0.121	0.416	0.447	0.000974	0.172973

Table 9.11-2: Rule of Mixtures, Synthetic Graphite Composite

	TC (W/mK)			29846.9	714497	23.9387
Vectra	0.22			epsilon(y)	sum((y(i)-y(mod))^2)	sum(y(i)^2)
Filler	600					
			TC (W/mK)	TC (W/mK)		
Formulation	wt% filler	vol% filler	Experimental	Calculated	(y(i)-y(mod))^2	y(i)^2
EVR	0	0.000	0.217	0.220	0.000010	0.047046
EBV10	10	0.065	0.294	39.164	1510.89	0.086142
EBV15	15	0.099	0.349	59.802	3534.63	0.122080
EBV20	20	0.135	0.387	81.250	6538.89	0.149692
EBV25	25	0.172	0.470	103.382	10590.9	0.220806
EBV30	30	0.211	0.546	126.954	15978.8	0.298553
EBV35	35	0.252	0.611	151.365	22726.8	0.372832
EBV40	40	0.293	0.706	175.956	30712.3	0.499001
EBV45	45	0.338	0.880	202.946	40830.4	0.775104
EBV50	50	0.385	1.108	230.895	52802.2	1.22789
EBV55	55	0.433	1.285	259.967	66916.2	1.65148
EBV60	60	0.484	1.559	290.514	83494.9	2.42923
EBV65	65	0.537	1.943	322.422	102707	3.77369
EBV70	70	0.593	2.323	355.890	125010	5.39401
EBV75	75	0.652	2.625	391.397	151143	6.89115

Table 9.11-3: Rule of Mixtures, Carbon Fiber Composite

	TC (W/mK)			119.638	448.065	3.74516
Vectra	0.22			epsilon(y)	sum((y(i)-y(mod))^2)	sum(y(i)^2)
Filler	20					
			TC (W/mK)	TC (W/mK)		
Formulation	wt% filler	vol% filler	Experimental	Calculated	(y(i)-y(mod))^2	y(i)^2
EVR	0	0.000	0.217	0.220	0.000010	0.047046
EHV5	5	0.041	0.238	1.031	0.628817	0.056644
EHV7.5	7.5	0.061	0.255	1.427	1.37260	0.065025
EHV10	10	0.082	0.271	1.842	2.46792	0.073441
EHV15	15	0.124	0.282	2.673	5.71554	0.079524
EHV20	20	0.168	0.320	3.543	10.3880	0.102400
EHV25	25	0.212	0.353	4.413	16.4865	0.124609
EHV30	30	0.255	0.365	5.264	23.9992	0.133225
EHV35	35	0.302	0.432	6.194	33.1956	0.186624
EHV40	40	0.349	0.527	7.123	43.5101	0.277729
EHV45	45	0.397	0.602	8.073	55.8108	0.362404
EHV50R	50	0.446	0.688	9.042	69.7873	0.473344
EHV55	55	0.496	0.838	10.031	84.5090	0.702244
EHV60R	60	0.547	1.030	11.040	100.193	1.06090

Table 9.11-4: Inverse Rule of Mixtures, Carbon Black Composite

	TC (W/mK)				0.080772	0.059687	0.738959
Vectra	0.22				epsilon(y)	sum((y(i)-y(mod))^2)	sum(y(i)^2)
Filler	2.1						
			TC (W/mK)	TC (W/mK)			
Formulation	wt% filler	vol% filler	Experimental	Calculated	(y(i)-y(mod))^2	y(i)^2
EVR	0	0.000	0.217	0.220	0.000010	0.047046
EAV2.5	2.5	0.019	0.242	0.224	0.000317	0.058419
EAV4R	4	0.031	0.258	0.226	0.001007	0.066616
EAV5R	5	0.039	0.269	0.228	0.001655	0.072200
EAV6	6	0.047	0.293	0.230	0.004062	0.086084
EAV7.5	7.5	0.060	0.322	0.232	0.007978	0.103491
EAV10	10	0.080	0.364	0.237	0.016021	0.132132
EAV15	15	0.121	0.416	0.247	0.028636	0.172973

Table 9.11-5: Inverse Rule of Mixtures, Synthetic Graphite Composite

	TC (W/mK)			0.528627	12.6547	23.9387
Vectra	0.22			epsilon(y)	sum((y(i)-y(mod))^2)	sum(y(i)^2)
Filler	600					
			TC (W/mK)	TC (W/mK)		
Formulation	wt% filler	vol% filler	Experimental	Calculated	(y(i)-y(mod))^2	y(i)^2
EVR	0	0.000	0.217	0.220	0.000010	0.047046
EBV10	10	0.065	0.294	0.235	0.003391	0.086142
EBV15	15	0.099	0.349	0.244	0.011055	0.122080
EBV20	20	0.135	0.387	0.254	0.017569	0.149692
EBV25	25	0.172	0.470	0.266	0.041706	0.220806
EBV30	30	0.211	0.546	0.279	0.071549	0.298553
EBV35	35	0.252	0.611	0.294	0.100184	0.372832
EBV40	40	0.293	0.706	0.311	0.156241	0.499001
EBV45	45	0.338	0.880	0.332	0.300453	0.775104
EBV50	50	0.385	1.108	0.357	0.563537	1.22789
EBV55	55	0.433	1.285	0.388	0.804885	1.65148
EBV60	60	0.484	1.559	0.426	1.28231	2.42923
EBV65	65	0.537	1.943	0.475	2.15337	3.77369
EBV70	70	0.593	2.323	0.540	3.17641	5.39401
EBV75	75	0.652	2.625	0.632	3.97200	6.89115

Table 9.11-6: Inverse Rule of Mixtures, Carbon Fiber Composite

	TC (W/mK)		TC (W/mK)	TC (W/mK)	0.181337	0.679135	3.74516
Vectra	0.22				epsilon(y)	sum((y(i)-y(mod))^2)	sum(y(i)^2)
Filler	20						
			TC (W/mK)	TC (W/mK)			
Formulation	wt% filler	vol% filler	Experimental	Calculated	(y(i)-y(mod))^2	y(i)^2
EVR	0	0.000	0.217	0.220	0.000010	0.047046
EHV5	5	0.041	0.238	0.229	0.000076	0.056644
EHV7.5	7.5	0.061	0.255	0.234	0.000436	0.065025
EHV10	10	0.082	0.271	0.239	0.000998	0.073441
EHV15	15	0.124	0.282	0.251	0.000976	0.079524
EHV20	20	0.168	0.320	0.264	0.003154	0.102400
EHV25	25	0.212	0.353	0.278	0.005571	0.124609
EHV30	30	0.255	0.365	0.294	0.005013	0.133225
EHV35	35	0.302	0.432	0.314	0.013996	0.186624
EHV40	40	0.349	0.527	0.336	0.036496	0.277729
EHV45	45	0.397	0.602	0.362	0.057495	0.362404
EHV50R	50	0.446	0.688	0.394	0.086656	0.473344
EHV55	55	0.496	0.838	0.432	0.164971	0.702244
EHV60R	60	0.547	1.030	0.479	0.303287	1.06090

Table 9.11-7: Geometric Rule of Mixtures, Carbon Black Composite

	TC (W/mK)				0.047189	0.034871	0.738959
Vectra	0.22				epsilon(y)	sum((y(i)-y(mod))^2)	sum(y(i)^2)
Filler	2.1						
			TC (W/mK)	TC (W/mK)			
Formulation	wt% filler	vol% filler	Experimental	Calculated	(y(i)-y(mod))^2	y(i)^2
EVR	0	0.000	0.217	0.220	0.000010	0.047046
EAV2.5	2.5	0.019	0.242	0.230	0.000141	0.058419
EAV4R	4	0.031	0.258	0.236	0.000482	0.066616
EAV5R	5	0.039	0.269	0.240	0.000801	0.072200
EAV6	6	0.047	0.293	0.245	0.002381	0.086084
EAV7.5	7.5	0.060	0.322	0.252	0.004913	0.103491
EAV10	10	0.080	0.364	0.263	0.010021	0.132132
EAV15	15	0.121	0.416	0.289	0.016123	0.172973

Table 9.11-8: Geometric Rule of Mixtures, Synthetic Graphite Composite

	TC (W/mK)			85.5646	2048.31	23.9387
Vectra	0.22			epsilon(y)	sum((y(i)-y(mod))^2)	sum(y(i)^2)
Filler	600					
			TC (W/mK)	TC (W/mK)		
Formulation	wt% filler	vol% filler	Experimental	Calculated	(y(i)-y(mod))^2	y(i)^2
EVR	0	0.000	0.217	0.220	0.000010	0.047046
EBV10	10	0.065	0.294	0.368	0.005507	0.086142
EBV15	15	0.099	0.349	0.483	0.017784	0.122080
EBV20	20	0.135	0.387	0.641	0.064366	0.149692
EBV25	25	0.172	0.470	0.858	0.150439	0.220806
EBV30	30	0.211	0.546	1.171	0.389570	0.298553
EBV35	35	0.252	0.611	1.615	1.00922	0.372832
EBV40	40	0.293	0.706	2.234	2.33369	0.499001
EBV45	45	0.338	0.880	3.189	5.33114	0.775104
EBV50	50	0.385	1.108	4.611	12.2710	1.22789
EBV55	55	0.433	1.285	6.766	30.0405	1.65148
EBV60	60	0.484	1.559	10.123	73.3514	2.42923
EBV65	65	0.537	1.943	15.420	181.652	3.77369
EBV70	70	0.593	2.323	23.978	468.953	5.39401
EBV75	75	0.652	2.625	38.301	1272.74	6.89115

Table 9.11-9: Geometric Rule of Mixtures, Carbon Fiber Composite

	TC (W/mK)			1.60887	6.02546	3.7452
Vectra	0.22			epsilon(y)	sum((y(i)-y(mod))^2)	sum(y(i)^2)
Filler	20					
			TC (W/mK)	TC (W/mK)		
Formulation	wt% filler	vol% filler	Experimental	Calculated	(y(i)-y(mod))^2	y(i)^2
EVR	0	0.000	0.217	0.220	0.000010	0.047046
EHV5	5	0.041	0.238	0.265	0.000712	0.056644
EHV7.5	7.5	0.061	0.255	0.290	0.001202	0.065025
EHV10	10	0.082	0.271	0.318	0.002251	0.073441
EHV15	15	0.124	0.282	0.385	0.010578	0.079524
EHV20	20	0.168	0.320	0.469	0.022296	0.102400
EHV25	25	0.212	0.353	0.572	0.048106	0.124609
EHV30	30	0.255	0.365	0.695	0.108776	0.133225
EHV35	35	0.302	0.432	0.859	0.182209	0.186624
EHV40	40	0.349	0.527	1.062	0.285838	0.277729
EHV45	45	0.397	0.602	1.318	0.512979	0.362404
EHV50R	50	0.446	0.688	1.644	0.914368	0.473344
EHV55	55	0.496	0.838	2.060	1.49357	0.702244
EHV60R	60	0.547	1.030	2.593	2.44257	1.0609

Table 9.11-10: Nielsen's Model, Carbon Black Composite

	TC (W/mK)	A	phi(m)			0.053869	0.039807	0.738959
Vectra	0.22					epsilon(y)	sum((y(i)-y(mod))^2)	sum(y(i)^2)
Filler	2.1	1.5	0.637					
			TC (W/mK)			TC (W/mK)		
Formulation	wt% filler	vol% filler	Experimental	psi	B	K	(y(i)-y(mod))^2	y(i)^2
EVR	0	0.000	0.217	1.000	0.773663	0.220000	0.000010	0.047046
EAV2.5	2.5	0.019	0.242	1.017	0.773663	0.228441	0.000176	0.058419
EAV4R	4	0.031	0.258	1.028	0.773663	0.233857	0.000588	0.066616
EAV5R	5	0.039	0.269	1.035	0.773663	0.237509	0.000973	0.072200
EAV6	6	0.047	0.293	1.042	0.773663	0.241136	0.002731	0.086084
EAV7.5	7.5	0.060	0.322	1.053	0.773663	0.247175	0.005554	0.103491
EAV10	10	0.080	0.364	1.071	0.773663	0.257399	0.011257	0.132132
EAV15	15	0.121	0.416	1.108	0.773663	0.279819	0.018518	0.172973

Table 9.11-11: Nielsen's Model, Synthetic Graphite Composite

	TC (W/mK)	A	phi(m)			11.8640	284.010	23.9387
Vectra	0.22					epsilon(y)	sum((y(i)-y(mod))^2)	sum(y(i)^2)
Filler	600	1.58	0.637					
			TC (W/mK)			TC (W/mK)		
Formulation	wt% filler	vol% filler	Experimental	psi	B	K	(y(i)-y(mod))^2	y(i)^2
EVR	0	0.000	0.217	1.000	0.999055	0.220000	0.000010	0.047046
EBV10	10	0.065	0.294	1.058	0.999055	0.260423	0.001094	0.086142
EBV15	15	0.099	0.349	1.089	0.999055	0.285333	0.004105	0.122080
EBV20	20	0.135	0.387	1.121	0.999055	0.314495	0.005243	0.149692
EBV25	25	0.172	0.470	1.154	0.999055	0.348912	0.014638	0.220806
EBV30	30	0.211	0.546	1.189	0.999055	0.391696	0.023933	0.298553
EBV35	35	0.252	0.611	1.225	0.999055	0.444715	0.027518	0.372832
EBV40	40	0.293	0.706	1.262	0.999055	0.510270	0.038467	0.499001
EBV45	45	0.338	0.880	1.302	0.999055	0.602230	0.077378	0.775104
EBV50	50	0.385	1.108	1.344	0.999055	0.731158	0.142085	1.22789
EBV55	55	0.433	1.285	1.387	0.999055	0.926638	0.128495	1.65148
EBV60	60	0.484	1.559	1.433	0.999055	1.26373	0.086949	2.42923
EBV65	65	0.537	1.943	1.481	0.999055	1.97947	0.001359	3.77369
EBV70	70	0.593	2.323	1.530	0.999055	4.56647	5.03542	5.39401
EBV75	75	0.652	2.625	1.583	0.999055	-14.0609	278.423	6.89115

Table 9.11-12: Nielsen's Model, Carbon Fiber Composite

	TC (W/mK)	A	phi(m)			431.171	1614.803	3.74516
Vectra	0.22					epsilon(y)	sum((y(i)-y(mod))^2)	sum(y(i)^2)
Filler	20	4.29	0.52					
			TC (W/mK)			TC (W/mK)		
Formulation	wt% filler	vol% filler	Experimental	psi	B	K	(y(i)-y(mod))^2	y(i)^2
EVR	0	0.000	0.217	1.000	0.944432	0.220000	0.000010	0.047046
EHV5	5	0.041	0.238	1.073	0.944432	0.267664	0.000880	0.056644
EHV7.5	7.5	0.061	0.255	1.108	0.944432	0.293086	0.001451	0.065025
EHV10	10	0.082	0.271	1.146	0.944432	0.321624	0.002563	0.073441
EHV15	15	0.124	0.282	1.220	0.944432	0.385630	0.010739	0.079524
EHV20	20	0.168	0.320	1.298	0.944432	0.465667	0.021219	0.102400
EHV25	25	0.212	0.353	1.376	0.944432	0.564536	0.044747	0.124609
EHV30	30	0.255	0.365	1.453	0.944432	0.687983	0.104318	0.133225
EHV35	35	0.302	0.432	1.536	0.944432	0.870634	0.192399	0.186624
EHV40	40	0.349	0.527	1.620	0.944432	1.13919	0.374778	0.277729
EHV45	45	0.397	0.602	1.705	0.944432	1.59042	0.976975	0.362404
EHV50R	50	0.446	0.688	1.792	0.944432	2.51752	3.34713	0.473344
EHV55	55	0.496	0.838	1.880	0.944432	5.55864	22.2844	0.702244
EHV60R	60	0.547	1.030	1.971	0.944432	-38.8127	1587.441	1.06090

Table 9.11-13: Modified Nielsen's Model, Carbon Black Composite

	TC (W/mK)	A	phi(m)			0.044397	0.032807	0.738959
Vectra	0.22					epsilon(y)	sum((y(i)-y(mod))^2)	sum(y(i)^2)
Filler	2.1	1.5	0.637					
			TC (W/mK)			TC (W/mK)		
Formulation	wt% filler	vol% filler	Experimental	psi	B	K	(y(i)-y(mod))^2	y(i)^2
EVR	0	0.000	0.217	1.570	0.773663	0.220000	0.000010	0.047046
EAV2.5	2.5	0.019	0.242	1.567	0.773663	0.230371	0.000128	0.058419
EAV4R	4	0.031	0.258	1.565	0.773663	0.237028	0.000444	0.066616
EAV5R	5	0.039	0.269	1.564	0.773663	0.241516	0.000739	0.072200
EAV6	6	0.047	0.293	1.562	0.773663	0.245973	0.002249	0.086084
EAV7.5	7.5	0.060	0.322	1.560	0.773663	0.253387	0.004667	0.103491
EAV10	10	0.080	0.364	1.556	0.773663	0.265919	0.009522	0.132132
EAV15	15	0.121	0.416	1.547	0.773663	0.293228	0.015048	0.172973

Table 9.11-14: Modified Nielsen's Model, Synthetic Graphite Composite

	TC (W/mK)	A	phi(m)			0.0302	0.723	23.9387
Vectra	0.22					epsilon(y)	sum((y(i)-y(mod))^2)	sum(y(i)^2)
Filler	600	1.58	0.637					
			TC (W/mK)			TC (W/mK)		
Formulation	wt% filler	vol% filler	Experimental	psi	B	K	(y(i)-y(mod))^2	y(i)^2
EVR	0	0.000	0.217	1.570	0.999055	0.220000	0.000010	0.047046
EBV10	10	0.065	0.294	1.559	0.999055	0.269836	0.000560	0.086142
EBV15	15	0.099	0.349	1.552	0.999055	0.300826	0.002359	0.122080
EBV20	20	0.135	0.387	1.543	0.999055	0.337135	0.002477	0.149692
EBV25	25	0.172	0.470	1.533	0.999055	0.379782	0.008121	0.220806
EBV30	30	0.211	0.546	1.521	0.999055	0.432145	0.013054	0.298553
EBV35	35	0.252	0.611	1.507	0.999055	0.495579	0.013230	0.372832
EBV40	40	0.293	0.706	1.492	0.999055	0.571230	0.018271	0.499001
EBV45	45	0.338	0.880	1.473	0.999055	0.671492	0.043643	0.775104
EBV50	50	0.385	1.108	1.452	0.999055	0.800097	0.094866	1.22789
EBV55	55	0.433	1.285	1.429	0.999055	0.969952	0.099318	1.65148
EBV60	60	0.484	1.559	1.401	0.999055	1.20399	0.125751	2.42923
EBV65	65	0.537	1.943	1.371	0.999055	1.53781	0.163853	3.77369
EBV70	70	0.593	2.323	1.336	0.999055	2.04136	0.07904	5.39401
EBV75	75	0.652	2.625	1.296	0.999055	2.8676	0.059	6.89115

Table 9.11-15: Modified Nielsen's Model, Carbon Fiber Composite

	TC (W/mK)	A	phi(m)			1.974	7.392	3.74516
Vectra	0.22					epsilon(y)	sum((y(i)-y(mod))^2)	sum(y(i)^2)
Filler	20	4.29	0.52					
			TC (W/mK)			TC (W/mK)		
Formulation	wt% filler	vol% filler	Experimental	psi	B	K	(y(i)-y(mod))^2	y(i)^2
EVR	0	0.000	0.217	1.923	0.944432	0.220000	0.000010	0.047046
EHV5	5	0.041	0.238	1.888	0.944432	0.276783	0.001504	0.056644
EHV7.5	7.5	0.061	0.255	1.871	0.944432	0.307523	0.002759	0.065025
EHV10	10	0.082	0.271	1.853	0.944432	0.342203	0.005070	0.073441
EHV15	15	0.124	0.282	1.817	0.944432	0.419870	0.019008	0.079524
EHV20	20	0.168	0.320	1.779	0.944432	0.515130	0.038076	0.102400
EHV25	25	0.212	0.353	1.740	0.944432	0.627664	0.075440	0.124609
EHV30	30	0.255	0.365	1.702	0.944432	0.758085	0.154516	0.133225
EHV35	35	0.302	0.432	1.661	0.944432	0.929332	0.247339	0.186624
EHV40	40	0.349	0.527	1.618	0.944432	1.13828	0.373669	0.277729
EHV45	45	0.397	0.602	1.575	0.944432	1.40153	0.639245	0.362404
EHV50R	50	0.446	0.688	1.530	0.944432	1.73773	1.10194	0.473344
EHV55	55	0.496	0.838	1.484	0.944432	2.17355	1.7837	0.702244
EHV60R	60	0.547	1.030	1.437	0.944432	2.7475	2.950	1.06090

Table 9.11-16: Optimized Nielsen's Model, Carbon Black Composite

	TC (W/mK)	A	phi(m)				0.000948	0.000701	0.738959
Vectra	0.22						epsilon(y)	sum((y(i)-y(mod))^2)	sum(y(i)^2)
Filler	2.1	47.3142	0.637						
			TC (W/mK)			TC (W/mK)			
Formulation	wt% filler	vol% filler	Experimental	psi	B	K	(y(i)-y(mod))^2	y(i)^2
EVR	0	0.000	0.217	1.000	0.150290	0.220000	0.000010	0.047046
EAV2.5	2.5	0.019	0.242	1.017	0.150290	0.251094	0.000088	0.058419
EAV4R	4	0.031	0.258	1.028	0.150290	0.270434	0.000152	0.066616
EAV5R	5	0.039	0.269	1.035	0.150290	0.283212	0.000211	0.072200
EAV6	6	0.047	0.293	1.042	0.150290	0.295703	0.000005	0.086084
EAV7.5	7.5	0.060	0.322	1.053	0.150290	0.316058	0.000032	0.103491
EAV10	10	0.080	0.364	1.071	0.150290	0.349327	0.000201	0.132132
EAV15	15	0.121	0.416	1.108	0.150290	0.417375	0.000002	0.172973

Table 9.11-17: Optimized Nielsen's Model, Synthetic Graphite Composite

	TC (W/mK)	A	phi(m)			3.83693	91.8511	23.9387
Vectra	0.22					epsilon(y)	sum((y(i)-y(mod))^2)	sum(y(i)^2)
Filler	600	0.0000	0.637					
			TC (W/mK)			TC (W/mK)		
Formulation	wt% filler	vol% filler	Experimental	psi	B	K	(y(i)-y(mod))^2	y(i)^2
EVR	0	0.000	0.217	1.000	0.999633	0.220000	0.000010	0.047046
EBV10	10	0.065	0.294	1.058	0.999633	0.236223	0.003281	0.086142
EBV15	15	0.099	0.349	1.089	0.999633	0.246672	0.010553	0.122080
EBV20	20	0.135	0.387	1.121	0.999633	0.259242	0.016297	0.149692
EBV25	25	0.172	0.470	1.154	0.999633	0.274449	0.038201	0.220806
EBV30	30	0.211	0.546	1.189	0.999633	0.293784	0.063815	0.298553
EBV35	35	0.252	0.611	1.225	0.999633	0.318240	0.085475	0.372832
EBV40	40	0.293	0.706	1.262	0.999633	0.349021	0.127720	0.499001
EBV45	45	0.338	0.880	1.302	0.999633	0.392886	0.237670	0.775104
EBV50	50	0.385	1.108	1.344	0.999633	0.455238	0.426228	1.22789
EBV55	55	0.433	1.285	1.387	0.999633	0.550869	0.539095	1.65148
EBV60	60	0.484	1.559	1.433	0.999633	0.71734	0.707722	2.42923
EBV65	65	0.537	1.943	1.481	0.999633	1.07356	0.755226	3.77369
EBV70	70	0.593	2.323	1.530	0.999633	2.37201	0.002451	5.39401
EBV75	75	0.652	2.625	1.583	0.999633	-6.8003	88.8373	6.89115

Table 9.11-18: Optimized Nielsen's Model, Carbon Fiber Composite

	TC (W/mK)	A	phi(m)			6.15553	23.0534	3.74516
Vectra	0.22					epsilon(y)	sum((y(i)-y(mod))^2)	sum(y(i)^2)
Filler	20	0.0000	0.52					
			TC (W/mK)			TC (W/mK)		
Formulation	wt% filler	vol% filler	Experimental	psi	B	K	(y(i)-y(mod))^2	y(i)^2
EVR	0	0.000	0.217	1.000	0.989000	0.220000	0.000010	0.047046
EHV5	5	0.041	0.238	1.073	0.989000	0.230005	0.000064	0.056644
EHV7.5	7.5	0.061	0.255	1.108	0.989000	0.235764	0.000370	0.065025
EHV10	10	0.082	0.271	1.146	0.989000	0.242532	0.000810	0.073441
EHV15	15	0.124	0.282	1.220	0.989000	0.258711	0.000542	0.079524
EHV20	20	0.168	0.320	1.298	0.989000	0.280506	0.001560	0.102400
EHV25	25	0.212	0.353	1.376	0.989000	0.309237	0.001915	0.124609
EHV30	30	0.255	0.365	1.453	0.989000	0.347197	0.000317	0.133225
EHV35	35	0.302	0.432	1.536	0.989000	0.406502	0.000650	0.186624
EHV40	40	0.349	0.527	1.620	0.989000	0.49886	0.000792	0.277729
EHV45	45	0.397	0.602	1.705	0.989000	0.66533	0.004010	0.362404
EHV50R	50	0.446	0.688	1.792	0.989000	1.04919	0.130461	0.473344
EHV55	55	0.496	0.838	1.880	0.989000	2.83706	3.99624	0.702244
EHV60R	60	0.547	1.030	1.971	0.989000	-3.3192	18.9157	1.06090

Table 9.11-19: Optimized Modified Nielsen's Model, Carbon Black Composite

	TC (W/mK)	A	phi(m)			0.000935	0.000691	0.738959
Vectra	0.22					epsilon(y)	sum((y(i)-y(mod))^2)	sum(y(i)^2)
Filler	2.1	41.5020	0.637					
			TC (W/mK)			TC (W/mK)		
Formulation	wt% filler	vol% filler	Experimental	psi	B	K	(y(i)-y(mod))^2	y(i)^2
EVR	0	0.000	0.217	1.570	0.167402	0.220000	0.000010	0.047046
EAV2.5	2.5	0.019	0.242	1.567	0.167402	0.250929	0.000085	0.058419
EAV4R	4	0.031	0.258	1.565	0.167402	0.270216	0.000147	0.066616
EAV5R	5	0.039	0.269	1.564	0.167402	0.282979	0.000204	0.072200
EAV6	6	0.047	0.293	1.562	0.167402	0.295469	0.000004	0.086084
EAV7.5	7.5	0.060	0.322	1.560	0.167402	0.315851	0.000034	0.103491
EAV10	10	0.080	0.364	1.556	0.167402	0.349230	0.000204	0.132132
EAV15	15	0.121	0.416	1.547	0.167402	0.417702	0.000003	0.172973

Table 9.11-20: Optimized Modified Nielsen's Model, Synthetic Graphite Composite

	TC (W/mK)	A	phi(m)			0.024971	0.597762	23.9387
Vectra	0.22					epsilon(y)	sum((y(i)-y(mod))^2)	sum(y(i)^2)
Filler	600	1.8538	0.637					
			TC (W/mK)			TC (W/mK)		
Formulation	wt% filler	vol% filler	Experimental	psi	B	K	(y(i)-y(mod))^2	y(i)^2
EVR	0	0.000	0.217	1.570	0.998954	0.220000	0.000010	0.047046
EBV10	10	0.065	0.294	1.559	0.998954	0.274177	0.000373	0.086142
EBV15	15	0.099	0.349	1.552	0.998954	0.307881	0.001724	0.122080
EBV20	20	0.135	0.387	1.543	0.998954	0.347386	0.001561	0.149692
EBV25	25	0.172	0.470	1.533	0.998954	0.393809	0.005790	0.220806
EBV30	30	0.211	0.546	1.521	0.998954	0.450838	0.009132	0.298553
EBV35	35	0.252	0.611	1.507	0.998954	0.519967	0.008214	0.372832
EBV40	40	0.293	0.706	1.492	0.998954	0.602462	0.010803	0.499001
EBV45	45	0.338	0.880	1.473	0.998954	0.711872	0.028402	0.775104
EBV50	50	0.385	1.108	1.452	0.998954	0.852321	0.065423	1.22789
EBV55	55	0.433	1.285	1.429	0.998954	1.037975	0.061071	1.65148
EBV60	60	0.484	1.559	1.401	0.998954	1.29400	0.070012	2.42923
EBV65	65	0.537	1.943	1.371	0.998954	1.65953	0.080129	3.77369
EBV70	70	0.593	2.323	1.336	0.998954	2.21141	0.012340	5.39401
EBV75	75	0.652	2.625	1.296	0.998954	3.1178	0.242778	6.89115

Table 9.11-21: Optimized Modified Nielsen's Model, Carbon Fiber Composite

	TC (W/mK)	A	phi(m)			0.000430	0.001609	3.74516
Vectra	0.22					epsilon(y)	sum((y(i)-y(mod))^2)	sum(y(i)^2)
Filler	20	0.0754	0.52					
			TC (W/mK)			TC (W/mK)		
Formulation	wt% filler	vol% filler	Experimental	psi	B	K	(y(i)-y(mod))^2	y(i)^2
EVR	0	0.000	0.217	1.923	0.988181	0.220000	0.000010	0.047046
EHV5	5	0.041	0.238	1.888	0.988181	0.238952	0.000001	0.056644
EHV7.5	7.5	0.061	0.255	1.871	0.988181	0.249095	0.000035	0.065025
EHV10	10	0.082	0.271	1.853	0.988181	0.260454	0.000111	0.073441
EHV15	15	0.124	0.282	1.817	0.988181	0.285623	0.000013	0.079524
EHV20	20	0.168	0.320	1.779	0.988181	0.316094	0.000015	0.102400
EHV25	25	0.212	0.353	1.740	0.988181	0.351687	0.000002	0.124609
EHV30	30	0.255	0.365	1.702	0.988181	0.392575	0.000760	0.133225
EHV35	35	0.302	0.432	1.661	0.988181	0.445926	0.000194	0.186624
EHV40	40	0.349	0.527	1.618	0.988181	0.51084	0.000261	0.277729
EHV45	45	0.397	0.602	1.575	0.988181	0.59278	0.000085	0.362404
EHV50R	50	0.446	0.688	1.530	0.988181	0.69830	0.000106	0.473344
EHV55	55	0.496	0.838	1.484	0.988181	0.83743	0.000000	0.702244
EHV60R	60	0.547	1.030	1.437	0.988181	1.0261	0.000015	1.06090